1-1-2014

Microvortices In Droplets: Generation & Applications

Gopakumar Kamalakshakurup
Wayne State University,

MICROVORTICES IN DROPLETS: GENERATION AND APPLICATIONS

by

GOPAKUMAR KAMALAKSHAKURUP

DISSERTATION

Submitted to the Graduate School

of Wayne State University,

Detroit, Michigan

in partial fulfillment of the requirements

for the degree of

DOCTOR OF PHILOSOPHY

2014

MAJOR: ELECTRICAL ENGINEERING

Approved by:

_____

Advisor Date

_____

_____

_____

DEDICATION

Dedicated to my "achhan & amma"

ACKNOWLEDGEMENTS

First of all, I would like to express my sincere appreciation to Dr. Amar Basu for introducing me to this exciting field of droplet microfluidics and his valuable guidance, without which this dissertation wouldn't have been possible.

Appreciation is also due to the committee members, Dr. Mark Cheng, Dr. Yong Xu, and Dr. Ming-Chia Lai for their constructive comments and valuable suggestions.

Finally, I would like to thank all my friends at WSU for giving me sweet memories during my graduate schooling which I can cherish for the rest of my life.

TABLE OF CONTENTS

LIST OF FIGURES

Chapter 1: Introduction to Droplet Microfluidics

Background and Overview

The advancement in the micro fabrication technology in the early century has led to a revolution in the sensing and detection of chemical and biological samples [1]. Specifically, it has led to a drastic reduction in the volumes requires for biochemical assays. Whereas traditional microplates and vials consume mL of reagents and sample, assays performed in microfluidic chips can range from μL to nL. The reduced reagent consumption not only reduces the cost of high throughput screening assays, but also helps to perform the processes in a faster, efficient and controlled manner. Using these miniaturized microfluidic chips, basic laboratory liquid handling operations can be performed and hence these chips are otherwise known as lab-on-chip devices.

Based on how the liquid is manipulated in a microfluidic chip, we can classify microfluidics into two categories: single phase or continuous microfluidics and multiphase or droplet microfluidics. Single phase microfluidics involves manipulation of miscible liquids inside a microfluidic chip consisting of channels and chambers. In such systems, multiplexing several chemical or biological reactions can be accomplished by integrating thousands of micromechanical valves and control components which direct the fluids into prescribed microchambers where assays are performed. These systems are often referred to as microfluidic large scale integration (mLSI) (figure 1) [2]. However, single phase microfluidics has limitations, including 1) the interaction of samples with the channels walls can cause chip contamination; 2) scaling up the screening process is limited by the need for chambers and isolating valves, leading to

an increase in overall chip size; and 3) reagent consumption, while small (μL by volume), can still become significant when doing large scale screening.

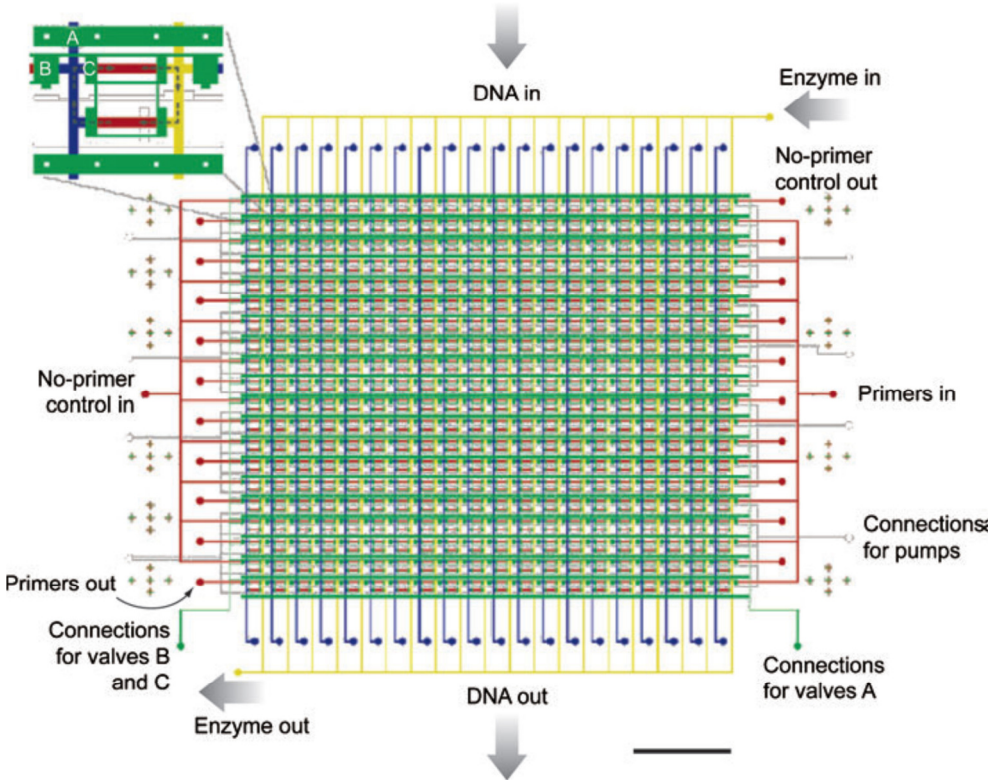

Figure 1: Microfluidic Large Scale Integration [2]

Many of the above limitations can be overcome by the 2nd category of microfluidics, referred to as droplet microfluidics. Droplet microfluidics offers compelling platform for high throughput detection and screening of biological or chemical samples. In contrast to the conventional single phase microfluidics, where the sample and reagents are flowed through the channel, droplet microfluidics deals with aqueous droplet samples encapsulated in an immiscible carrier phase, typically a silicone or fluorocarbon oil [3]. The droplet is separated from the channel walls by a thin film of carrier phase which forms if the surface tension between the droplet and wall is greater

than that of the carrier phase and the wall [4]. Droplet technology offers several advantages over conventional single phase methods: 1) Droplets can have volumes as little as 10fL, leading to a reduction in reagent consumption and therefore the cost of biological screening, 2) the thin carrier phase around the droplet prevents evaporation or contamination [5], 3) the small volume enables single cell culture in pL or fL volumes [6], [7], 4) droplets can be generated and detected with ultra-fast assay throughputs (up to 10KHz) [3], [8], 5) many tools have evolved to perform numerous unit operations [9]. The unit operations, which emulate the basic fluid handling processes performed on the laboratory bench top, are described below.

1.1 Droplet Unit Operations

One of the major capabilities of droplet microfluidics is that it has tools to perform numerous unit operations such as droplet generation, droplet merging, droplet splitting, droplet sorting and fluorescent sensing or assay read out [9]. These unit operations can emulate most of the laboratory operations such as fluid dispensing, mixing of two reagents, aliquoting and fluorescent detection in the microfluidic chip. Due to the rapid development of this field, more technologies are available today to control, manipulate and functionalize the droplets [10]. In addition to above unit operations, there exist other techniques such as single cell encapsulation, droplet polymerization, encapsulation of proteins and DNA, synthesis of nano particles etc [11].

1.1.1 Droplet Generation

The primary aspect of droplet microfluidics is the capability of generating uniformly sized monodisperse droplets. The fine control over the generation parameters such as channel geometry, flow rate of both phases, capillary number is very important

to achieve a reliable droplet production. The two basic device configurations to generate droplets are T-Junction and cross junction/flow focusing. In most cases, the microfluidic devices are manufactured using polydimethyl siloxane (PDMS), which is inexpensive, flexible and transparent elastomeric polymer.

T-junction configuration: In this configuration the dispersed phase and the continuous stream intersect perpendicular to each other [12], [13]. The continuous phase exerts unidirectional shear at the dispersed phase and the subsequent pressure build up results in the elongation of the dispersed phase into the main channel until the neck of the dispersed phase thins and eventually breaks off into droplets (figure 2). Here the droplet size depends on the relative flow rates of the streams, channel geometry and also the relative viscosity of the two phases [14]. To perform the more sophisticated assays, alternate droplet generation with multiple T junction has also been reported (figure 5) [15].

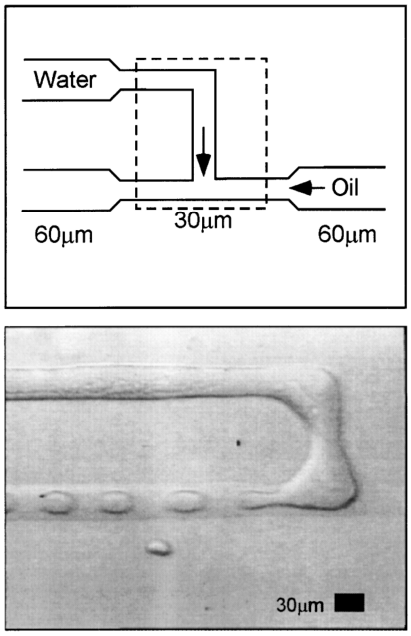

Figure 2: T Junction microfluidic droplet generator [12]

Cross-junction or flow focusing configuration: In this configuration the dispersed phase and the continuous phase are forced to pass through a small and narrow region in the microfluidic device [16]. When the droplet phase enters the junction, it blocks the flow of continuous phase and results in the pressure build up in the continuous phase inlets. The subsequent bidirectional shear as a result of the pressure build up pinches off the dispersed phase to form droplets (figure 3 & 4) [17]. Under flow focusing geometry there are two configurations: confined configuration and unconfined configuration. In the confined configuration, both the dispersed phase inlet and the continuous phase inlets have same width whereas in unconfined configuration, the dispersed phase inlet has smaller width than the continuous phase inlets. Based on the mode of drop formation in these channels, three regimes are defined [18]. (i) Squeezing regime (ii) Dripping regime and (iii) Jetting regime. Squeezing regime and jetting regime occurs at low capillary number and high capillary numbers respectively. In the dripping regime, which occurs at moderate capillary numbers, the geometry of the microchannel has very important role in determining the size of the droplets. The flow focusing geometry enables controlled and stable drop generation compared to T-junction geometry [19].

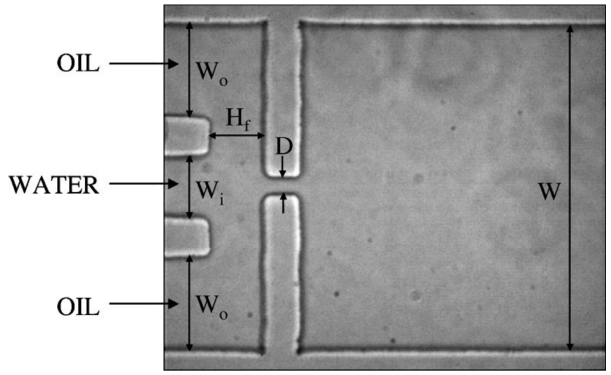

Figure 3: Flow focusing geometry implemented in a microfluidic device [16]

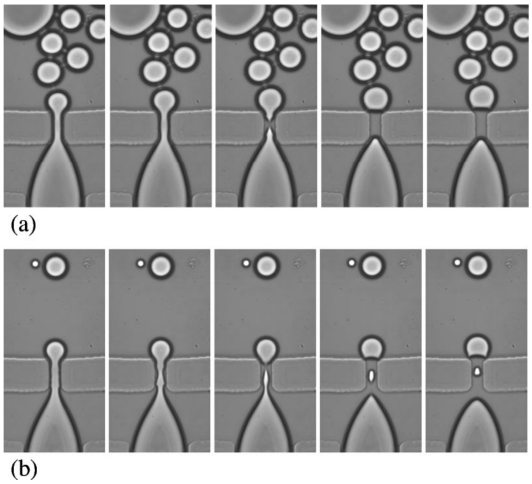

Figure 4: Droplet generation using Flow focusing/cross junction geometry [16]

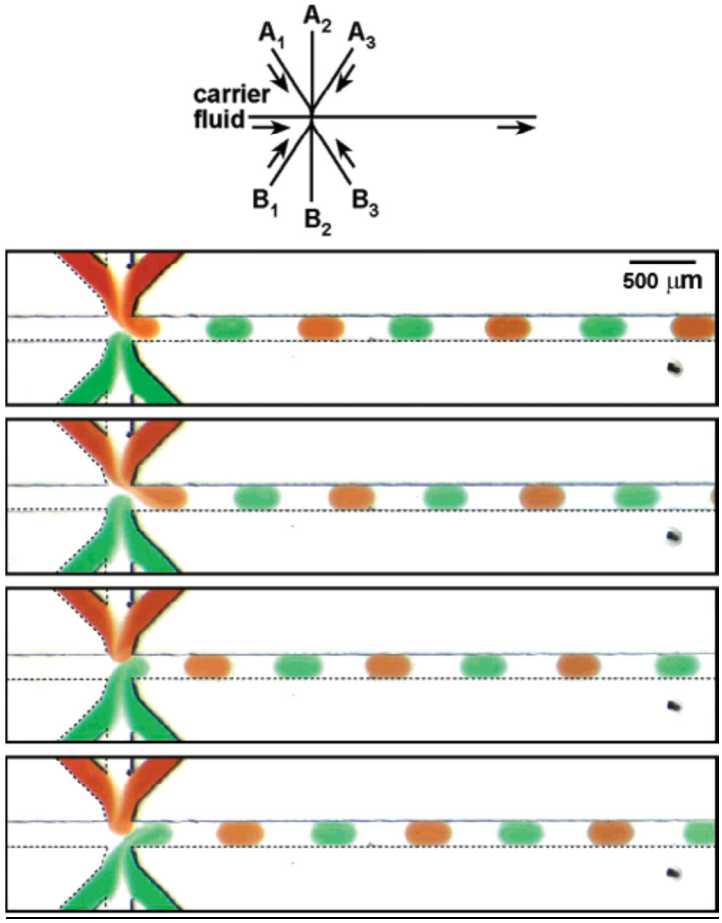

Figure 5: Alternating T junction droplet generator [15]

1.1.2 Droplet Merging/Fusion

Controlled fusion of droplets is an important unit operation when performing reaction in droplets including the synthesis of chemicals and biomolecules, protein and cell based assays, drug discovery etc [9]. To study the activity of certain drugs against a particular disease causing proteins, both the reagent and the protein sample is generated separately in the form of droplets under different conditions. The individually generated droplet samples are made to merge and then the activity is monitored using the microfluidic detection technologies. Droplet merging can be accomplished using both passive and active methods.

(a) Passive Merging

Passive techniques involve smart ways in designing microfluidic channel geometries to ensure controlled and efficient merging. Two well-known techniques to perform passive droplet fusion is the channel expansion design (figure 6) [20] and pillar induced droplet merging [21]. The expansion channel design helps in draining the continuous phase between the droplets and ensures rapid merging. In pillar induced technique, the merging mechanism depends on the pillar geometry, flow rate, interfacial tension and viscosity of the continuous and dispersed streams. When a droplet enters the pillar structure, it slows down, stops and merges with the successive droplets until the hydraulic pressure exceeds the surface tension which pushes the droplet out of the chamber (figure 7).

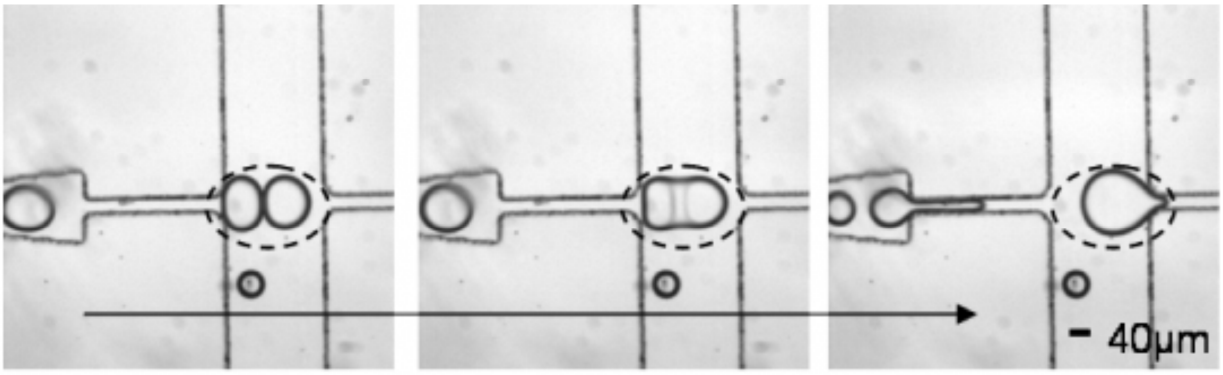

Figure 6: Channel expansion design for droplet fusion [20]

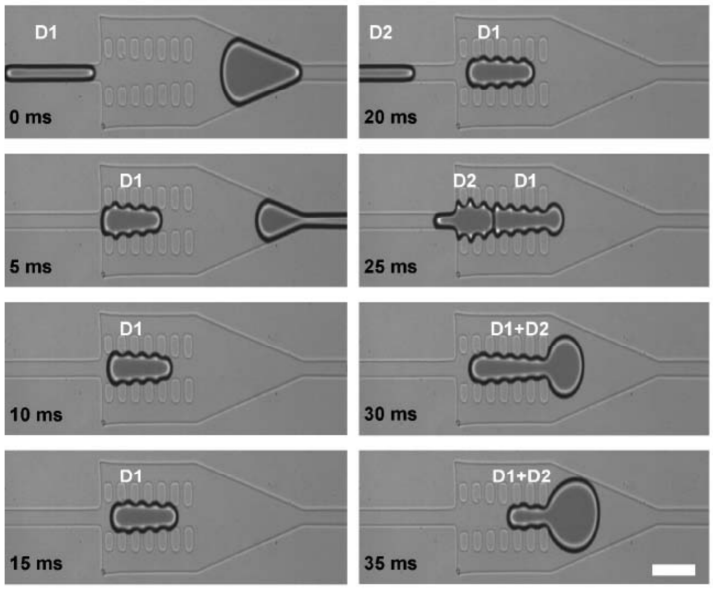

Figure 7: Droplet merging by pillar structures. Sequence of images demonstrate the merging of two droplets [21]

(b) Active Merging

Active methods employ electrical, thermal and optical fields to perform droplet merging. Electrical techniques include DEP [22] and EWOD [23] based methods where the droplets are merged using the electrical actuation of the electrodes (figure 9 & 10). Droplets are arranged in line with a series of electrodes and the controlled actuation of a pair of electrodes coalesce the respective droplets. By also actuating series of adjacent electrodes, a droplet can be moved to another droplet until they merge. Droplet merging

can also be initiated by temperature [24]. Temperature can alter the viscosity of the fluid (continuous phase), which in turn changes the drainage rate of the carrier resulting in the droplet fusion (figure 8). Optical methods generally rely on electromagnetic gradient force generated by focused laser beam to merge two droplets, but the low actuation force and low throughput makes this method less attractive [25]

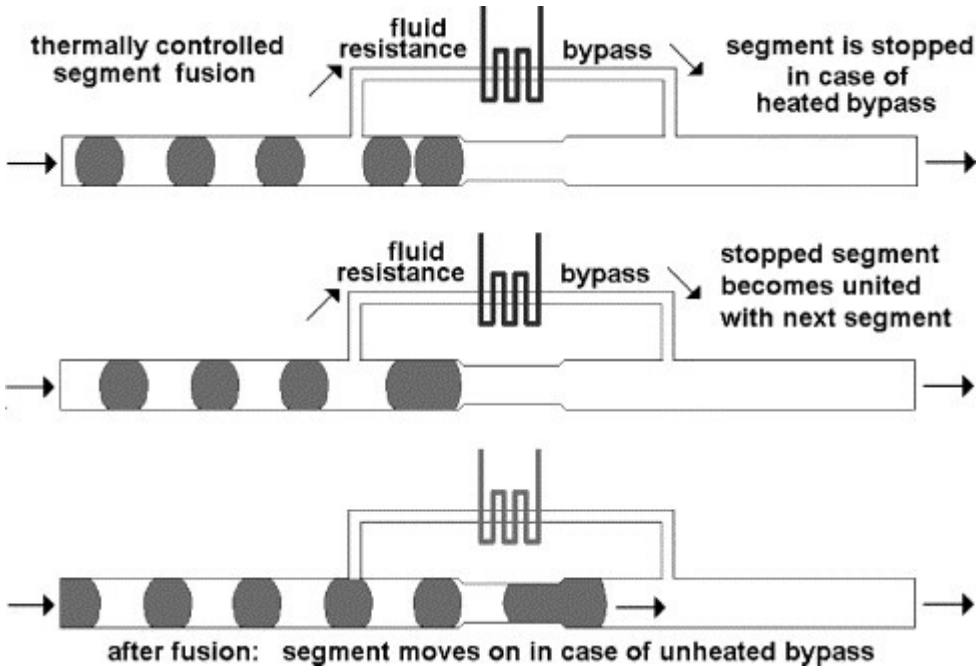

Figure 8: Thermally controlled stopping and pairwise fusion of fluid segments in a channel configuration [24]

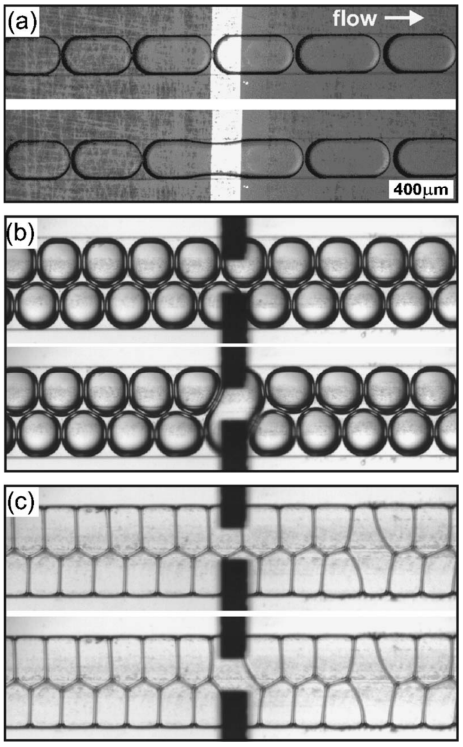

Figure 9: Targeted electrocoalescence of droplets in a microchannel using EWOD [23]

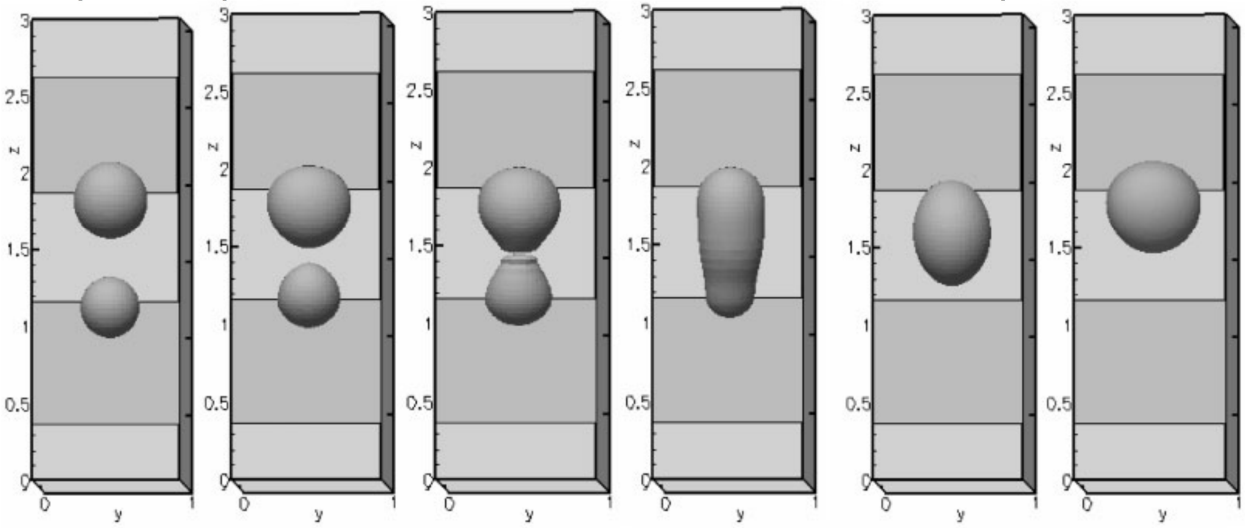

Figure 10: Coalescence of droplets using DEP [22]

.

1.1.3 Droplet splitting

Droplet splitting is a unit operation akin to aliquotting which helps to increase the throughput of the process by splitting a sample into smaller volumes for subsequent process steps. Splitting can also be done using both passive and active techniques.

Passive fission generally relies on the shear force alteration at the channel bifurcation to precisely split the parent drop into two daughter droplets [20], [26], [27]. The size of the daughter droplets can be controlled by altering the flow rate of the continuous stream and the resistance of the channels. For example, if the resistance of the bifurcating channels is equal, then the shear force at the bifurcation is same on either half of the droplet which eventually leads to symmetric splitting of the droplet (figure 11, 12, 13). Splitting can also be accomplished by incorporating a PDMS obstacle in the channel [26]. In contrast to passive splitting, active splitting employs set of electrodes to electrically control the splitting mechanism. Several groups have used EWOD technology to perform active fission (figure 14). The electrodes at the two ends of the droplet are actuated while the central electrode is grounded. Opposite end electrodes pull the droplet to either side with reference to the center leading to droplet break up [28]. Thermally induced surface gradients can also be used to split the droplets by modulating the interfacial stress [29]

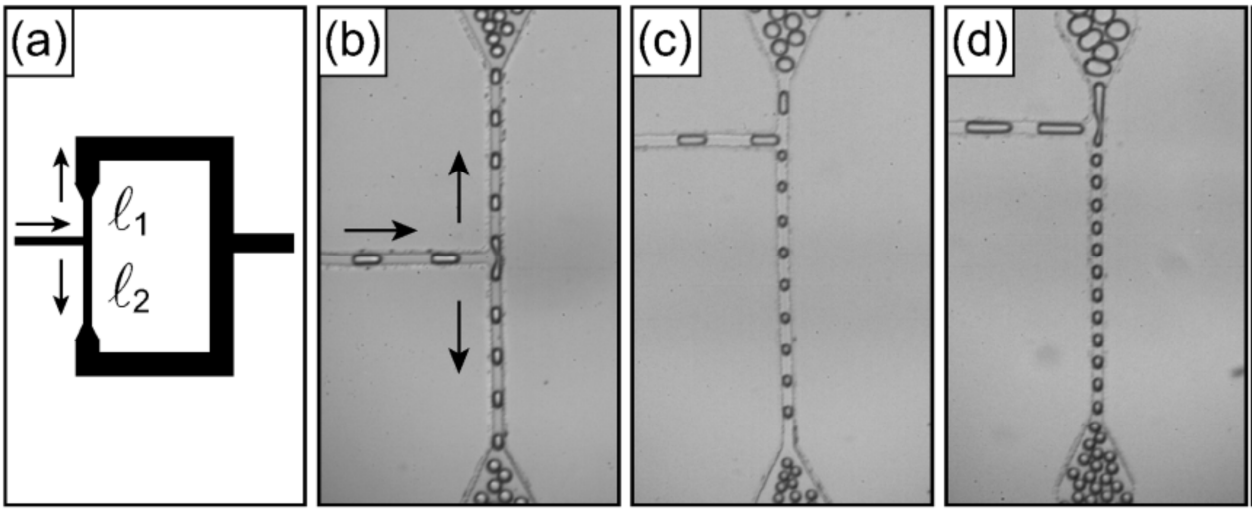

Figure 11: Passive drop splitting using T junction [26]

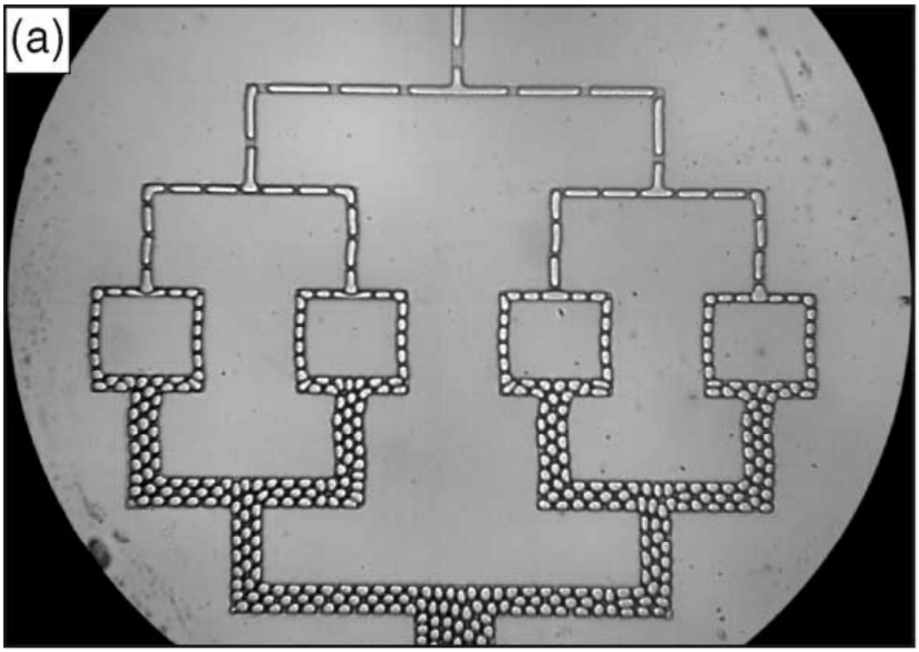

Figure 12: Sequential droplet breaks up [26]

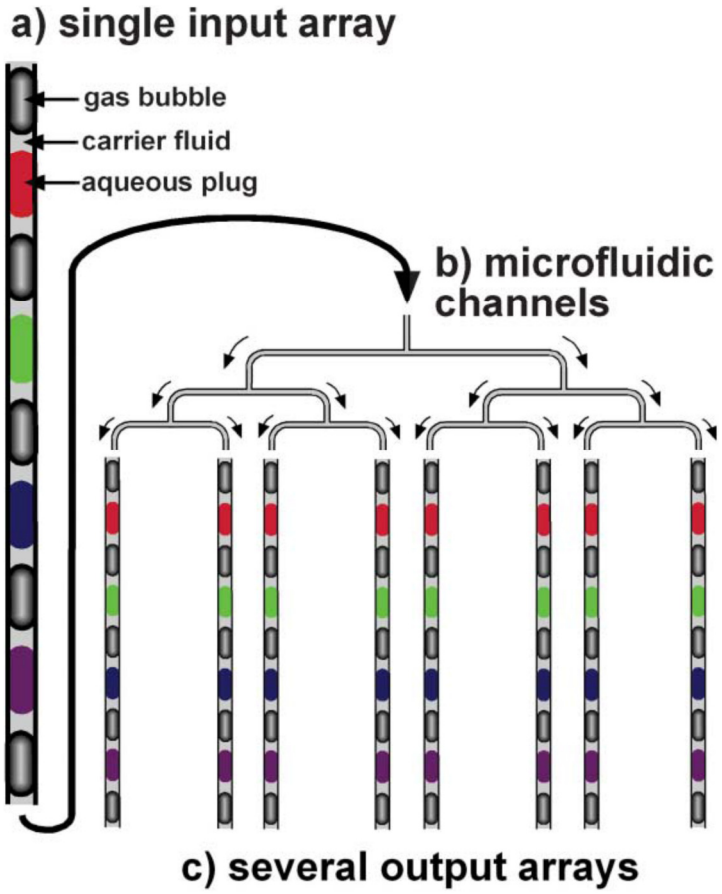

Figure 13: T junction drop splitter for HTS [27]

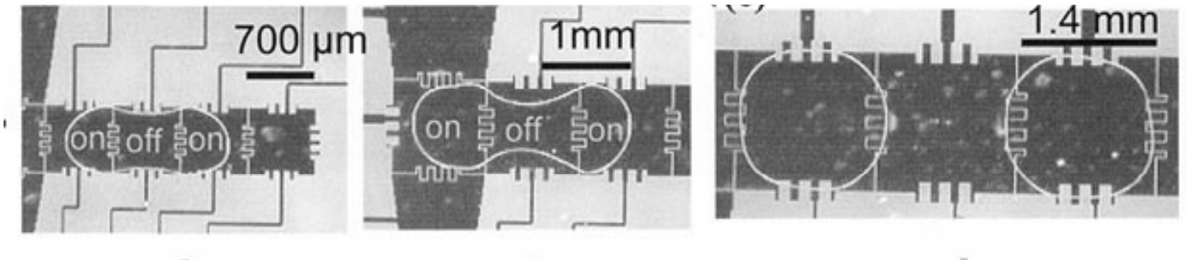

Figure 14: Droplet splitting by EWOD [28]

1.1.4 Droplet sorting

Droplet sorting enables one to separate individual droplets from a library as a function of its size or chemical contents. Like the other unit operations, droplet sorting can be categorized into two types- passive and active.

(a) Passive sorting

As the name suggests, passive sorting techniques do not require any active components such as on-chip electrodes or control electronics. Passive techniques are generally used to sort the droplets based on size. Existing size based sorting techniques generally rely on hydrodynamic techniques. In 2007, Tan et.al demonstrated a passive droplet sorting technique which utilized the channel geometry to alter the flow rate at the bifurcation [31]. Different size droplets were successfully sorted into the respective outlets determined by the shear force ratio which depends on the area of projection and shear rate imposed across the droplet (figure 16).

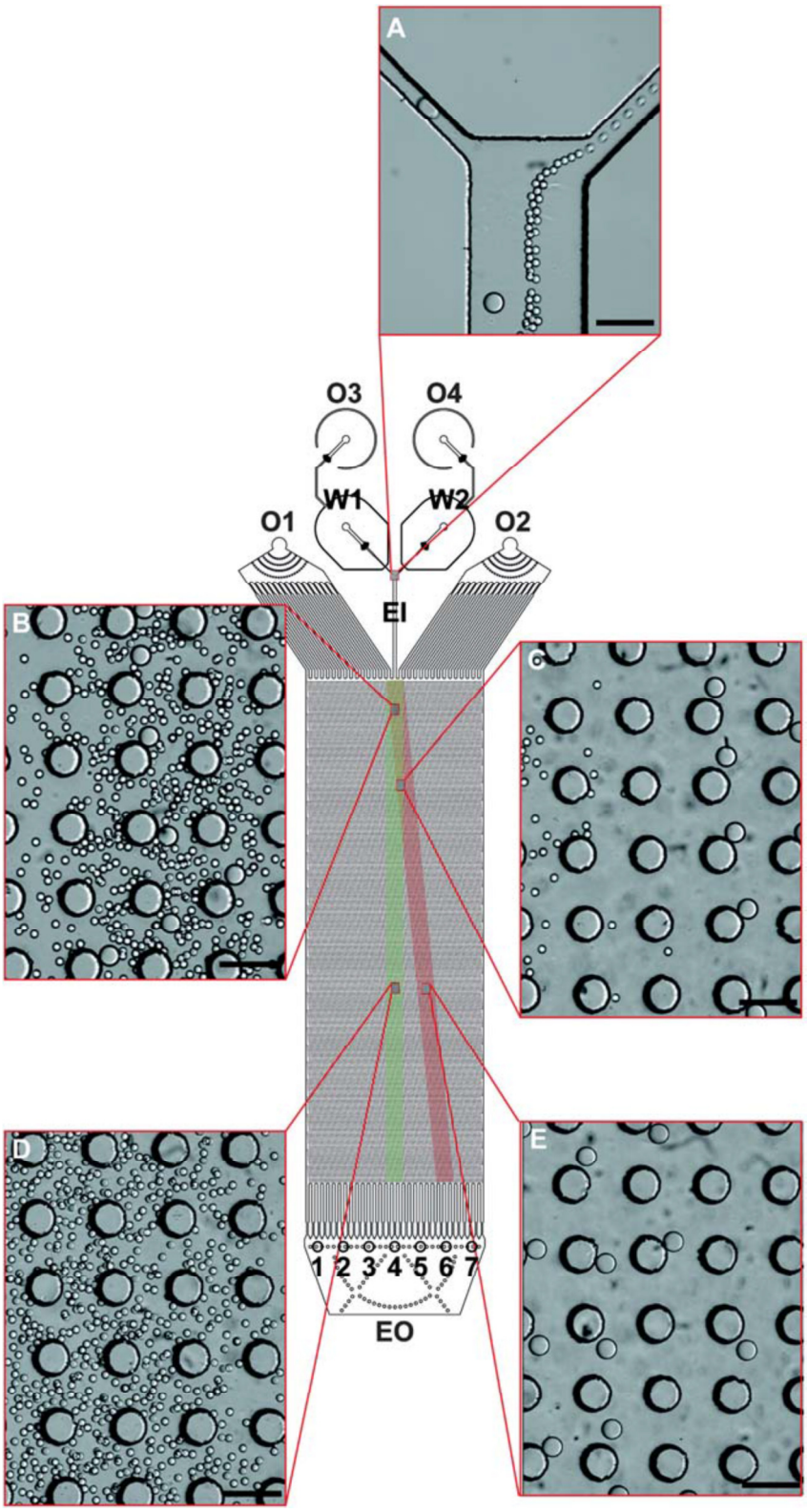

Figure 15: Size based droplet sorting in a DLD device [30]

In 2008, Chabert et.al presented a hydrodynamic technique for cell encapsulation and subsequent sorting of the droplets at the channel bifurcation [32]. The cell encapsulated droplet which is larger than the empty droplet gets sorted into the 'left' outlet by the combined effect of lateral shear induced drift generated by the asymmetric oil flow rates, and the steric interactions between the droplets at the bifurcation. In 2011, Joensson et.al demonstrated a deterministic lateral displacement (DLD) pillar array which could successfully sort 11 μm droplets from 30 μm droplets at a frequency of 12,000 droplets/sec (figure 15) [30].

(b) Active sorting

Whereas the passive droplet sorting techniques can sort by size only, the active techniques are able to sort by both their size and chemical contents. However, they generally require chemical labeling and on-chip electrodes. In fluorescence activated droplet sorting (FADS) [8], [33], the fluorescent signal from the positive droplets is used as a feedback mechanism to actuate the on chip electrodes which pulls the respective droplets into the channel outlet via dielectrophoretic forces [3]. This is an efficient and well known technique which can do selective sorting of the droplets based on the chemical contents. Some of the other active techniques include piezoelectric technique which utilizes surface acoustic waves (SAW) [34], electrically actuated membrane valves [35] which hydro dynamically sort droplets or laser induced thermo capillary valves which can block the advance of droplets [36].

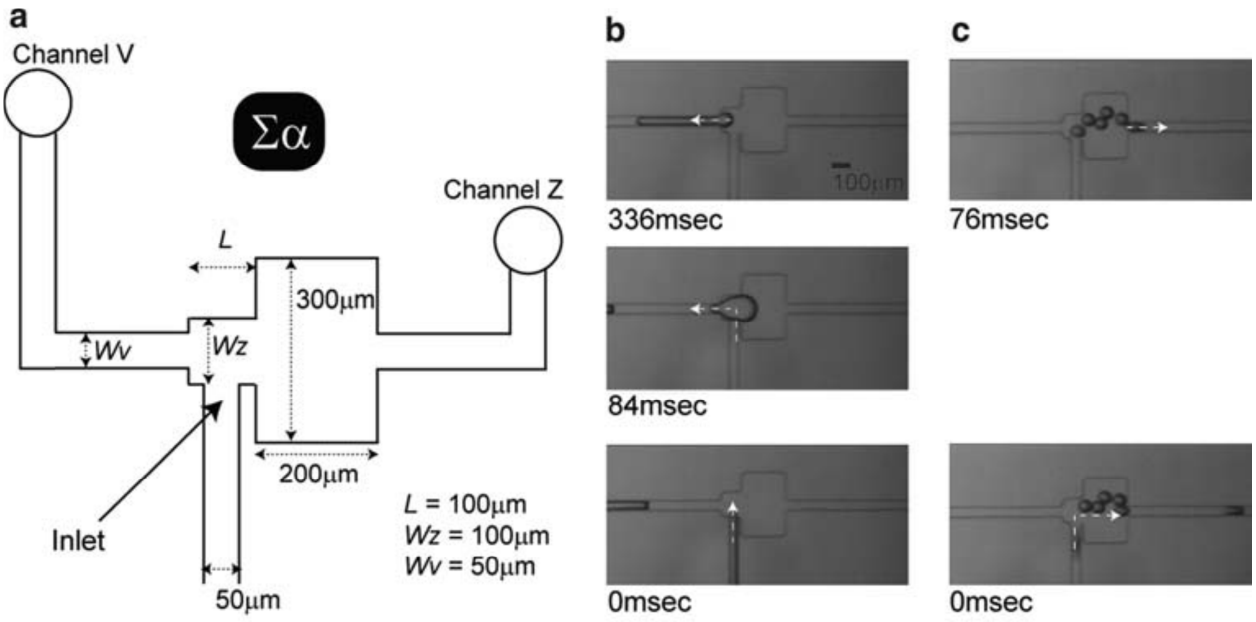

Figure 16: Sorting of droplets based on size in a bifurcating channel [31]

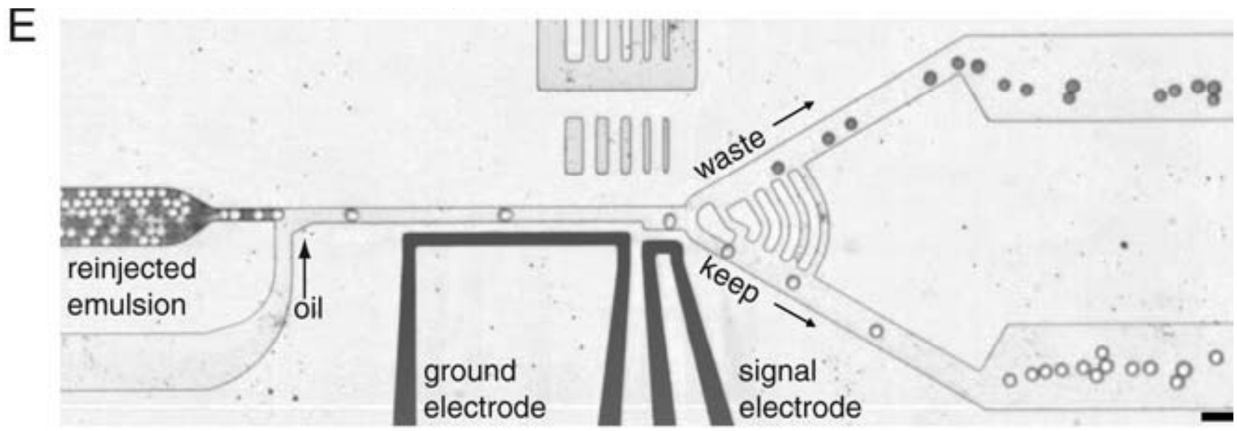

Figure 17: Fluorescence activated sorting of droplets by DEP [33]

1.1.5 Assay Readout/Detection Technique

Sensing and detection is a critical part of high throughput biological screening. The current state of art technique in sensing droplets relies on laser-Induced fluorescent (LIF) detection [33]. LIF requires that the assay is chemically labeled with a fluorophore which fluoresces in the presence of the target biomolecule or enzymatic activity. The laser source is focused through a small window into the microfluidic chip, where it is either

scattered or absorbed by particles, cells or biomolecules. If the sample emits fluorescence, the resulting emission wavelength is captured by multiple photomultiplier tubes arranged symmetrically around the flow cell. In addition to the LIF detection, there are other techniques such as electrochemical detection [37], [38], mass spectroscopy (figure 19) [39], HPLC [40], capillary electrophoresis [41], surface enhanced Raman spectroscopy (figure 18) or combinations of the above mentioned methods [42], [43].

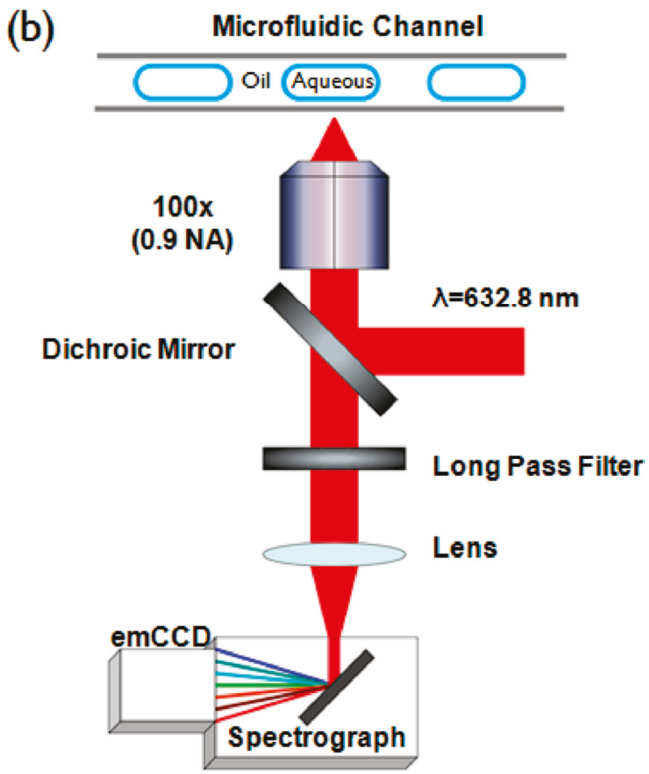

Figure 18: Schematic of surface -enhanced Raman spectrometer used for droplet detection [43]

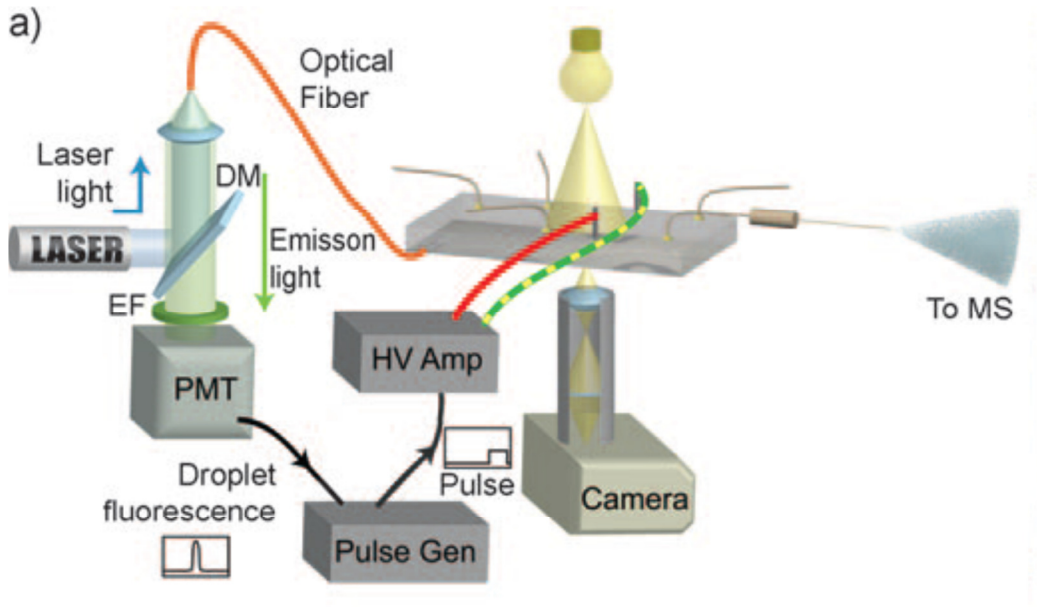

Figure 19: Schematic of the experimental set up which integrates both fluorescent screening and mass spectroscopy analysis of droplets [39]

In addition to aforementioned unit operations, there exist many other operations such as droplet mixing [44], phase change in droplets [45] and photo-initiated polymerization to create microbeads and hydrogels [46].

1.2 Applications of Droplet Technology: Present and Future

With the development of tools to perform numerous operations such as droplet mixing, merging, splitting, sorting etc, droplet microfluidics offers tremendous platform to carry out diverse set of applications from chemical synthesis, particle manipulation, bioassays and drug discovery to point of care diagnostic chips [9]–[11][47]. This section discusses the current and potential applications of droplet microfluidics.

1.2.1 Chemical Reactions in Droplets

The tools to achieve exquisite control and manipulation of droplet reactors help to perform various chemical reactions within the droplets [5]. Each droplet acts as a separate container while performing chemical reactions and offer several advantages: 1. less consumption of expensive reagents 2. Reduce the exposure to hazardous chemicals 3. Large surface to volume ratio ensures greater diffusion and mass flow rates 4. Ensure proper mixing of the reactants by recirculation vortices 5. Scale up the process by parallelization.

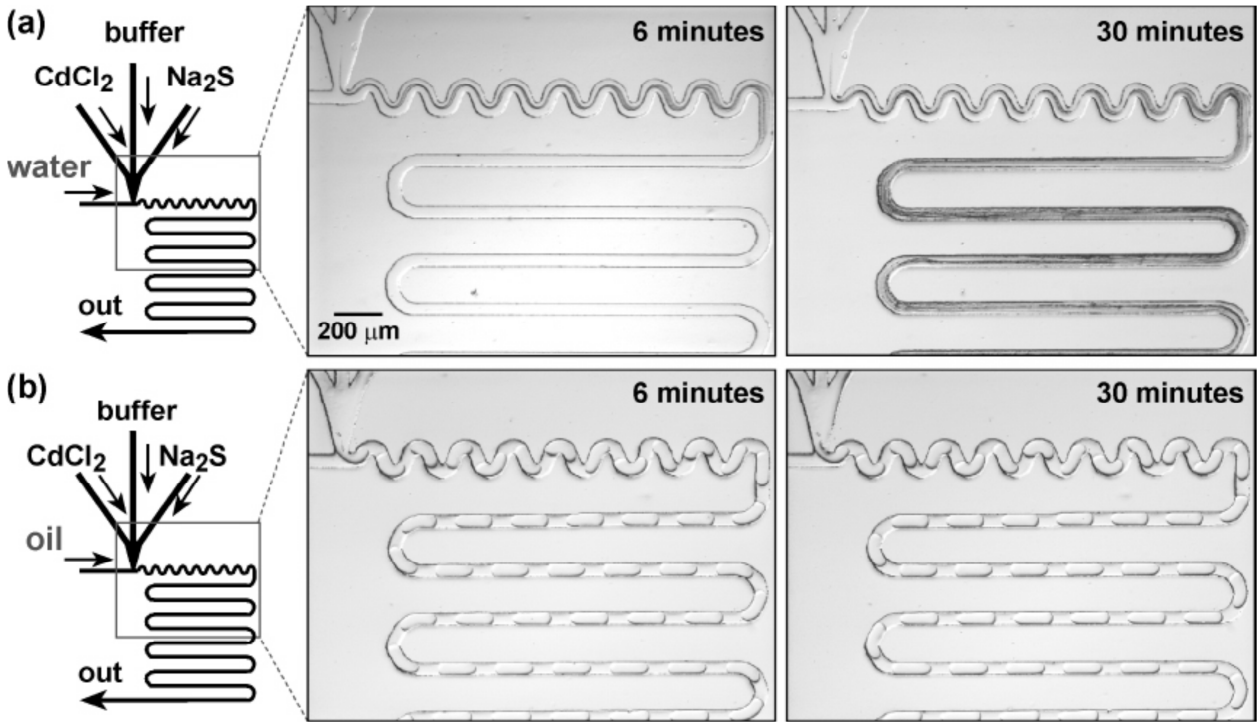

Figure 20: Comparison of the nano-particle (CdS) synthesis in (a) single phase flow and (b) droplet phase. Unlike the droplet system, the single phase system results in nano-particle accumulation inside the channel and eventually leads to clogging [48]

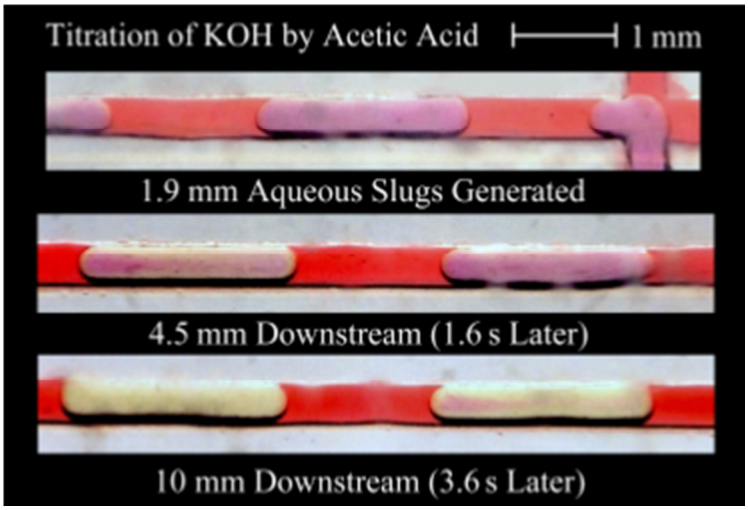

Figure 21: Titration reactions in droplets. The acetic acid present in the continuous phase diffuse into the KOH/NaOH droplets containing phenol red pH indicator [49]

The hydrolysis reaction between sodium hydroxide and the p-nitro phenyl acetate was performed in droplets, where the reaction occurs as result of the mass transfer of p-nitro phenyl acetate into the droplet containing sodium hydroxide. Similar experiment done in single phase showed that the micro reactor based platform gave a dramatic increase in the yield [50]. Diffusion rate studies have been conducted by performing neutralization reaction in droplets [49]. The acetic acid present in the continuous phase diffuse into the KOH/NaOH droplets and the color variation of the pH indicator is indirectly used to calculate the diffusion rates (figure 21). It is found that the diffusion occurs much faster in the small droplets than the plugs. Other chemical reactions include precipitation reactions [51], anticoagulants [52], organic phase reactions [53] and generation of CdSe nanoparticles inside the droplets [48], [54]. The reagents were separately generated in the form of droplets, merged in a controlled environment to induce reaction inside the fused droplet to generate nano particles (figure 20).

1.2.2 Biomolecule Synthesis

Droplet microfluidics is capable of carrying out the synthesis of wide range of biomolecules [9] which includes realization of artificial cells, high throughput directed evolution of proteins, and polymerization chain reaction (PCR) is few of them. The ability of droplet microfluidics to generate uniform and homogeneous droplets with a controlled environment is the fundamental requirement for the synthesis of artificial cells [55]. The formation of an artificial cell helps to study life's fundamental reactions. A cell like bioreactor was realized by encapsulating E coli cell free expression system in a phospholipid vesicle [56]. The phospholipid bilayer acts as a semi-permeable membrane that helps in exchange of nutrients in and out of the cell (figure 22). Huebner et al demonstrated protein expression by encapsulating single cell inside the droplet and detecting the expression of fluorescent proteins within the cell [57]. This in-vitro protein expression in the droplet vesicles offers potential applications in the high throughput directed evolution of proteins (figure 23). In genomics, droplet microfluidics offer compelling platform to perform PCR in droplets. Compared to the conventional approach, droplet based PCR technique offer advantages especially in making the process quantitative and sensitive [58]. It also increases the amplification efficiency by minimizing the reagent dispersion and surface adsorption. Generally, the droplet based PCR is performed in two different ways. 1) Fully chip based approach: A droplet based micro-oscillation flow PCR chip was designed and implemented by Wang et al [59]. Injected droplets, containing PCR mixture, pass through the three distinct temperature zones (denaturation, extension and annealing) in the microfluidic channel to attain required temperature transition. They could successfully amplify HPV-DNA sample and were

analyzed by using gel electrophoresis. They also have shown that the whole process takes less than 15 minutes when compared to 2 hour conventional process. 2) Second approach is widely accepted and commercialized technique, where the microfluidic chips are used only for the generation and detection process [60]. The process flow occurs in three steps: i) Uniform sized droplets with template DNA were created by a microfluidic drop generation device. ii) These droplets are transformed manually into a 96 well plates and are placed in a thermo-cycling device which is programmed to control the temperature required for the DNA amplification iii) Thermo-cycled droplets with amplicons are automatically transferred to the detection device, which has a microfluidic chip built in it. The LIF detection system helps to quantitatively estimate the DNA expression based on the fluorescence associated with each droplet (figure 24).

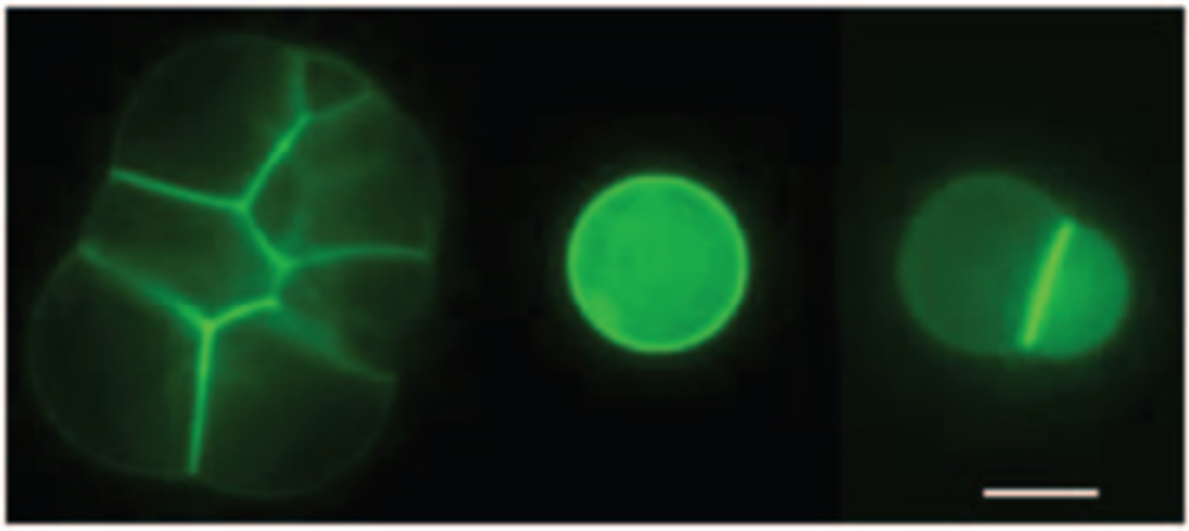

Figure 22: A cell like bioreactor realized by encapsulating E coli cell free expression system in a phospholipid vesicle [56]

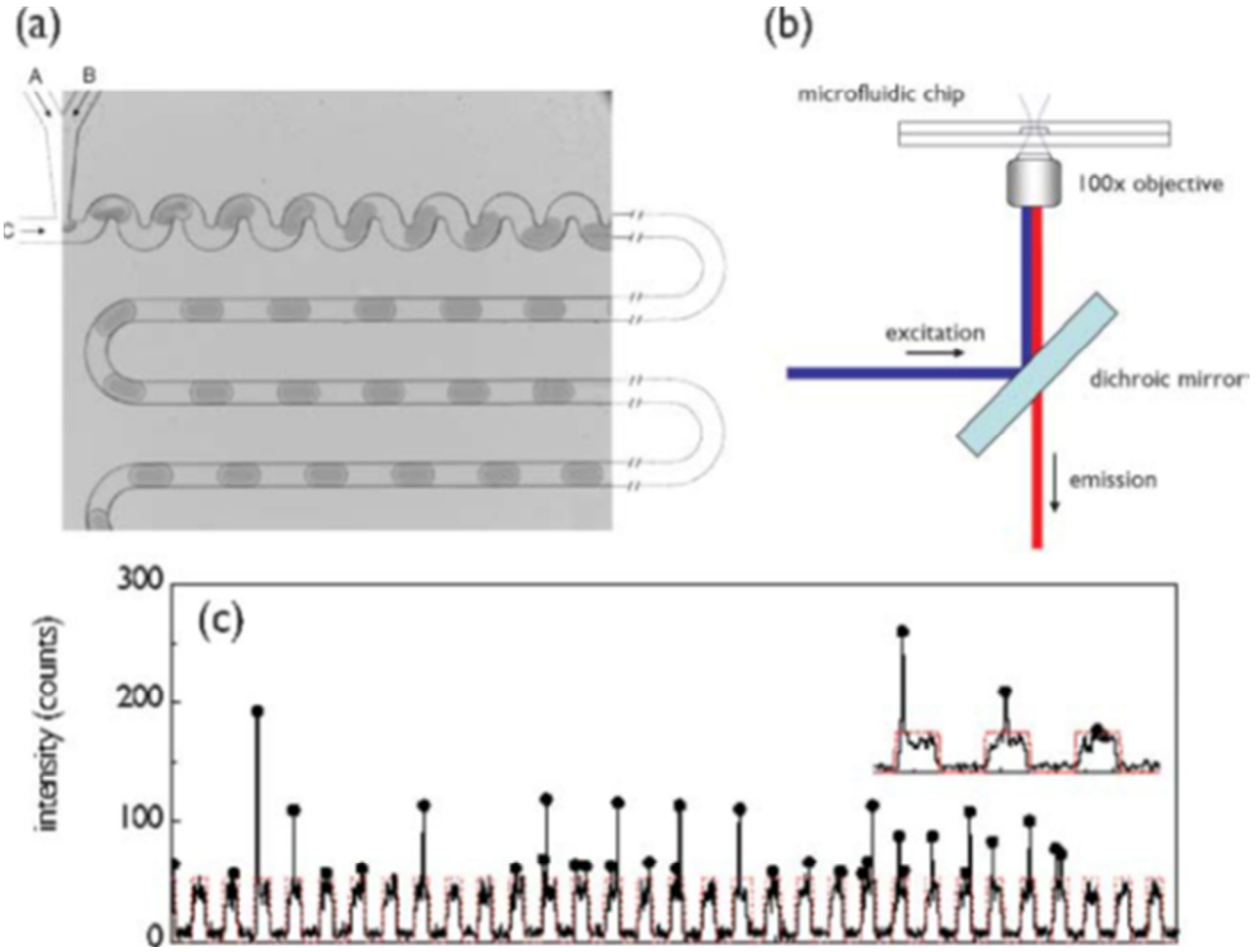

Figure 23: Protein expression studies by encapsulating single cell inside the droplet and detecting the expression of fluorescent proteins within the cell. Droplet containg cells are distinguished by a vertical spike arising from the expressed fluorescent protein [57]

1.2.3 Drug Discovery

With the advent of high speed and sensitive detection technologies such as LIF detection, mass spectroscopy, capillary electrophoresis, x-ray crystallography, high pressure liquid chromatography (HPLC) etc, the droplet microfluidics has the capability to perform high-throughput screening of target molecules against the potential drugs [9]. In a typical example, to study the activity of certain drug against the disease causing cells or proteins, both the labeled cells/proteins and drugs are encapsulated separately in the form of droplets using suitable droplet generation configuration. These two specific

droplet groups are subjected to droplet merging/fusion using any passive or active fusion techniques. The after effect of the reaction happened inside the fused droplet is picked up by the fluorescent detection techniques. Since the droplet generation frequency is reached up to 10 KHz, one can screen up to 10,000 droplets in one second and that had revolutionized the high through put industry. As a result of this, the whole screening process has been transformed from the conventional well plates to the droplet technology. Another tool to perform high throughput protein analysis is matrix assisted desorption or ionization (MALDI) (figure 25). MALDI spectroscopy has been integrated with droplet technology to achieve high throughput analysis of proteins and chemicals [61]. Wheeler et al illustrated a EWOD based technique to purify the sample and analyze them using MALDI-TOF mass spectroscopy [62][63]. The interesting aspect of their method is that the whole process is automated but the surface contamination issues still poses a question over the EWOD techniques (figure 27). Protein characterization can also be done by using x-ray diffraction of protein crystals. Proteins (glucose isomerase, thaumatin, and ferritin) are subjected to crystallization inside the droplets and were characterized using x-ray crystallography technique [64] (figure 26). Another technique to characterize a drug compound is by performing kinetic studies, which helps to explore the activity of enzyme and chemicals. Song and Ismagilov have conducted kinetic measurements of ribo nuclease A (R Nase A) with millisecond temporal resolution [65]. The enzymatic activity is determined by the fluorescence resulting from the cleavage of a fluorogenic substrate by R Nase A. The intensity of the fluorescence is used to figure out the duration of reaction process. In general, droplet microfluidics offers standardized platform to perform high-throughput screening of biomolecules. As such, the droplet

microfluidics does not change the format of the drug screening but it added functionality and performance to the existing platform.

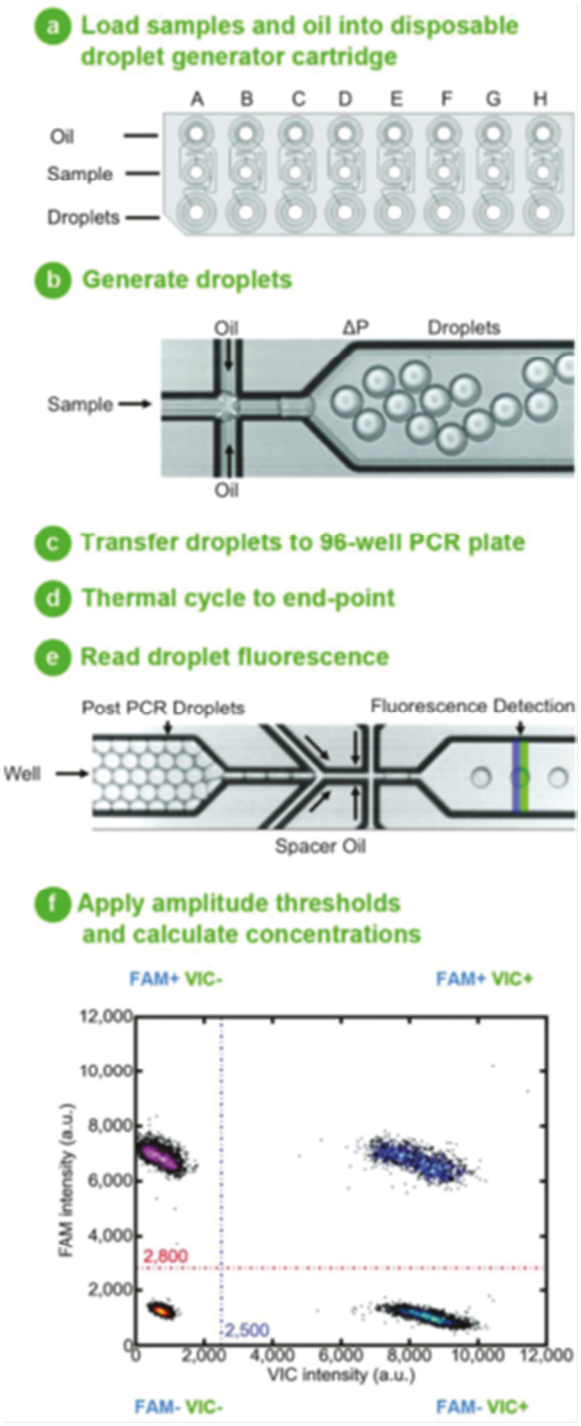

Figure 24: Droplet PCR work flows [60]

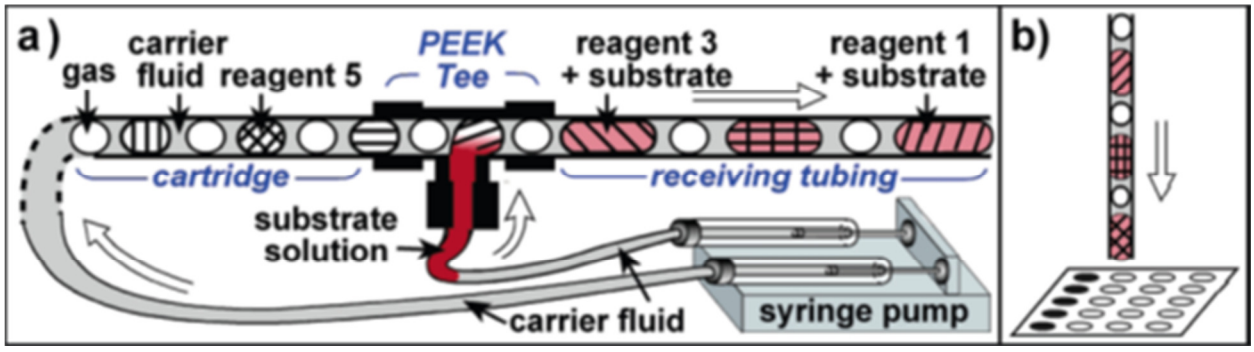

Figure 25: Work flow of screening system (a) serial merging of reagent with substrate solution (b) After incubation, the reaction plugs are deposited onto sample plate for MALDI-MS [61]

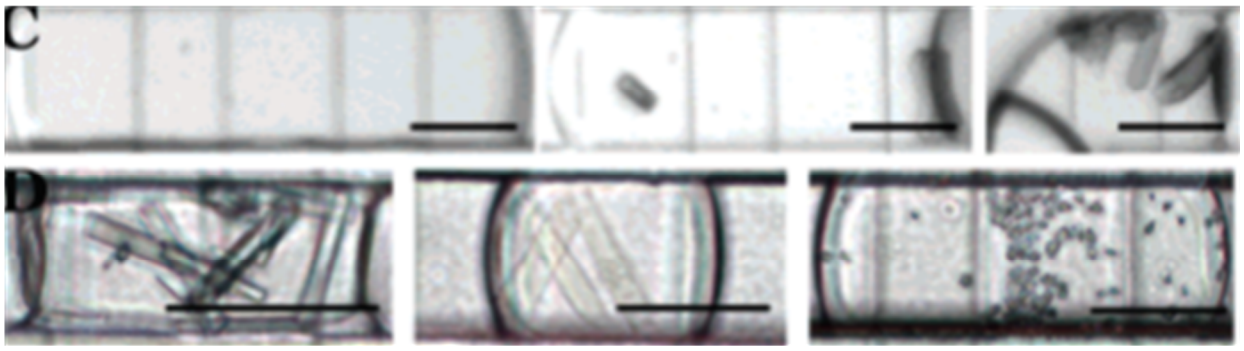

Figure 26: Protein crystallization in droplets. Crystals are from glucose isomerase (left), atalase (middle), and thaumin (right),[64]

Although the droplet microfluidics has been evolved as an excellent platform for biological and pharmaceutical research, this field is still encountering few challenges. One of the primary challenges pertains in the sensing and detection of the droplets. At present there exists many efficient detection technologies such as fluorescence detection, surface enhanced Raman spectroscopy, electrochemical detection, mass spectroscopy, HPLC, capillary electrophoresis etc. How well these techniques are in terms of high throughput sensing and detection? Are we able to extract complete information from the pico-liter volume reactors? As the miniaturization effort is still on, droplet microfluidics would encounter further scale down in future- in terms of the device size, droplet size, and reagent volume and that would seriously challenge the existing detection systems.

Another challenge is the material used in the fabrication of microfluidic devices. In most of the research applications, PDMS is used to make the microfluidic chips. PDMS is transparent, flexible, biocompatible and permeable to gases. These features are good for culturing biomolecules and cells, but PDMS is also auto fluorescent. If the signal to noise ratio of the signal is low, that would affect the fluorescence measurements of the sample. PDMS has low thermal conductivity and also absorbs dyes and swells in certain organic solvents (eg. Silicone oil).These demerits would prevent commercialization of the PDMS chips.

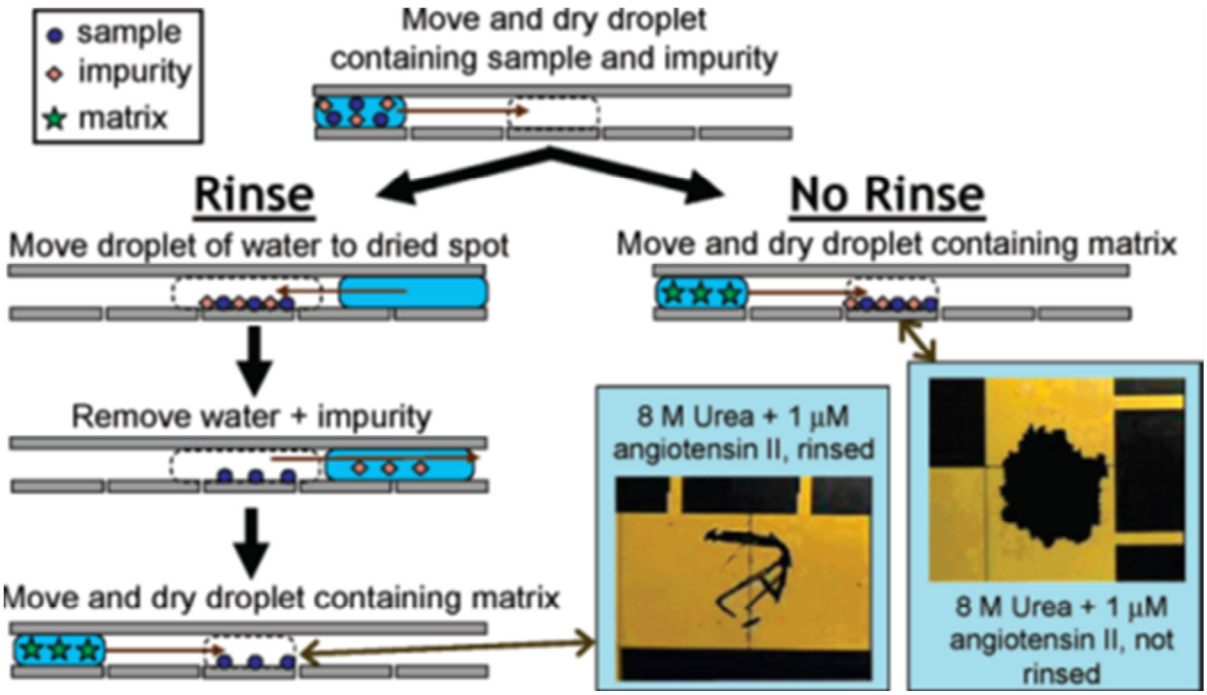

Figure 27: Schematic of EWOD-driven on-chip sample purification for MALDI analysis [62]

Another challenge is the synthesis of ideal surfactants to perform the assays within the microfluidic channels. Although there are many commercially available organic solvents, proper incubation of the droplet emulsions require standardized surfactant and that limits the choice of organic solvents. The problems encountered while incubating the

droplets is imperfect partitioning, inter-droplet cross talk which limits the stability of the emulsions leading to droplet shrinkage or coalescence. Since this is a relatively new and rapidly developing field, more work has to be done to solve the issues and challenges associated with it. With this pace of advancement, in future one could foresee the development of a portable-miniaturized automated microfluidic platform with large number of functional components, which can perform many complex biological processes in less time with high efficiency and precision.

1.3 Motivation

Droplet microfluidics is an emerging platform which has revolutionized the pharmaceutical industry, food industry, cosmetic industry and biomedical or life science industry in less than a decade. With the aid of microfluidic unit operations, it can perform wide set of applications such as chemical synthesis, genomics and proteomics, drug discovery, drug delivery, high throughput screening of wide variety of assays, particle synthesis etc. However, sensing and sorting of the droplets by their contents is still a challenging problem in terms of complexity and cost of the device. Existing sensing technique relies primarily on fluorescence detection coupled with an active actuation mechanism to perform sorting. Using this technique, a fluorescent signal (resulting from the reactions inside the droplet) is used as a feedback mechanism to either i) actuate the on-chip electrodes and sort the droplets by DEP ii) energize the piezoelectric transducers which generates surface acoustic waves to sort the droplets iii) actuate the high speed membrane valves to redirect the droplets into respective outlets. These methods are both sensitive and fast, but they require fluorescent labeling, along with on-chip structures and an active feedback to control sorting signals. Also the need for

several photomultiplier tubes (PMTs), lasers and other related detection electronics around the microfluidic chip makes the system bulky and expensive. To date, there is no simple, passive and label-free sensing and sorting technique based on the chemical composition of the droplets. Here, we present a novel phenomenon which can simultaneously sense and sort the droplets based on the chemical contents inside it. The technique is based on micro-vortices which are naturally generated when a droplet is subjected to an interfacial tension (IFT) gradient.

It has been discussed in the previous session that one of the critical advantages of the droplet microfluidic systems is the tools to perform a set of unit operations including drop generation, merging, mixing, splitting, sorting, and fluorescence detection. However, one of the limitations is that the droplet microfluidics cannot perform an important operation of particle concentration. Particle concentration inside the droplet is an important step to perform bead based (heterogeneous) assays in droplets. Bead based assays are used throughout the life sciences for protein and DNA purification and detection. Inability to concentrate beads in droplets limits droplet systems to simple homogeneous (mix and read) assays. In this thesis, we utilize the naturally occurring hydrodynamic recirculation vortex to concentrate the beads inside the droplets, and demonstrate it applicability to bead based purification.

1.4 Outline of Thesis

This thesis describes two unique ways of generating microvortices in microfluidic droplets, namely (i) recirculation drag and (iii) surfactant microgradient (tensiophoresis), and demonstrates how these vortices can be manipulated to perform useful operations on microfluidic droplets, including the sorting of droplets by size and chemical composition, protein segregation and extraction, and particle concentration. The general outline of the thesis is shown below.

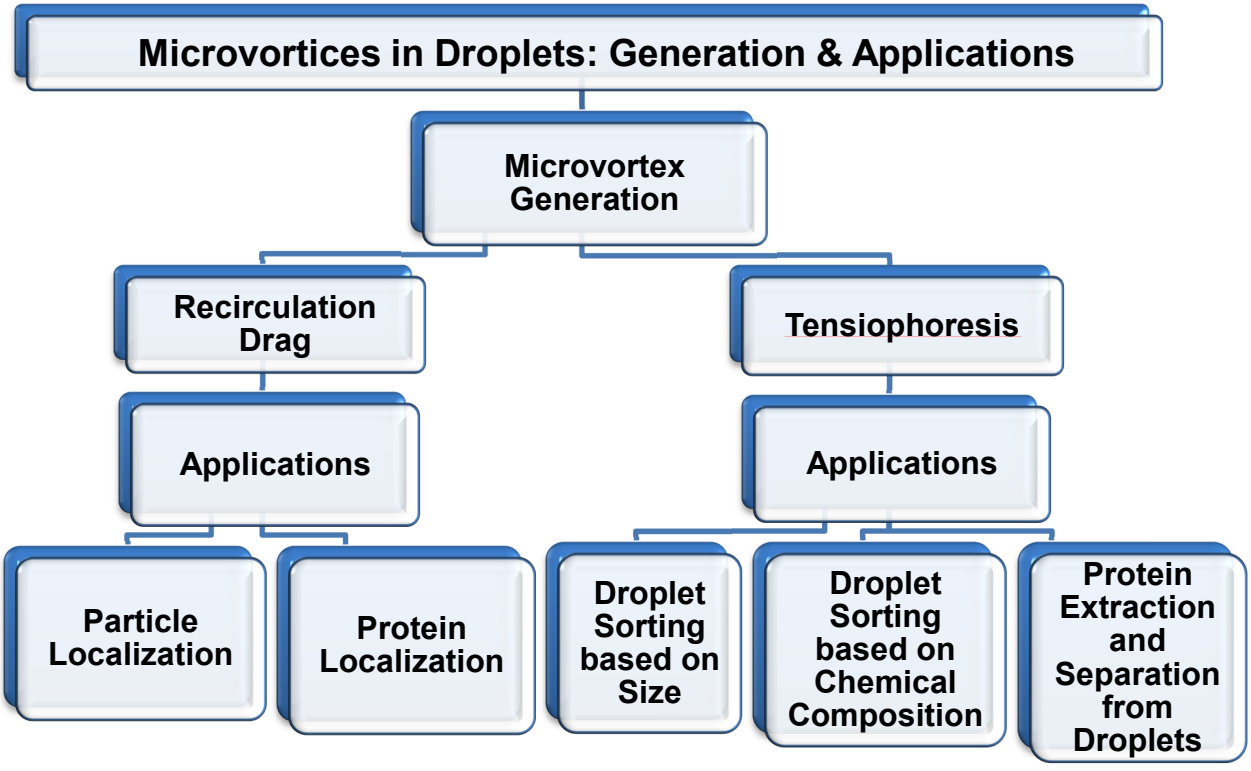

Chapter 2: Micro-Vortex Generation in Droplets

2.1 Micro-Vortex Generation Techniques

In fluid dynamics, vortex is defined as a spinning motion of a region of fluid within a bulk fluid about an imaginary axis [66]. Common examples of vortices found in nature are smoke rings, whirlpools, hurricanes, tornadoes, dust devils etc. Vortices are often formed in turbulent flow regimes (high Reynolds number) where inertial forces are several orders greater than viscous forces. In many macro-scale fluidic systems, such vortices are common, and efforts are often made to avoid them or to mitigate flow perturbations caused by unsteady vortices (for example, in commercial aircraft). At the microfluidic length scales, where low Reynolds number prevails, vortex flow rarely occurs unless they are generated within the laminar regime (recirculation flow inside a moving droplet is one example). Without vortices, mixing within microfluidic channels occurs only by diffusion; and therefore mixing occurs relatively slowly. In microfluidic devices, in order to perform certain applications including biological assays and chemical synthesis, it is important to have a deliberate and controlled agitation of the fluids [67]. Methods to generate vortices in microfluidics are discussed in this session.

2.1.1 Acoustic Streaming

Acoustic based technique utilizes surface acoustic waves (SAW) to induce vortices inside a single phase or droplet systems (figure 28). The microfluidic device is acoustically coupled to a piezoelectric substrate coated with of a set of interdigitated metal electrodes for SAW generation. The acoustic wave propagates through the base of the device, enters the fluid and generates the recirculating vortex flows [67]. Acoustic

waves propagate by adiabatic compression and decompression and the speed of the waves depends on the medium through which they propagate. The acoustic wave equation is

$$\frac{\partial^2 P}{\partial x^2} - \frac{1}{c^2}\frac{\partial^2 P}{\partial t^2} = 0$$

where P is acoustic radiation pressure, x is particle or fluid displacement, c is speed of sound and t is time. This acoustic radiation pressure is responsible for displacing the fluid element in axial and radial directions [68]. When the acoustic wave enters the fluid, the absorption of wave by the fluid generates a gradient in the radiation pressure. This pressure gradient displace the fluid elements at different speed resulting in vortices [69].

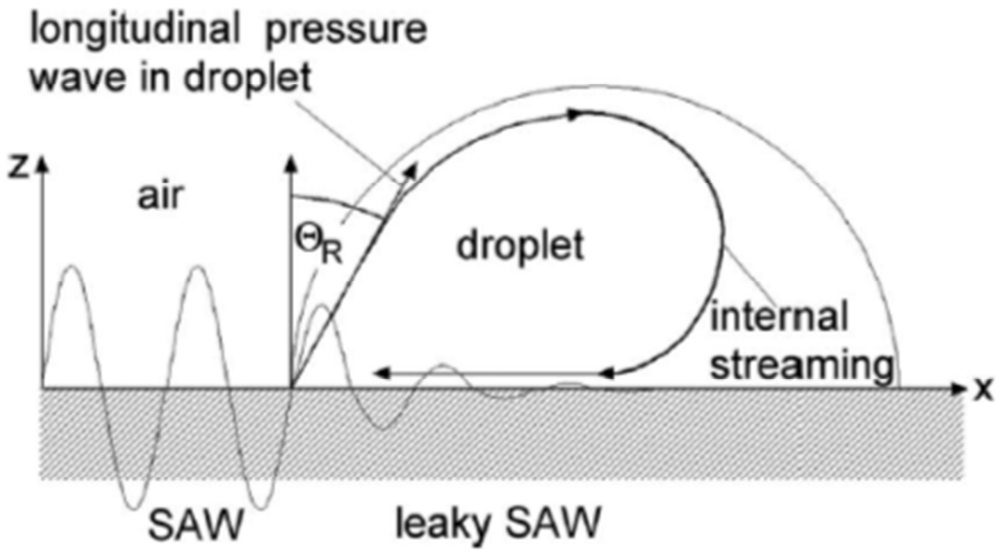

Figure 28: Sketch of the acoustic streaming acting on a small droplet on the surface of a piezoelectric substrate [67]

2.1.2 Channel Geometry

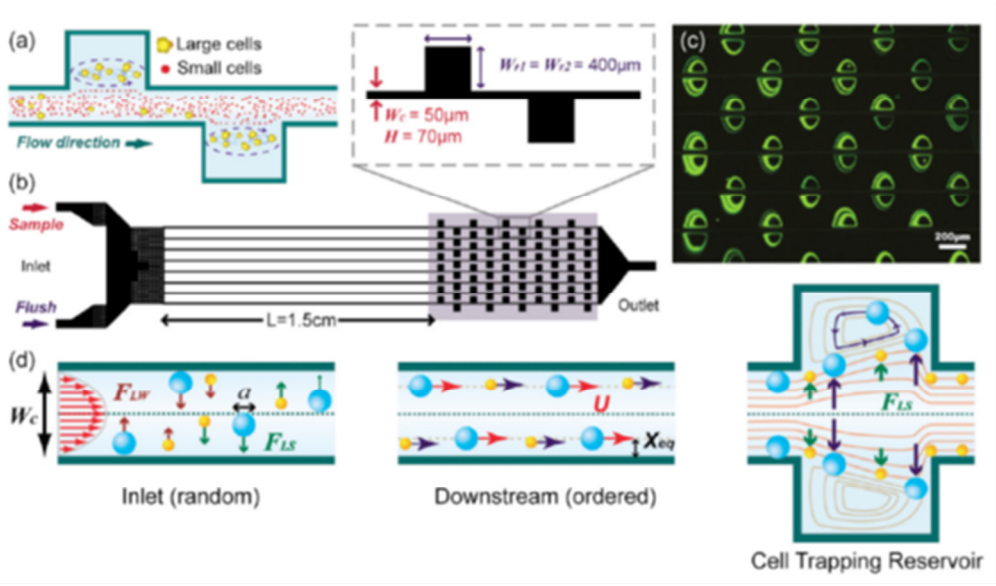

Figure 29: Schematic showing how the microvortices are formed in the expansion chamber. Larger cells are trapped in these vortices by inertial focusing [70]

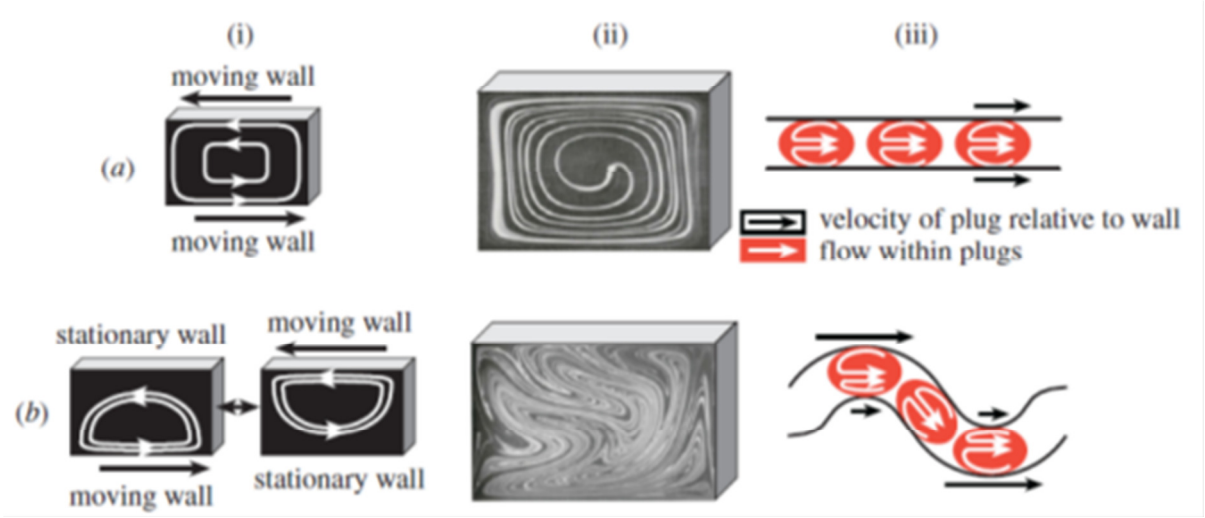

Figure 30: Comparison of mixing inside a straight channel and winding channel geometry. (a) Steady recirculation flow (b) chaotic mixing [44]

Microvortices can also be generated via interactions of the fluid with structures within the microchannel. An advantage of this passive approach is that it doesn't require external actuators or energy input. In single phase systems, the vortices are

generated by pushing the liquid at a high flow rate (Re ~1000) through a microfluidic channel containing a set of series and parallel expansion chambers [71]. The portion of fluid entering the expansion chamber continues to recirculate in the form of vortex [70]. It has been shown that these vortex flows can be used to focus large size particles (10 μm polystyrene beads) and cells (large size cancerous cells from small sized erythrocytes and leukocytes) by the technique called inertial focusing. At the expansion zone, the large particles/cells are subjected to larger lateral lift force which guides them to the vortex. Once trapped in the vortices, these cells continue to recirculate within the expansion chamber (figure 29).

In two-phase microfluidics, the recirculation vortices are naturally generated inside the droplet/plug/slug when it moves through the channel [72]. Recirculation vortex is caused due to the relative displacement of the droplet and the carrier fluid. Within the reference frame of the droplet, the recirculation flow is forward-oriented at the center and reverse-oriented at the periphery. These flows are exploited in many droplet based enzymatic screening applications where the contents of the droplet must be agitated and mixed properly to get better results. The recirculation vortex inside a droplet that moves through a straight channel is shown in figure 30a. In this case, both the recirculation flows within the droplets are isolated and both halves of the droplet will not mix each other. Ismagilov et al demonstrated chaotic mixing of the multiple reagents isolated in the droplets by designing a combination of straight and winding channel geometry [44]. More details will be provided in chapter 3.

2.1.3 Electrokinetic Vortex Flow

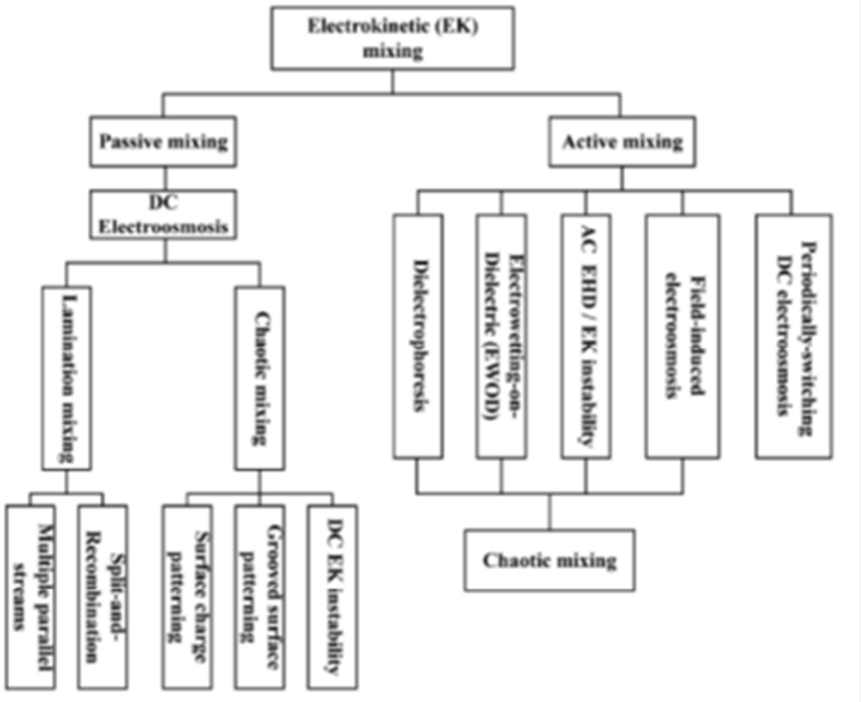

Figure 31: Classification scheme for microfluidic mixing based on electrokinetics [73]

Electrokinetic flow occurs when an electric field imparts a net electrostatic force in polarized surface regions in an electrolyte to induce flow both within and outside the charged region [74]. Electrokinetic mixing is a broad field which includes DC electroosmosis, DEP, EWOD, AC electrohydrodynamic (EHD), and field induced electroosmosis [73]. The details are shown in the figure 31. Electroosmotic flow is the movement of fluid due to the electric field applied across a porous material (eg. silicon, glass). The effect is caused due to the formation of electrical double layer formed at the solid liquid interface. In presence of electric field, a coulombic force will be exerted on the double layer resulting in fluid motion. Capillary electrophoresis works on the principle of electroosmotic flow. Dielectrophoresis (DEP) is the manipulation of dielectric particles or droplets in presence of a non-uniform electric field. The DEP force depends

on the dielectric properties of particle and medium, size of the particle, amplitude and frequency of the voltage applied. EWOD induce flow by modifying the wetting property of the surface with electric field. A recent electrokinetic mixing device proposed by Kim et al [75] is shown in figure 32. It has a U-shaped microchannel and nanochannels across it. When voltage is applied, high electric field intensity is induced near and around the nano channels. This is because the resistance of the nano channel is high compared to the microchannel. This high electric field near the nano channel induces joule heating that change the electrical property (conductivity and permittivity) of the fluid resulting in a body force which induces the flow. As a result, strong vortex is formed at the inlet of the nanochannels which ensure greater mixing of the solutions inside the microchannel.

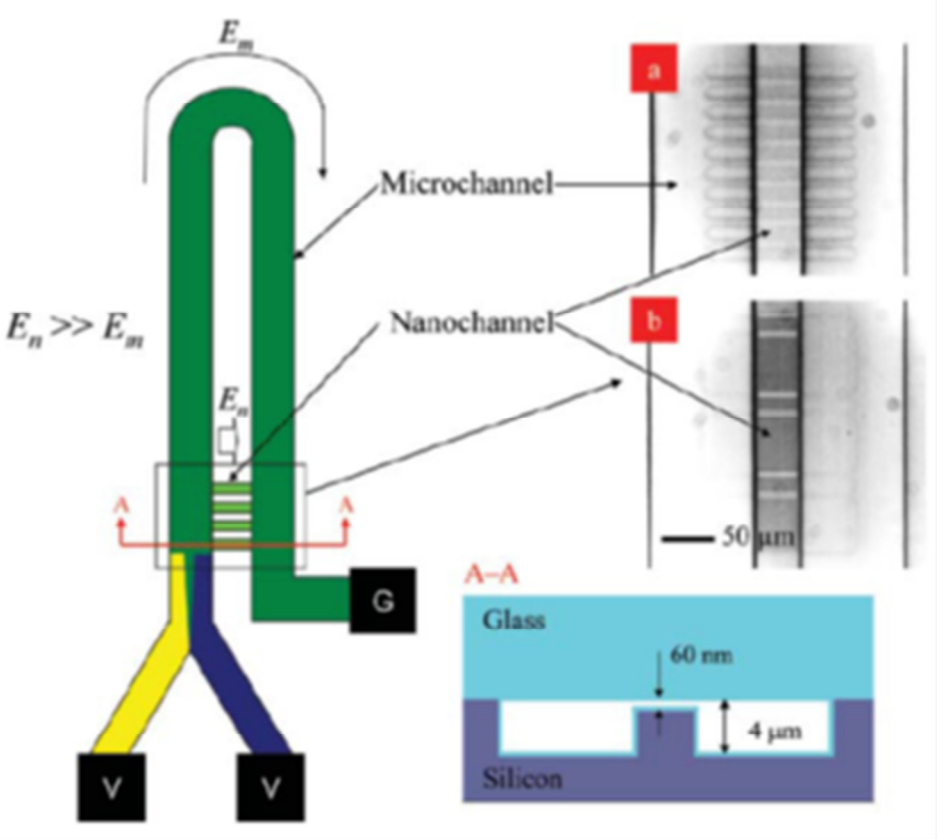

Figure 32: Schematic of an electrokinetic fluidic mixer [75]

2.1.4 Optical methods

2.1.4.1 Optoelectrically generated microvortices

Simultaneous laser irradiation along with the application of uniform or non-uniform electric field can generate strong microvortices which can be utilized for microfluidic mixing [76]. Focused laser beam heats the liquid locally causing a gradient in electrical permittivity and conductivity [77]. When an electric field acts on this gradient, it induces a body force on the fluid (Figure 33). This body force is responsible for the generation of microvortices. Since the body force is a function of temperature gradient, sharp illumination with a highly focused laser beam induces strong, localized microvortices. Wereley et al has demonstrated the optoelectric generation of microvortices by focusing a near-infrared laser beam (1064 nm) in presence of AC electric field [76].

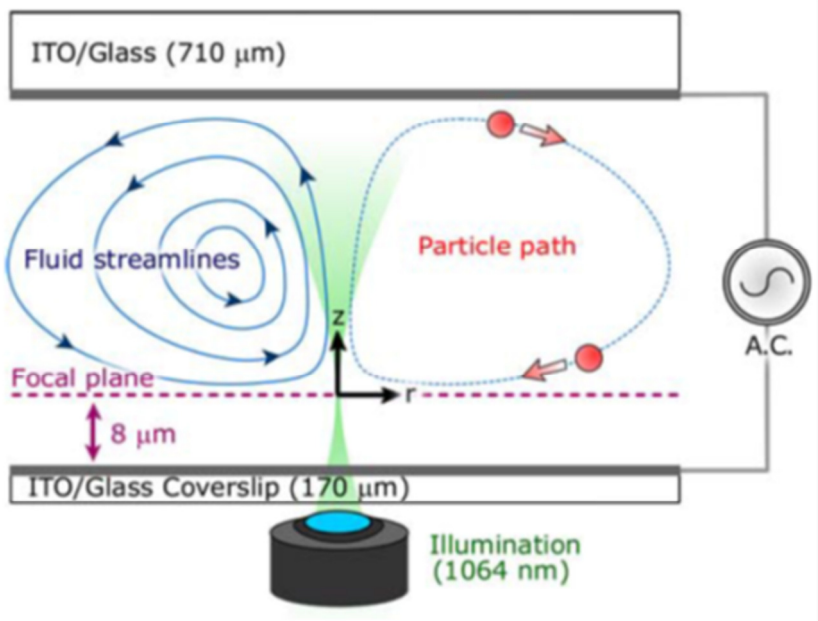

Figure 33: Schematic of the microvortices generated by optoelectic method [76]

2.1.4.2 Optical Tweezers (OT)

Optical tweezers can manipulate particles utilizing the electromagnetic field gradient force generated by laser beam [78]. It can generate forces in the order of pN and can manipulate particles 25nm- 10μm range. Chiu et al have demonstrated a modified optical tweezer technique to generate vortex traps to manipulate the droplets [25]. A Laguerre-Gaussian (LG) laser beam focused on the carrier phase creates a zero intensity propagating dark core in the middle of the beam. The ring of the laser intensity that surrounds the dark core acts as a cage to trap the droplets. They successfully demonstrated the vortex trapping and translation of water droplets in oil.

2.1.4.3 Optoelectronic Tweezers (OET)

OET can perform parallel manipulation of single particles by dielectrophoretic force [79], [80]. The particles or cells are sandwiched between upper transparent Indium tin oxide (ITO) coated glass and lower opaque photoconductive material with a bias voltage (10Vpp) applied across the two surfaces [79]. When light is projected on the photoconductive material, virtual electrodes are created which generates non-uniform electric field required for DEP actuation. This technique can generate forces in the range of nN, but the opaque photoconductive material makes it difficult for microscope visualization.

2.1.4.4 Optoelectrowetting (OEW)

OEW, also known as optical electrowetting on dielectric (EWOD) is also used to manipulate droplets [81]. OEW can generate stronger force than OET. OEW also works by the principle of generating virtual electrodes on photoconductive material by light actuation. Unlike OET, the electrodes in OEW are coated with a dielectric material, usually Teflon. The droplet wetting the surface poses serious issues on device contamination. For more details on optical manipulation of droplets, see this review article [82]. Comparison of optical methods in terms of force is shown in figure 34.

2.1.4.5 Thermocapillary

Kotz et al have shown that the water droplets in oil can be manipulated utilizing Marangoni microvortices generated as a result of temperature gradient induced by the laser beam heating the continuous phase [83]. The study has shown that the droplets can be repelled away from the laser spot at a speed of several mm/s due to the surface flows created as a result of spatial variation in surface tension. Thermocapillary methods can generate forces in the range of μN's.

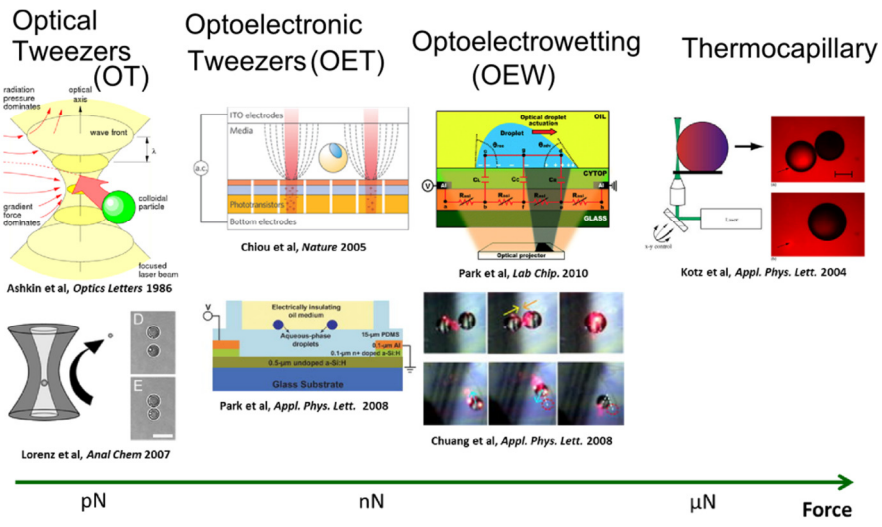

Figure 34: Comparison of existing optical manipulation techniques

2.1.5 Thermal

Marangoni microvortices can also be generated by imposing a temperature gradient and that can be done by suspending miniaturized heat sources on the liquid surface (figure 35). Basu et al have shown that by using a heat source of different geometries (point, linear, ring, and tapered heat sources); it is possible to engineer the Marangoni flows to perform droplet and particle manipulation [84]. The point source generates toroidal flows which are used to manipulate particles and droplets (translation, mixing, merging). Linear sources mimic virtual channel and filters; ring source helps to trap a droplet of interest and the tapered heat source mimic a pump.

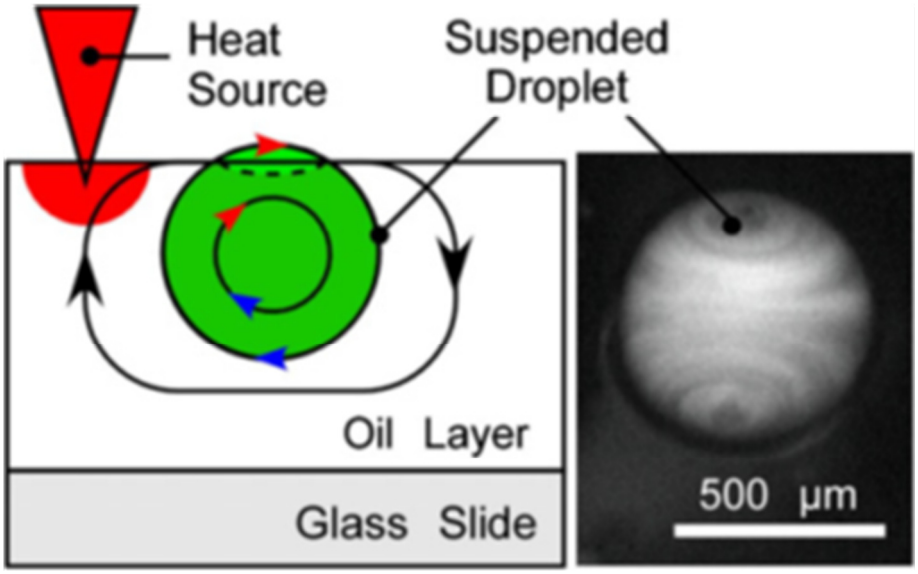

Figure 35: Microvortices in droplet generated by a heat source (Basu et al, JMM, 2008)

2.2 Our techniques to generate micro-vortices in droplets

In addition to all these well-known techniques, this thesis describes two distinct ways to generate microvortices in droplets and extend these techniques to perform

various applications in droplet microfluidics including particle segregation, droplet sorting based on size and chemical composition, and protein localization and extraction.

2.2.1 Recirculation Drag

When a droplet/plug moves through the channel, recirculation vortices occur inside the droplets due to the relative displacement of the droplet w.r.t the continuous phase/channel wall (figure 36, 37). We engineered these vortex flows to successfully segregate and extract the hydrophilic high density silica beads. We also have demonstrated a deterministic protein extraction from droplets by the combination of recirculation drag and tensiophoresis. Hydrodynamic recirculation flows and its applications [72] are discussed in chapter 3.

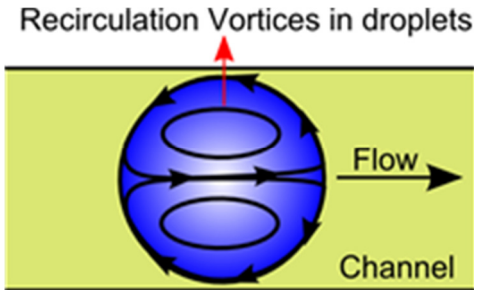

Figure 36: Recirculation vortices in droplet

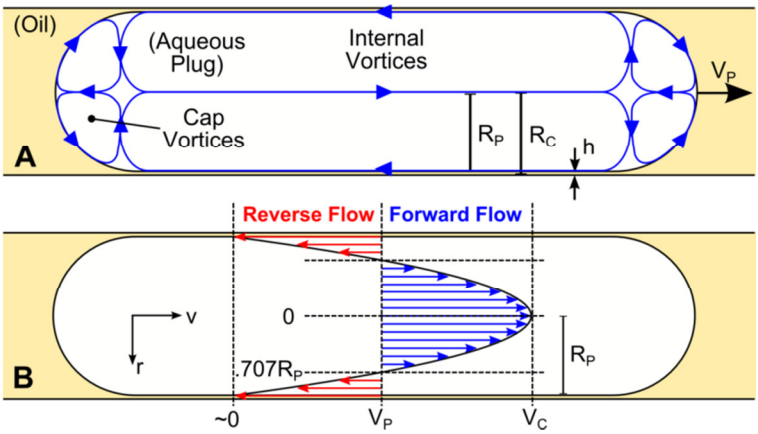

Figure 37: Recirculation vortices in plugs

2.2.2 Surfactant micro-gradient (Tensiophoresis)

When a droplet is subjected to a surfactant gradient as shown in the figure 38, it migrates toward the region having higher surfactant concentration. We define this phenomenon as Tensiophoresis. The migration is due to the formation of Marangoni vortices which directs from the low interfacial tension (high surfactant stream) to the high IFT (no surfactant) stream. Tensiophoresis and its applications are explained in detail in chapter 4.

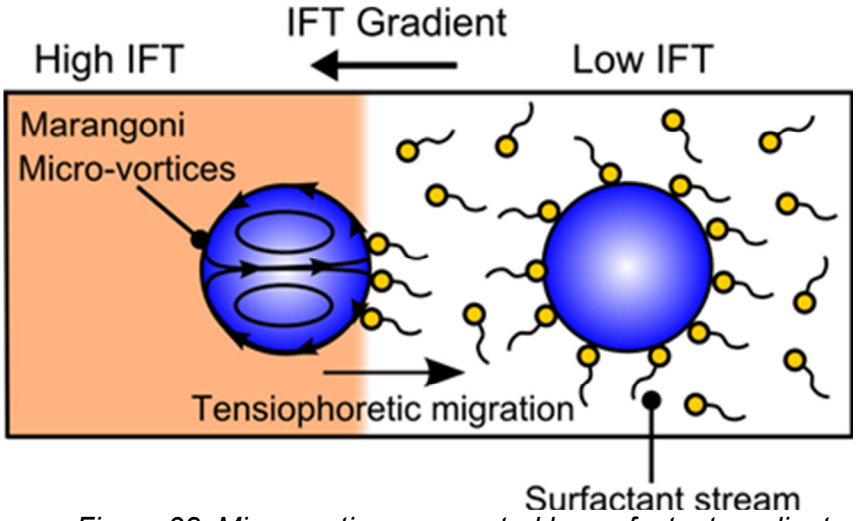

Figure 38: Micro-vortices generated by surfactant gradient

Chapter 3: Hydrodynamic Recirculation Vortices in the Droplets/Plugs

3.1 Introduction

The plug based microfluidics also referred to as microreactors or microdroplets is potentially emerged as a system platform for performing high-throughput biomedical applications, explicitly in the field of biotechnology where samples are encapsulated in aqueous plugs or droplets in an immiscible carrier fluid. The plug is separated from the channel walls by a thin film of carrier fluid which forms if the surface tension between the plug and wall is greater than that of the carrier fluid and the wall [4]. In droplet based microreactors, recirculating flow occurs naturally inside the plugs caused by the relative displacement of plug and carrier fluid [85]. This recirculating flow pattern inside the plug is influenced by a several factors including flow velocity, plug length, channel size and viscosity ratio between the plug and carrier fluid [86], [87]. The recirculating flow can be utilized for effective mixing of reagents in different channel geometries [5], [88]and also for enhanced mass transfer [89]. The majority of prior experimental studies reported two recirculating vortices inside the plug [8]. In contrast to their findings, here we present simulation and experimental results which reveal multiple (4 or more) co-rotating vortices located at the front and rear of the plug. We refer to these as Laplace vortices because they are caused by the deformation of the plug by Laplace pressures [90]. This chapter discusses the theoretical framework of the recirculation flows inside a plug and also demonstrates how this recirculation phenomenon is applied to segregate the hydrophilic silica beads and protein molecules at the rear end of the plug.

3.2 Theory of Multiphase Plug Flow

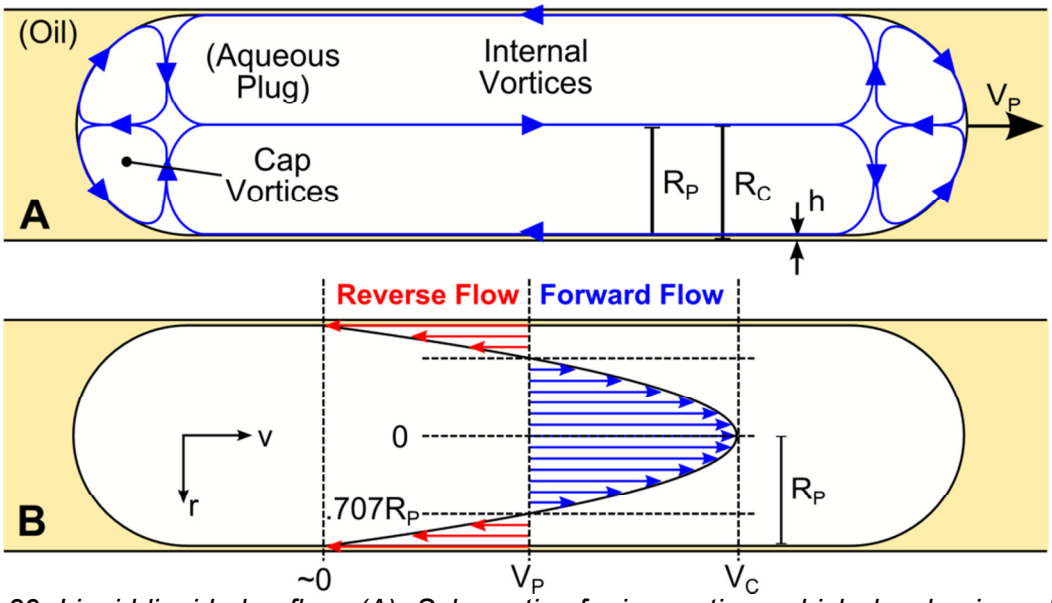

Figure 39: Liquid-liquid plug flow. (A) Schematic of microvortices which develop in a plug as it moves through the channel at a velocity VP. The plug radius is RP, the channel radius is RC, and the wetting film has a thickness h. (B) Analytical model illustrating forward and reverse flow in the reference frame of the plug. The flow can be approximated as a classic Poiseuille

Aqueous plugs of uniform length can be generated by combining aqueous sample and an immiscible carrier fluid (typically a hydrocarbon or fluorocarbon oil) in a tee or cross junction [91], [92]. In a laminar flow environment, the plug breakoff process occurs in a repeatable manner, resulting in monodisperse plugs. Each plug is separated from the channel walls by a thin film of carrier fluid (ie a wetting film) which spontaneously forms if the surface tension between the plug and wall is greater than that of the carrier fluid and the wall [88], [93]. The thickness of the wetting film *h* scales according to Brethertons' law, $h \propto R_C Ca^{2/3}$, where R_C is the capillary radius [94]. The capillary number *Ca* is given by $\mu_C V_P/\gamma$, where μ_C is the viscosity of the carrier fluid, V_P is the plug velocity, and γ is the interfacial tension. Although Brethertons' law was derived specifically for gas–liquid flow, the same scaling holds true in liquid-liquid plug

flows when the viscosity of the carrier exceeds the viscosity of the plug and *Ca*<.01 [95]. This is generally the case in droplet microfluidics, and has been experimentally verified in prior experimental results from Ghaini and Agar [96] and our group [97]. At low *Ca*, the thickness of the wetting film is generally 1-5% of the channel radius [95], and the velocity at the plug's exterior surface is close to zero.

Microvortices in Liquid-Liquid Plug Flow. In Taylor's classic model of gas-liquid plug flow in a cylindrical channel, shear forces exerted by the wetting film generate axisymmetric vortices within the plug [98]. The same holds true for liquid-liquid plugs [95], [99]–[101]. Within the reference frame of the plug, the internal vortices are oriented backward near the plug's outer surface, and forward along its interior axis (Figure 39 A). If the viscosity ratio of plug and carrier fluid μ_P/μ_C is << 1, there are additional co-rotating vortices at the front and rear cap of the plug [101]. Computational fluid dynamics simulations of the caps have been shown in our prior publication [97]. Both the internal and cap vortices are responsible for the concentration phenomena to be discussed later.

A first order analytical model we reported previously [97] is useful for understanding the parabolic flow profile which occurs in the internal vortices (Figure 39 B). It should be noted that multiphase flow is influenced by a wealth of factors, including the capillary number, channel radius, cross sectional geometry, and the viscosity ratio between the plug and carrier fluid [95], [102]–[104]. However, if *Ca* << 1 and $\mu_P/\mu_C \leq 1$, which is often the case in droplet microfluidics, the internal vortices follow a simple model where the circulation velocity V_C scales proportionally with the plug velocity V_P [101]. At small *Ca*, the wetting film is <5% of the channel radius, and we can

reasonably assume the axial velocity at the plug's exterior surface is negligible [101]. Under this boundary condition, the flow follows the classic Poiseuille profile in a cylindrical pipe (Figure 39 B). The parabolic, axisymmetric flow profile is given by $v(r) = (V_C/R_P^2)(R_P^2 - r^2)$, where *r* is the radius, $V_C = 1/(4\mu_P)(dP/dx)R_P^2$ is the circulation velocity, dP/dx is the axial pressure gradient, and R_P and μ_P are the radius and viscosity of the plug (respectively). The circulation velocity V_C is the difference between the forward and reverse flows, which is important to this work because it defines the strength of the microvortices. The plug velocity V_P can be found by taking the average flow velocity along a cross section, and is found to be $V_P = V_C/2$. Therefore, within the reference frame of the plug, the direction of flow transitions from forward to reverse when $v = V_P = V_C/2$, which occurs at a radius $r = (\sqrt{2}/2)R_P$. The maximum shear stress at the plug surface ($r = R_P$), used later for calculating the shear velocity, is given by $\tau = 2\mu_P V_C/R_P$.

3.3 Applications

3.3.1 Particle Segregation in a Microfluidic Plug

Particle concentration is a key operation in biochemical assays. In traditional single-phase microfluidic devices, high-throughput continuous particle separation can be achieved using several techniques which typically focus particles within selected streamlines in a channel (see topical reviews [105], [106]). Active focusing techniques exploit the interaction of particles with external electric, magnetic, and acoustic fields. Passive techniques generally rely on the interaction of particles with laminar flows in microfluidic structures; these include pinched flow fractionation, lateral displacement,

and hydrophoretic separation. Inertial microfluidic techniques utilize particle migration and secondary flows to focus and separate particles with high throughput [107], [108]. Gravity-driven particle concentration has also been demonstrated using a hydrodynamic amplification principle to improve separation fidelity [109].

By comparison, the emerging field of multiphase microfluidics has relatively few particle concentration techniques available. In general, the existing approaches utilize active electric or magnetic fields. Using local electric fields, Cho and Kim segregated charged particles in a droplet with 83% efficiency in an electrowetting platform [110]. Valley and Wu demonstrated a similar approach using an optoelectrowetting platform [111]. Magnetic fields can be used to localize paramagnetic beads in a droplet, and when functionalized, the beads can capture biomolecules in the droplet. This approach was used to purify proteins [112], DNA [113], and virus particles [114]. All of these techniques are promising; however, the requirement of external field generators can add additional complexity to the microfluidic system, which may be undesirable.

Theory

Particle Concentration: The sedimentation velocity of a spherical particle with radius *a* can be found by equating the gravitational force $F_G = (4/3)\pi a^3 \Delta\rho g$ with the Stokes drag force $F_D = 6\pi\mu_P a v$. Here, $\Delta\rho$ is the difference in density between the particle and fluid, g is the gravitational constant, μ_P is the plug viscosity, and v is the velocity of the fluid relative to the particle. The sedimentation velocity is

$$V_S = \frac{2}{9}\frac{a^2(\Delta\rho)g}{\mu_P} \qquad (1)$$

For example 1 μm polystyrene particle ($\rho = 1.03 g/cm^3$) in water sediments at 16 nm/s. By contrast, a 38 μm glass bead ($\rho = 2.52 g/cm^3$) sediments at ~1.19 mm/s, nearly 100,000X larger. In the latter case, particle sedimentation is a useful mechanism which can be exploited for particle concentration. As a rule of thumb, particles will sediment if the sedimentation velocity exceeds the fluid velocity.

Particle Concentration Model:. Under appropriate flow conditions, the interaction of particle sedimentation with the circulating microvortices can concentrate particles in the rear of the plug. Their combined effect results in two distinct particle concentration phenomena (Figure 40): 1) the localization of particles in a circulation zone (circulation effect), and 2) the aggregation of particles near the rear cap (aggregation effect). Scaling of both phenomena can be suitably described by the Shields parameter θ, a dimensionless number which describes the ratio of the drag force exerted by the fluid on a particle to the particle's weight [115]. There are two forms useful for our analysis:

$$\theta = \frac{Particle\ Drag}{Particle\ Weight} = \frac{\tau}{a\Delta\rho g} = 9\frac{\mu_P}{a^2\Delta\rho g}V_P \qquad (2)$$

Here, τ is the shear stress exerted by the liquid on the particle, and the other parameters are as described earlier. The first form, commonly used in sedimentation engineering, is useful for determining the minimum shear force needed to resuspend a bed of sedimented particles [116]. When θ exceeds the movement threshold, the particles are suspended in the moving fluid, and in the opposite case, the particles sediment. If a particle is spherical, we can recast the Shields parameter into a 2nd form, which is simply the ratio of Stokes drag to weight. This is found by taking F_D/F_G as described earlier, and recalling that $V_P = V_C/2$. The 2nd form is equivalent to the ratio of

circulation velocity to sedimentation velocity V_C / V_s, which is useful for calculating the trajectory of particles in circulating flows. In our analysis, we will use the 2nd form because it conveniently depends on the plug velocity and the particle properties.

Circulation Effect. We first consider the circulation effect in three different flow regimes, governed by the Shields parameter (Figure 40, column 2). When θ is less than the movement threshold θ_M, the particle's gravitational force exceeds the drag force exerted by the fluid. In order for particle circulation to occur, particles at the rear of the plug must be lifted vertically to the interior streamline by drag forces. When the lift force is insufficient, particles remain in a sediment bed at the rear of the plug, similar to conventional sedimentation theory [116], [117]. The tensile interface between the aqueous plug and oil phase keep the particles within the plug. As more particles are added to the sediment bed, the velocity profile in this region vanishes, which in turn draws in additional particles. As a consequence of the positive feedback, all particles in the plug ultimately collect in the rear of the droplet, thus providing virtually 100% collection efficiency. In region II, when $\theta \sim \theta_M$, gravitational and drag forces are comparable. Here, particles circulate within a well-defined zone which begins at the rear of the plug. To understand why this occurs, we consider a particle at the rear of the plug which is entering the interior, forward-directed streamline. Ignoring relaxation time for simplicity, we assume that the particle travels with a horizontal velocity V_C. Simultaneously, it also experiences a sedimentation velocity V_S, directed to the bottom of the channel. Combining both velocity components, the particle follows a trajectory which ultimately brings it to the lower region of the plug, where the reverse-oriented flow then returns it to the rear of the plug. This process repeats for all particles, forming a

circulation zone where particles are confined. The length of the circulation zone, denoted L_C, can be found using the Poiseuille model shown in Figure 39 B. The time required for a particle to reverse direction is $V_S/(.707R_P)$, where V_S is the sedimentation velocity and R_P is the plug radius. During this time, the particle travels a horizontal length L_C, which can be found by integrating the velocity profile over this time period. Scaling L_C by R_P gives the aspect ratio of the circulation zone, and the non-dimensional form can be expressed as a function of the plug velocity or the Shields parameter.

$$\frac{L_C}{R_P} = \frac{5\sqrt{2}}{24}\frac{V_P}{V_S} = \frac{5\sqrt{2}}{48}\theta \qquad (3)$$

When $\theta \gg \theta_M$ (Region III), drag forces greatly exceed the particle's weight, and sedimention is negligible. In this regime, particles circulate uniformly throughout the plug, and no concentration occurs. We note, however, that after an asymptotically long period of time, particles subject to any gravitational force will eventually migrate to the lower vortex and remain there. The time required for this to occur is simply the particle's sedimentation velocity divided by the plug radius.

Aggregation Effect:. The aggregation effect (Figure 40, column 3) refers to the collection of particles in the rear cap. This effect is believed to be due to the interplay between the cap vortices (Figure 39) and the internal vortices at the rear of the plug. Particles at the rear of the plug which enter the cap will remain there because it is an independent, co-rotating vortex. As additional particles collect in the cap, the effective viscosity will increase, forming a stagnant region which, in turn, will collect additional particles. In dilute suspensions, the effective viscosity scales according to Einstein's relationship, $\mu_P = \mu_{P0}(1 + k_e\phi)$, where μ_{P0} is the initial plug viscosity, k_e is a constant

~2.5, and ϕ is the volume fraction of particles [118], [119]. At higher concentrations, other models (such as Mooney's equation) must be used, and the linear scaling described by Einstein's relationship generally does not hold [119]. As particles pack into a sufficiently high volume fraction, the viscosity can become very large, leading to a positive feedback effect where a nucleated particle bed can quickly grow by stagnating the local fluid. In addition to the viscosity effects, particle aggregation can also occur by colloidal interactions such as electrostatic double layers, Van der Waals interactions, hydration effects, and steric interactions [120]. In our experiments, which typically use particles with diameters of 30-40 μm, such colloidal effects typically are not observed. However, if the concentration technique were to be scaled down, such effects would need to be considered. This would require a more complex model because many such interactions depend heavily on the physicochemical properties of the fluid and the particle surface. Like the circulation zone, the aggregation effect also scales with the Shields parameter. Gravitational forces cause the particle to segregate to the lower half of the cap, while fluidic drag induced by the internal vortices (F_{D1} and F_{D2}) seek to maintain a symmetric aggregation in the cap. Thus, when θ is small, the particles gather toward the lower half of the cap, and when θ is large, particles tend to distribute symmetrically within the cap.

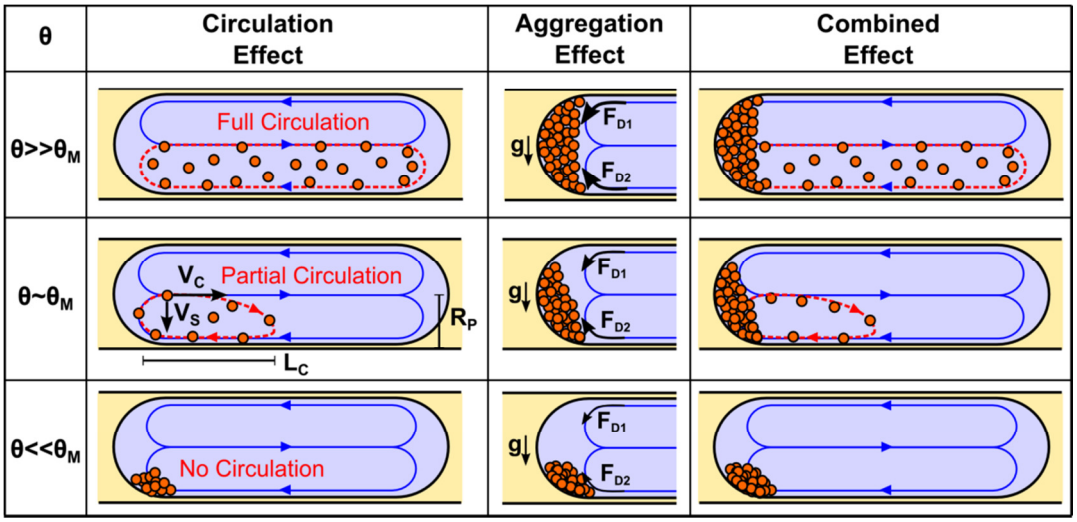

Figure 40: Schematic of the 3 flow regimes, described by the dimensionless Shields parameter θ (column 1). In each regime, the circulation effect and the aggregation effect are illustrated in columns 2 and 3, respectively. The combined behavior is shown in column 4. Note: all the schematics show a side (cross sectional) view of the plug.

Experimental Set up

The experimental setup is shown in Figure 41. Plugs are generated by combining an aqueous bead suspension with oleic acid ($\mu_C = .027\ Pa \cdot s$) in a 500 μM bore PEEK T-junction (IDEX Health and Science). Microcapillary Teflon tubing with 500 μm ID (IDEX) are used as the microchannel as well as the syringe interconnect. The bead suspension consists of deionized water containing soda-lime glass beads with mean diameter 38 μm and a D50 distribution ranging from 34-42 μm (Cospheric). Each syringe is controlled by an independent syringe pump to maintain relative flow rates. The syringe containing the beads is periodically agitated to maintain suspended particles. The flow rates for oil and water range from 0.6-10 μL/s, which generates plug velocities between 1-50 mm/s. This corresponds to Reynolds number <25, well within the laminar regime. To image the particle concentration profiles, we use a standard

inverted microscope with a 4X objective. The objective is placed several cm downstream the drop generator to allow sufficient time for particle profiles to form. Equilibration typically occurs in the time it takes for the plug to travel several plug lengths, typically <1 second. Digital videos are recorded with a high speed camera (Casio EX-F1) at 1200 frames per second (FPS) with 336x96 pixel resolution, at 600 FPS with 432x192 resolution, and 30 FPS with 1280x720 resolution. To obtain grayscale intensities vs. time, an image analysis program implemented in Matlab extracts grayscale pixel values on a pixel on the channel centerline.

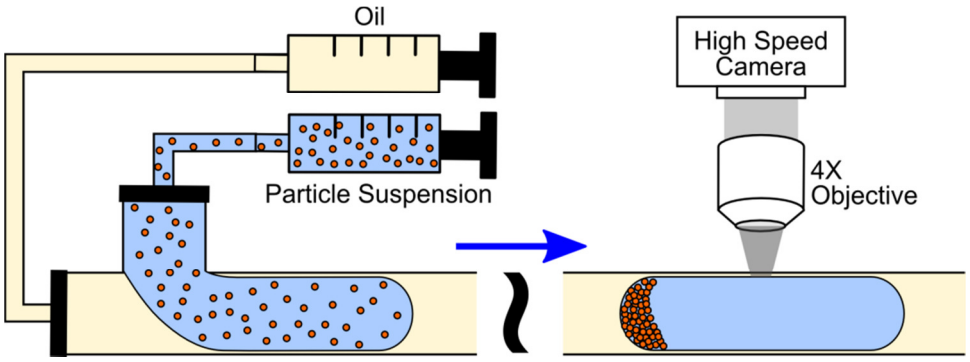

Figure 41: Experimental set up

Results and Discussion

Effect of Particle Size: To illustrate the importance of particle size, figure 42 compares concentration profiles of beads with a small and large settling velocity V_S when both are subject to identical plug velocity of 3 mm/s. In the case of the 1 μm polystyrene particle ($\rho = 1.03 g/cm^3$), the Shields parameter is $\theta \sim 3.7x10^5$. As expected with large θ, the particles are uniformly distributed throughout the plug. In contrast, with 38 μm glass beads ($\rho = 2.52 g/cm^3$), $\theta \sim 5$. In this case, the particles do not circulate and sediment

near the rear of the plug. Under each of the images is a line plot which gives the grayscale intensity along the length of the plug. The graphs are inverted, and they are provided as a means to compare the length of the circulation zone (L_C) with the total length of the plug (L_P). The two peaks at the front and rear of each graph represent the shadow at the front and rear each plug. The ratio of L_C/L_P indicates the enrichment factor.

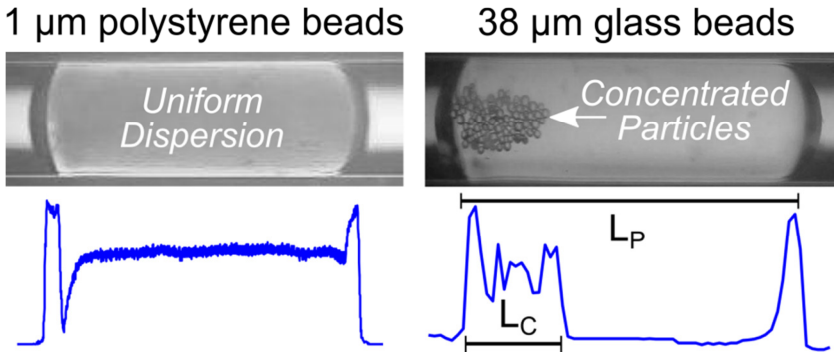

Figure 42: : Top view comparison of experimental concentration profiles with small, light particles versus large, heavy particles at an identical flow rate of 3 mm/s in a 500 µm diameter circular channel. Both experiments use a high particle loading of >10^5/mL.

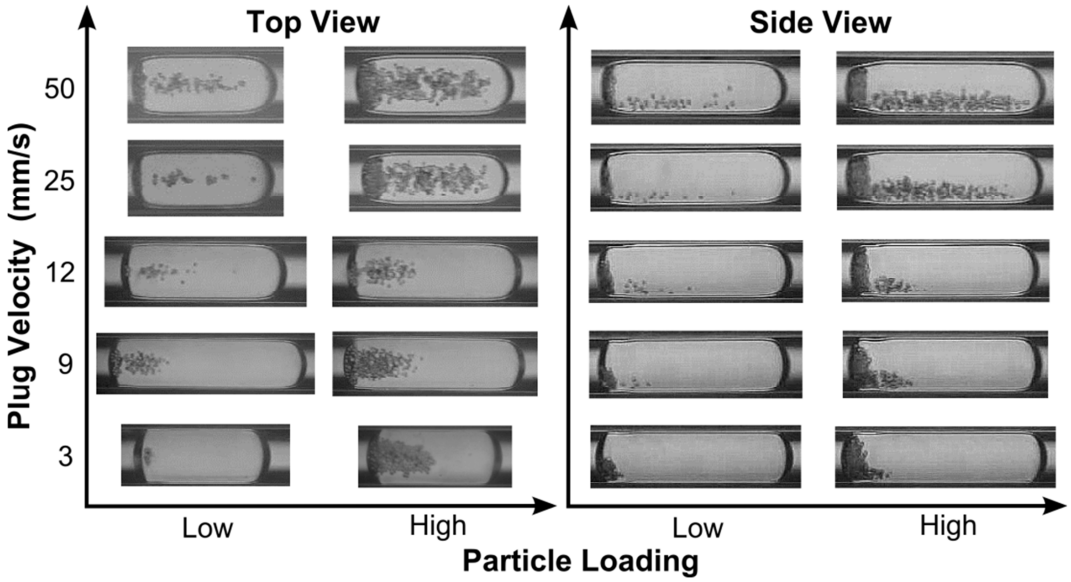

Figure 43: (enhanced): Particle concentration profiles as a function of flow velocity and particle loading (38 µm glass beads). Images shown are high speed video (1200 fps) taken in a circular, 500 µm capillary tubing at the indicated flow velocity.Both the top view and side are shown. High concentration is defined as >10^5/mL, and low concentration is defined as <10^4/mL.

Effect of Flow Velocity: Figure 43 (enhanced) compares the effect of flow velocity on particle circulation patterns. All experiments are conducted with 38 μm glass beads at high or low concentration (experimental parameters given in the caption). Both the top view and side view are shown to fully illustrate the particle behavior in each flow regime. The non-dimensionalized experimental data is shown in figure 44, where 3 distinct regimes can clearly be identified. In region I, which occurs at low plug velocity (3 mm/s), the Shields parameter θ is sufficiently small such that the particles are not suspended by the flow. Instead, they sediment in a single bed at the rear of the plug as a result of the lack of circulation as well as the aggregation effect. This flow regime is most suitable for high efficiency particle concentration, since virtually all particles collect near the rear cap (see Supplementary Multimedia). Region II begins when θ exceeds the movement threshold, which is experimentally found to be at $\theta \sim 10$, or a flow velocity of ~6 mm/s. This can be compared to previous sedimentation data described by Miller [116]. According to Miller's modified Shield diagram, a 38 μm particle would require a minimum shear velocity of 8 mm/s. Taking the shear rate at the plug surface, this correlates to a minimum plug velocity of about the same, 8 mm/s. Thus, the movement threshold obtained in our experiments is consistent with basic sedimentation theory. In region II, the particles are suspended, and they circulate in a well-defined zone which begins at the rear of the plug. The length of the circulation zone (L_C) scales scales linearly with flow velocity, increasing from 0.4 to 1.4 mm over plug velocities ranging from 9 to 25 mm/s ($\theta \sim 15 - 42$). The measured L_C values match the theoretical values calculated using equation (3). In region III, which occurs at flow velocities greater than 25mm/s, the predicted L_C is >1.5 mm, which is longer than the plugs generated in the

experiment. As a result, the circulation zone is constrained by the plug length, and particles circulate through the entire length of the plug. The concentration profile is therefore independent of flow rate.

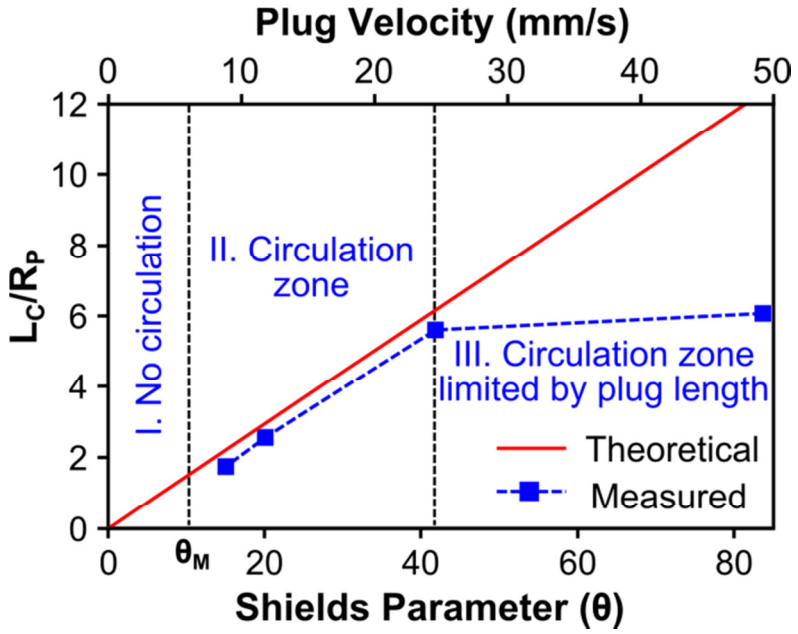

Figure 44: Variation in the length of the circulation zone as a function of plug velocity. The data is given in non-dimensional form by scaling LC by the plug radius (which gives the aspect ratio of the circulation zone), and expressing plug velocity in terms of the Shields parameter. The dotted lines demarcate the 3 flow regimes. The data is taken with experimental conditions identical to figure 43.

Parabolic Particle Profiles in Circulation Zones: When viewed from above, the circulation zones appear to have a roughly parabolic boundary (Figure 45, enhanced). This highlights the point that particles may travel streamlines other than the center axis. Particles which occupy streamlines away from the axis will have a slower axial velocity, and therefore will sweep a smaller circulation length before being swept to the rear of the droplet. Conversely, particles close to the axial streamline will attain faster velocities and sweep a longer trajectory before returning. The parabolic shape reflects

the radial Poiseuille flow profile described earlier. The parabolic circulation zones are especially apparent in long plugs at large flow velocities. Figure 46 B and C (enhanced) show the top view of plugs containing ~38 µm glass beads, traveling at 10 mm/s and 30 mm/s, respectively.

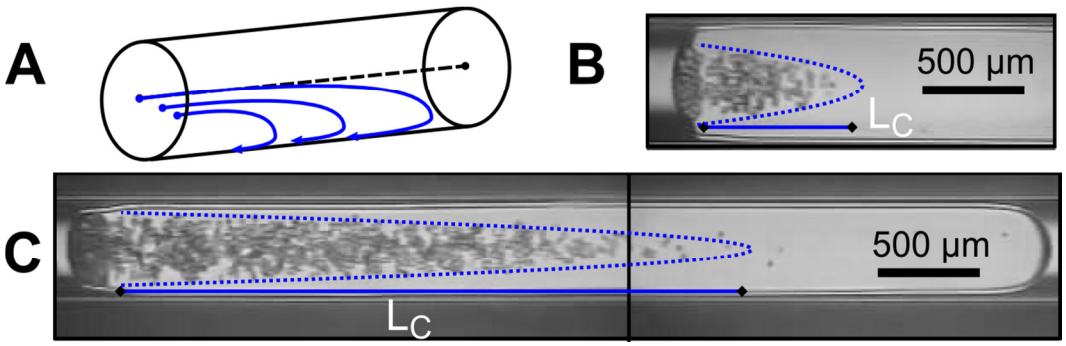

Figure 45: (enhanced): (A) Schematic of multiple possible trajectories for circulating particles. B,C) Parabolic particle distribution in at 10 and 30 mm/s flow velocity, respectively (Top view).

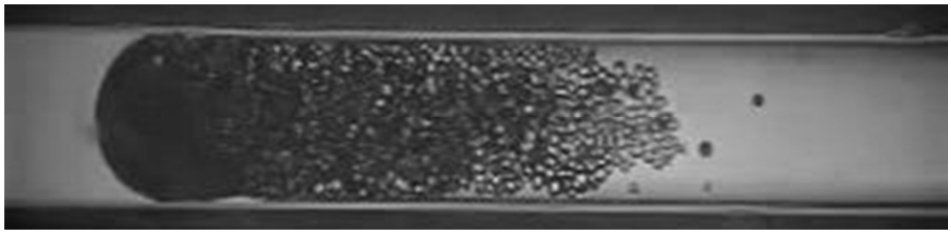

Figure 46: Very high particle loading (>107/mL) causes the aggregate in the rear cap to extend into the plug, extending the length of the stagnation zone. The channel diameter is 500 µm. (Top view)

Effect of Particle Loading: Figure 43 (enhanced) also shows the effect of particle loading on concentration profiles. In these experiments, a high concentration is defined as $>10^5$/mL, and a low concentration is defined as $<10^4$/mL. High particle loading favors the formation of the aggregation zone in the rear cap, regardless of flow velocity. As described earlier, high particle loading contributes to a positive feedback effect, where the deposition of particles reduces the local flow velocity, which in turn leads to further aggregation. This is particularly apparent in the side view images at high concentration,

where the aggregate fills the cap. At low flow velocity (3mm/s, $\theta = 5$), the distribution is biased toward the lower half because gravitational forces dominate. As the flow velocity increases, the balanced drag of the symmetric internal vortices becomes significant, the particles become evenly distributed. At low flow velocity, the cap is hemispherical, whereas at larger flow velocity (ie larger capillary number), the interface adopts bullet shape similar to what is observed in gas-liquid plug flow at high *Ca* [121]. Future research is needed to understand how aggregation in the cap affects its shape. At very large particle concentration (>10^7/mL), the aggregate can extend well beyond the cap region (Figure 46). Since the flow stagnates wherever the aggregate exists, these particles are essentially dragged by the motion of the plug. The particles are held within the plug due to the tensile interface between the two phases. We have found this to be the case even when the interfacial tension is reduced to 2-5 mN/m by adding surfactants.

This session demonstrated a field-free, gravitationally driven approach to perform particle concentration inside microfluidic plugs. The first notable advantage of this technique is that it is passive, requiring no external components, and it can be controlled simply by changing the flow velocity. Second, whereas prior approaches have reported 83% particle collection efficiency [110], this technique can achieve an efficiency of nearly 100%. One important requirement is that particles must have a sufficiently large settling velocity. Since V_S scales as the square of the radius, it is best to use dense particles in the 10-50 μm range. Although this is larger than the magnetic beads often used in biological assays, there are nonetheless a wide variety of commercial beads available in this range. Such sizes would be compatible with

microchannels with diameters 100-500 μm. Many beads, including the glass beads used here, can be functionalized to adsorb biomolecules. On a broader note, particle concentration techniques expand the capabilities of plug-based systems to include particle filtration, an operation that was previously limited to continuous flow systems. An advantage of droplet microfluidics is that it can perform batch-mode processing of very small assay volumes. The ability of this technique to switch between circulation and aggregation has promise in heterogeneous bead-based assays, which require resuspension and concentration of beads in solution. High plug velocities, which cause beads to circulated throughout the plug, is useful for mixing and agitating the particles with the sample. Decreased flow velocities, where particles sediment, can then be used for collecting the functionalized particles.

3.3.2 Label-Free Detection of proteins by Drop Shape Analysis

Introduction: In clinical proteomics, there is a growing demand for performing high throughput protein detection in low sample volumes. In single phase microfluidics, the sample is flushed through the channel containing immobilized antibodies [122] or functionalized magnetic beads [123] which can capture the targeted proteins. After capture, they can be detected by ELISA, fluorescent tagging, electrochemical techniques, and others. In droplet systems, protein detection is often realized by light induced fluorescence by chemically tagging the protein molecules with specific fluorophores [33]. Although these techniques are sensitive, they require chemical labels along with instrumentation such as photomultiplier tubes, laser, and actuators. It is desirable to perform sensitive detection without the use of the chemical labels and active components. In this paper, we present a label-free method for protein localization

and detection inside the droplets due to the combined effect of hydrodynamic recirculation drag [72] and interfacial adsorption [124]. The protein localization at the rear end of the droplet changes its shape, which is used as a label free indicator of protein concentration in the droplet. The model is validated in simulations and experiments

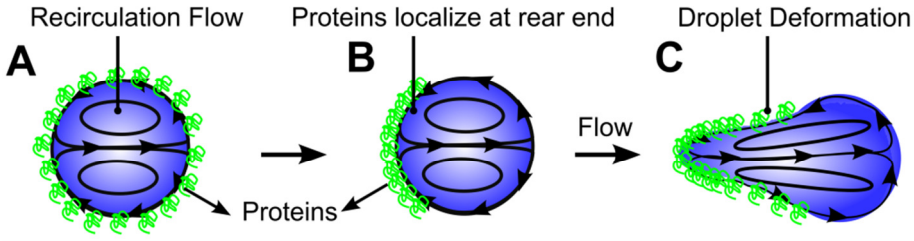

Figure 47: Mechanism of shape-based protein detection in droplets. (A) Proteins adsorb at the surface of a water-in-oil droplet. (B) Hydrodynamic recirculation convects adsorbed proteins to the rear of the droplet. (C) Aggregated proteins reduce the interfacial tension locally, deforming the rear end of the drop. The length of the deformed region scales predictably with protein concentration and flow rate.

Concept: The method is based on the adsorption and localization of proteins in a droplet flowing through a microchannel, causing the droplet to deform in a concentration-dependent manner (Figure 47). Proteins in the droplet adsorb to the surface due to hydrophobic partitioning [124], as described by the Langmuir isotherm. The adsorbed molecules are then convected to the rear of the drop by recirculation flows which naturally occur in a moving droplet [72]. The aggregated proteins locally reduce the interfacial tension at the rear of the drop, leading to a local increase in the capillary number (*Ca*). The oil film between the droplet and channel wall scales as $Ca^{2/3}$, as described by Bretherton [94]. Due to the increased *Ca*, the rear of the droplet tapers (Figure 47 C). Notably, the length of the deformed region is proportional to the number of protein molecules on the droplet interface. Therefore, it serves as a label-free indicator of the droplet's protein content.

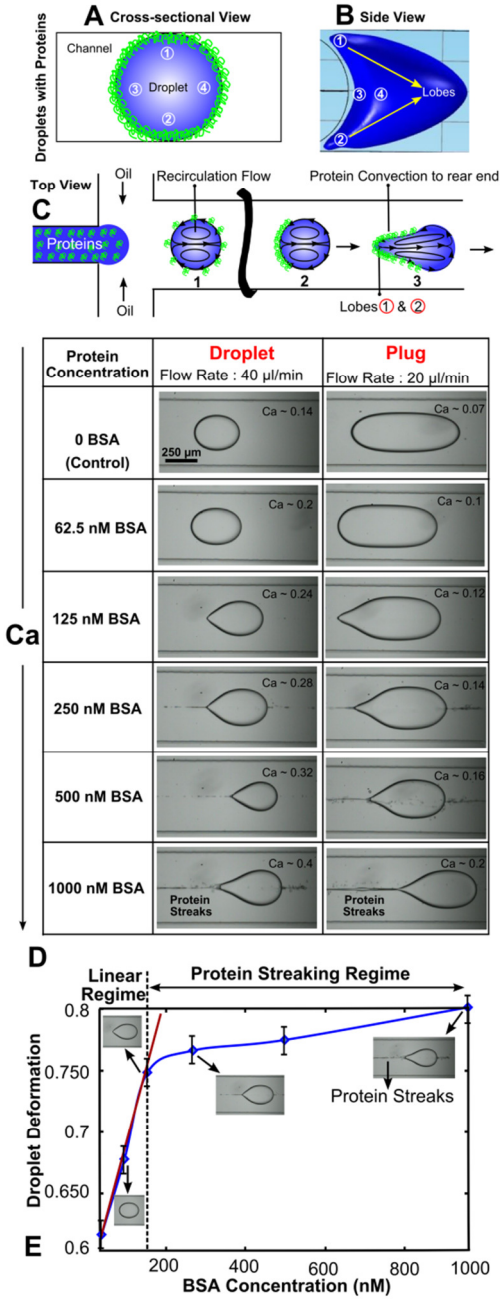

Figure 48: Protein localization and detection in an unconfined geometry (A) Cross sectional view of droplet in the channel. (B) 3D CFD model showing two lobes. (C) Schematic of unconfined channel illustrating protein localization. (D) Protein concentration in droplet vs. plugs. (E) Label-free protein measurement.

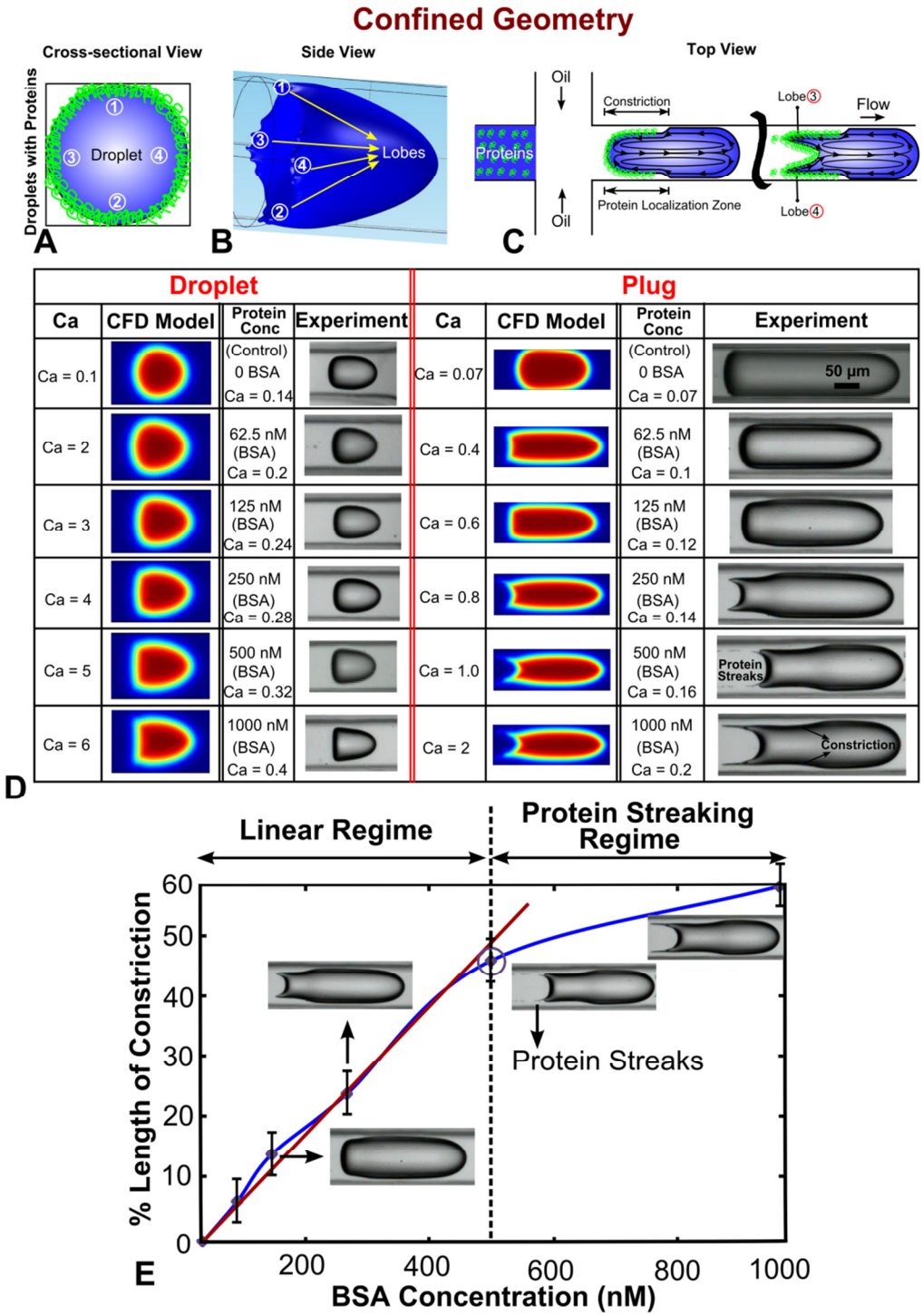

Figure 49: Protein localization and detection in a confined geometry (A) Cross sectional view of droplet in channel. (B) 3D CFD model showing all 4 deformation lobes. (C) Schematic representation of a confined channel illustrating droplet constriction and protein localization. (D) Chart comparing simulation and experimental details of protein concentration in droplets vs. plugs. (E) Label-free protein measurement.

Results & Discussion: Using experiments and simulations, the concept is studied in both confined and unconfined channel configurations. In the unconfined geometry (Figure 48), only the upper and lower surfaces of the droplet are in contact with the channel walls. As the proteins aggregate at the rear of the drop, the shear stress exerted by the walls causes 2 protruding lobes at the upper and lower surface (Figure 48 B-D). The elongation of the lobes increases with protein concentration (Figure 48 D&E). In the confined geometry, where the droplet is in contact with all 4 walls (Figure 49 A), 4 lobes form at the rear end of the droplet (Figure 49 B&C). Furthermore, in long plugs, the aggregation of proteins (and local change in *Ca*) results in a constriction at the rear end of the drop (Figure 49 D). Two flow regimes are observed, depending on *Ca*. In the linear regime (small *Ca*), the length of the constriction scales linearly with protein concentration, and therefore can be used as a label-free measure of protein concentration (Figure 49 E). At high *Ca*, proteins aggregated at the rear of the drop are stripped from the droplet due to high shear forces (Figure 48 E& 49 E). Drop shape can be analyzed in real-time using our image processing software [6], thus providing a label-free measure of protein concentration for droplet-based proteomic assays.

Chapter 4: Tensiophoresis: Migration of Droplets in a Micro-Surfactant Gradient

4.1 Introduction

Phoretic transport can be broadly defined as the migration of a particle or droplet due to a field which interacts with its surface [125]. Existing phoretic techniques generally rely on electric fields, either directly or indirectly. In electrophoresis and dielectrophoresis, externally generated electric fields interact directly with charges or induced charges on the dispersed phase [126], [127]. Electrophoretic forces can only act on charged species and the induced force is proportional to the electrode voltage. Dielectrophoresis can manipulate dielectric/neural species - since the induced force scales proportional to the particle volume, it can manipulate rather larger droplets/particles (>10 μm). Both these techniques are efficient; however, they require either charged or dielectric particles in addition to on-chip electrodes which causes issues like electrode polarization and joule heating. In diffusiophoresis, the electric field is formed indirectly as a result of electrolyte concentration [128] gradients around the dispersed phase. Analogously, in thermophoresis, the electric field is established based on temperature gradients across the particle [129]. In thermophoresis, few colloids exhibits thermophilic as well as thermophobic behavior at certain temperatures which helps to microfractionate biomolecules such as DNA, proteins etc [130]. But both diffusiophoresis and thermophoresis are incapable of generating appreciable force so that their applications are limited to micro/nano species such as ions, colloids and biomolecules. Here, we introduce a novel phoretic transport technique, tensiophoresis, which we define as the capillary migration of droplets in a surfactant micro-gradient.

The adsorption of surfactants at a liquid interface locally reduces the interfacial tension. Therefore, if a surfactant concentration gradient is presented across the length of the droplet, it induces a corresponding interfacial tension gradient (IFT) on the droplet surface. The surface stress is relieved by capillary flow which propels the droplet toward the stream containing higher surfactant concentration. In previous studies, IFT gradients were generated by applying a nonuniform temperature profile on the droplet surface [131], resulting in the well-known phenomenon of thermocapillary migration. Extensive fundamental studies explored all aspects of thermocapillary migration by generating a temperature gradient in the continuous phase [83], [132]–[135]. However, the relatively weak forces associated with thermocapillary migration limits its practical applications. Typical experiments achieve temperature gradients of 0.2 K/mm [136]. Coupled with IFT temperature coefficients of <1 mN/m-K [131], this results in an IFT gradient (and corresponding capillary stress) of $\nabla\gamma \sim .02\ N/m^2$. Surfactants, in contrast, can dramatically change IFT with a small change in concentration [137]. Using microfluidics to generate co-flowing laminar streams that differ in surfactant concentration; our approach can achieve capillary pressures > 100 mN/m^2, enabling novel methods for droplet manipulation and sorting.

4.2 Concept of Tensiophoresis

Capillary migration of a liquid droplet can be explained by a thermodynamic or physical argument (Figure 50). A spherical drop in an immiscible fluid has free surface energy $E = A\gamma$, where A is the surface area and γ is the IFT [138]. If the continuous phase has a spatial gradient in IFT, the droplet will migrate down the gradient in order to minimize its surface energy. At the physical level, the migration is initiated by the

Marangoni surface flow, generated as a result of the capillary stress imposed at the droplet surface by the IFT gradient ($\nabla\gamma$). At low Reynolds number, the flow forms the so-

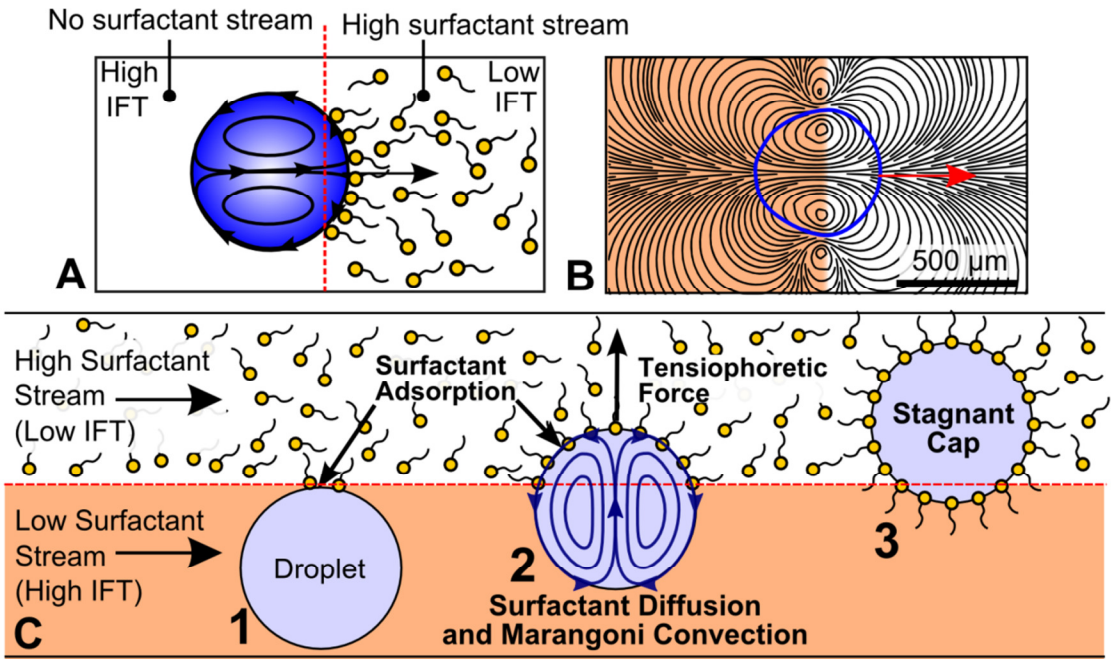

Figure 50: Concept of tensiophoresis (A) Schematic showing the tensiophoretic migration of a droplet when subjected to surfactant gradient. Droplet migrates towards the region of higher surfactant concentration.(B) During the tensiophoretic migration, the secondary vortices are observed using a CFD solver. (C) Capillary migration of droplets in a binary concentration gradient: 1) when the droplet comes in contact with the interface, the surfactant molecules from the upper stream adsorb to its proximal surface. 2) Non uniform IFT generates surface Marangoni stress which propels the droplet towards the upper stream, and the simultaneous convection of the surfactant molecules to the second half of the droplet. 3) Droplet either migrates completely or immobilized by the stagnant cap which is regulated by the surfactant concentration in the bulk.

called Hill spherical vortices [139], with flow directed forward along the axis of the droplet, and reverse on its surface. The surface stress is transmitted to the surrounding continuous phase, propelling the droplet towards the low IFT stream[131]. Figure 50 C illustrates how the tensiophoresis concept is realized in a microfluidic channel, exploiting laminar flow. A carrier fluid containing surfactant solution is flowed through the upper half of the channel, while an unmodified carrier fluid is flowed through the

lower half. When a droplet introduced in the low surfactant stream (high IFT) comes in contact with the laminar interface, the surfactant molecules from the upper stream adsorb onto the proximal surface of the droplet (**1**). This creates a non-uniform IFT across the droplet which generates surface flow directed from low to high IFT, resulting in the migration of the droplets into the upper stream. During the process of migration, the surfactant molecules are convected to lower half of droplet by the surface flow (**2**). Simultaneously, the surfactant molecules are replaced by the additional surfactants from the upper stream, and this process continues until the droplet surface becomes saturated with the surfactant molecules (**3**), forming a stagnant cap which prevents further migration [140], [141]. The rate of formation of the stagnant cap depends on the concentration of the surfactant molecules in the upper laminar stream. In dilute surfactant concentrations, the droplet migrate completely to the upper stream, while at concentrations above the critical micelle concentration (CMC), the stagnant cap prematurely arrests migration.

The capillary force F_C and migration velocity V_C are[131]

$$F_C = \gamma_C \nabla C \frac{4\pi r^2}{(1+\alpha)(2+\mathrm{K}\beta)} \qquad V_C = \gamma_C \nabla C \frac{2r}{\mu_C (2+3\alpha)(2+K\beta)}$$

where ∇C is the concentration gradient (evaluated at the droplet centroid), $\gamma_C = d\gamma/dC$ is the sensitivity of IFT to concentration, the product $\gamma_C \nabla C$ is the IFT gradient, r is the radius, μ_C is the viscosity of the continuous phase, α is the viscosity ratio between the droplet and carrier, K is the ratio of concentration between droplet and bulk, and β is the ratio of diffusion coefficients. It should be noted that this is a first order model which assumes a spherical droplet and also neglects the effects of surfactant solubility or adsorption dynamics.

4.3 Results and Discussion

Droplet trajectory, Migration velocity & Deformation

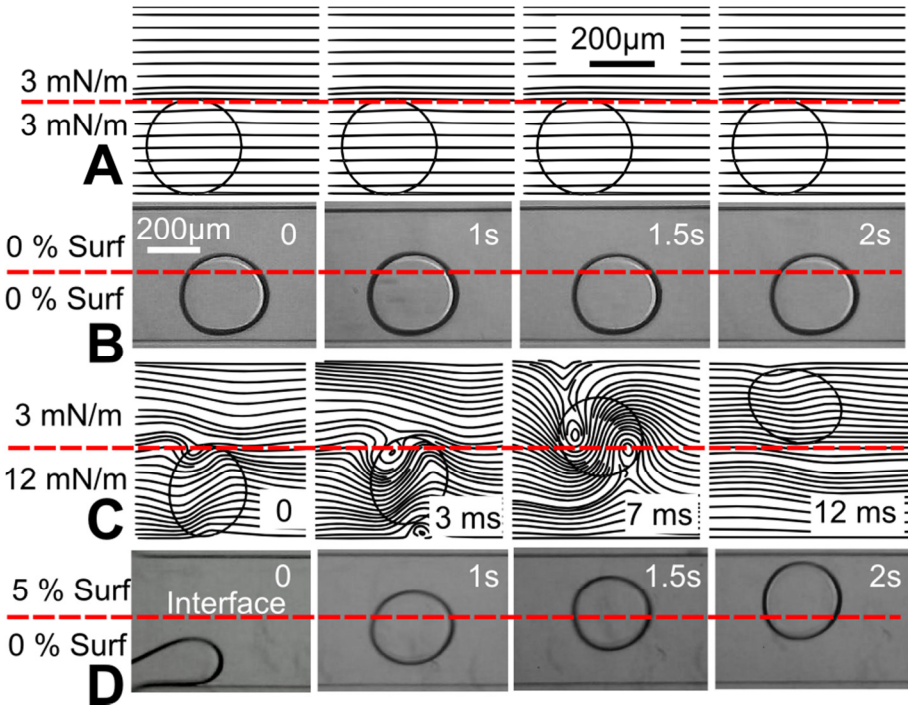

Figure 51: (A&B) Control experiment: Two streams have same IFT gradient. Both CFD simulation (A) and the experiment (B) show no migration and the droplet advances through the lower stream. C) CFD simulation of the droplet migration. The upper half of an 800 μm channel is set to a 3 mN/m IFT, while the lower half is set at 12 mN/m, creating a $\Delta\gamma$~9mN/m D) Tensiophoretic migration of droplet in a binary surfactant concentration profile. At 5 % v/v surfactant concentration, the droplet migrates completely into the upper stream.

Experimental results are shown in Figure 51. If the two streams have the same IFT (control), both the computational simulation and experiments show that the droplet does not migrate and continues to advance through the lower stream (Figure 51 A&B). As we introduce the IFT gradient between two streams, a droplet touching the interface migrates to the lower IFT stream (Figure 51 C&D). Unlike the experiment, the simulation ignores the stagnant cap effect because it doesn't consider the effect of surfactant adsorption, only the IFT profile. At low IFT gradients (less than CMC), the possibility of

the formation of a stagnant cap is almost negligible; therefore, the droplet migrates completely into the high surfactant stream. To illustrate the dependence of IFT gradient on the migration pattern, we tracked the trajectories of a 400 μm droplet subjected to various surfactant concentrations (Figure 52 A) using a custom image processing software. When the surfactant concentration is 20% v/v, the droplets migrate completely into the low IFT stream. Beyond the critical micelle concentration (CMC) (Figure 52 B), the droplet migrates abruptly and does not fully enter the low IFT stream. Instead, it settles at a position where its center aligns with the interface and further migration of the droplet is arrested due to the stagnant cap formation. In a microfluidic chip, the location of the interface can be precisely controlled by adjusting the relative flow rates of the two continuous phases. This allows for exquisite control of the migration pattern and settling location of the drop. The migration velocity increases rapidly with surfactant concentration until the CMC, beyond which it saturates (Figure 52 C). The abrupt migration is due to the increase in the IFT gradient imposed across the droplet at high surfactant concentration. This IFT gradient generates non uniform capillary pressure across the droplet; therefore, the droplet deforms when it encounters such pressure variation (Figure 52 D). Deformation also depends on the width of the low IFT stream. If the width of the low IFT stream is less than the droplet diameter, it deforms in order to stay inside the low IFT stream to reduce its overall energy, and that result in increased deformation.

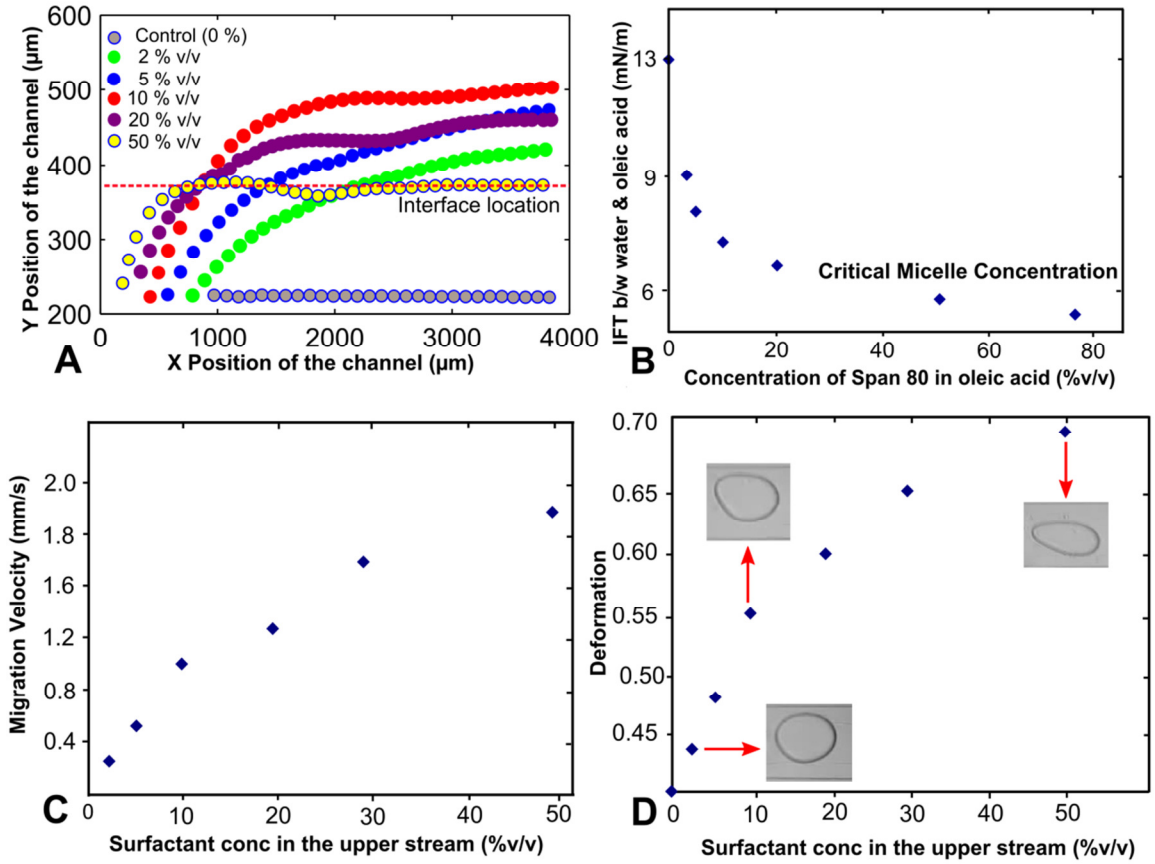

Figure 52: A) Migration trajectories for different surfactant concentrations. Steady and continuous migration is observed for the droplets subjected to 2%, 5% and 10 % v/v surfactant concentrations. Beyond CMC (50% v/v), the droplet settles at a position where its center aligns with the interface. B) IFT measurement by pendant drop method between water and various concentrations of surfactants (span 80) in oleic acid C) Migration velocity of 400 micron droplet at different concentrations of surfactant in the upper stream D) Droplet deformation at various surfactant concentrations in the upper stream

4.3 Applications

The growing trend of performing biological assays in water-in-oil droplet microreactors with nL-fL volumes has renewed interest in the ability to physically manipulate drops and query their biological contents. Leveraging microfluidic laminar flows to precisely control the IFT gradients, we demonstrate how tensiophoresis can be

engineered to enable droplet sorting and detection. Controlling the width of the surfactant streams enables a passive, tunable method to sort droplets by size with 3.3% sorting resolution. Droplets can also be sorted by chemical composition. Notably, the migration velocity depends on biochemical composition of the drop. Proteins and other surface active molecules within the drop undergo Langmuir adsorption, creating a saturated interface which inhibits droplet migration. The migration velocities can be correlated to protein concentration with a 1 femtomole limit of detection (LOD) in a 100 nL droplet. The results suggest a highly sensitive method for label-free detection in droplet microreactors.

4.4.1 Droplet Sorting based on Size

Droplet sorting based on size is an important unit operation in droplet microfluidics which helps to improve the uniformity of droplet populations. Existing size-based sorting techniques generally rely on hydrodynamic techniques. In 2007, Tan et.al demonstrated a passive droplet sorting technique, where different size droplets were successfully sorted into the respective outlets determined by the shear force ratio which depends on the area of projection and shear rate imposed across the droplet [31]. In 2008, Chabert et.al presented a hydrodynamic technique for cell encapsulation and subsequent sorting of the droplets at the channel bifurcation by the combined effect of lateral shear induced drift generated by the asymmetric oil flow rates, and the steric interactions between the droplets at the bifurcation [32]. In 2011, Joensson et.al demonstrated a deterministic lateral displacement (DLD) pillar array which could successfully sort 11 μm droplets from the 30 μm droplets at a frequency of 12,000

droplets/sec [30]. These techniques are well-known and efficient; however, they require either fixed channel designs or precise control over the flow regime, which limits the size-sorting dynamic range and simplicity of the system. Here, we demonstrate a size based droplet sorting device with wide tuning range using tensiophoresis.

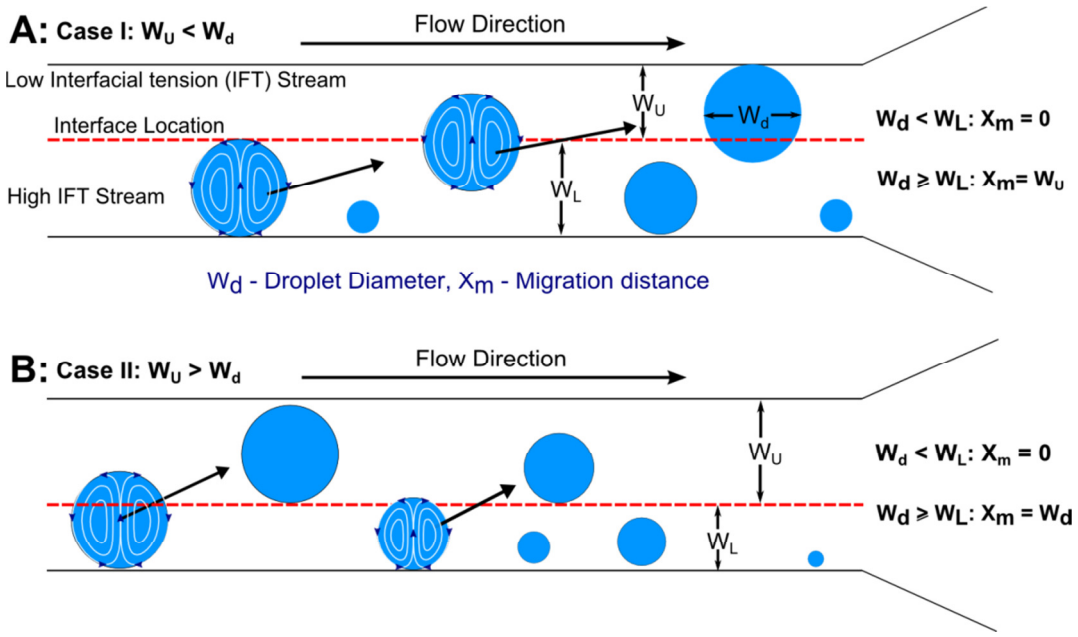

Figure 53: Size-based droplet using Tensiophoresis. (A & B) Effect of WU, WL and Wd on the migration distance (Xm) and sorting behavior

.

When a droplet is placed between two streams of different interfacial tension (IFT), it migrates toward the stream with lower IFT. The migration is initiated only when the droplet touches the interface ($W_d > W_L$); therefore, the size sorting threshold can be dynamically tuned by changing the width of the upper (W_U) and lower (W_L) stream. The widths can be easily controlled by changing the relative flow rates of the upper and lower streams. For a migrating droplet ($W_d > W_L$), two different cases have been observed based on W_U and the drop diameter (W_d). **Case I** (Figure 53 A): If $W_d > W_U$, the droplet migrates completely to the upper stream in order to minimize its overall

surface energy. In this case, the migration distance of the droplet (X_m) is equal to W_U. **Case II** (Figure 53 B): If $W_d < W_U$, then X_m is equal to droplet diameter (W_d). In this case, the droplet does not migrate completely to the upper wall. This is because once the droplet is fully enclosed in the upper stream; it no longer experiences an IFT gradient across it and therefore stops migrating. In both **case I and II**, small droplets ($W_d < W_L$) do not contact the interface, and therefore do not migrate and are collected at the lower outlet. Case I is ideal to separate the larger droplets from the population while case II is useful to collect the smallest droplets from the library.

To demonstrate size based sorting of droplets, microfluidic devices were fabricated in poly dimethylsiloxane (PDMS) using soft lithography. The aqueous phase was injected through the lower inlet while the middle and top inlets were used to inject surfactant free oil (oleic acid) and an oil+surfactant (10% v/v Span 80) mixture, respectively. This effectively creates two streams of different IFT. Measured by pendant drop method, the IFT of surfactant free oil is 13mN/m, while that of the oil+surfactant is 8mN/m. The observation channel is 800 μm in width and the droplet sorting was visualized using a bright field microscope. Bright field images were acquired using a high speed camera. The droplet's velocity, diameter, migration profile, and final y-position were tracked using DMV, a droplet tracking software previously developed in our group [142].

When the droplet's diameter is greater than W_L, it migrates to the upper stream and the final settling position of the droplets depends on the interface location (Figure 54). Figure 54 A is the example of case I. Here, the droplet diameter (W_d) is greater than both the width of the lower stream (W_L) and the width of the upper stream (W_U). In this

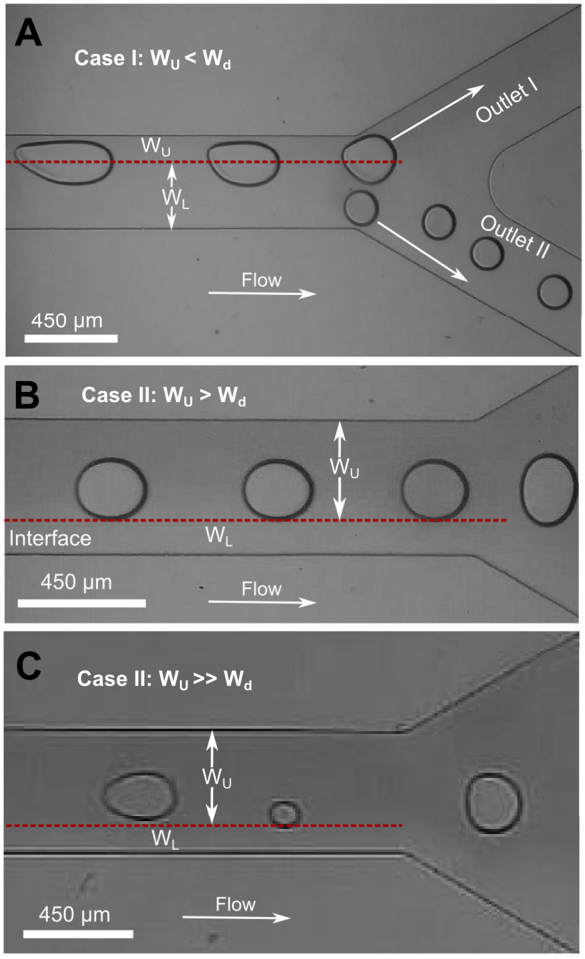

Figure 54: Case study of droplet size tuning range. (A) Case 1: (a) If WU < Wd > WL, the migration distance (Xm) is limited to WS. (b) If $W_U < W_d < W_L$, the droplet will not migrate (X_d = 0). (B & C) Case 2: (a) If $W_U > W_d > W_L$, then $X_m = W_d$ and (b) if $W_U > W_d < W_L$, then $X_m = 0$. (W_d is the drop diameter).

case the droplet migrates completely to the upper stream and the migration distance (X_m) is limited by the width of the upper stream. In case I, larger droplets ($W_d > W_L$) are collected at the upper outlet while the smaller droplets ($W_d < W_L$) are directed towards the lower outlet. Figure 54 C is the examples of case II. Here, the droplet diameter is greater than the width of the lower stream but less than the width of the upper stream. Droplets will not migrate completely to the upper wall; instead, it settles just inside the upper low IFT stream. This is because once the droplet migrates to the low IFT stream;

it no longer experiences an IFT gradient across it and remains just inside the stream. In case II, the migration distance is maximum and it is equal to the droplet diameter. In both case I & II, if the droplet's diameter is less than the width of the lower high IFT stream, the droplet will not migrate because it never see the IFT gradient. The quantitative data of case I and II are shown in Figure 55. Figure 55 B&C is the example of case I and case II respectively. If the width of the lower stream (W_L) is 150 μm, the droplets with diameter greater than 150 μm will migrate to the upper stream while the others remain in the lower stream (Figure 55 B). The non-uniformity of droplet's final position (lower left quadrant) is due to droplet-droplet interactions as a result of a sudden decrease in the flow rate at the channel expansion. Figure 55 C is an example of case II. If W_L is 100 μm, droplet after migration settles just inside upper stream. In this case, all the migrating droplets, irrespective of diameter, will settle in the same plane (along the interface). Case II is suitable for collecting small droplets ($W_d < W_L$) from the library. The variable interface allows us to dynamically tune the droplet size thresholds (Figure 56). Figure 56 A-C shows the tuning of the size threshold from 490-620μm in an 800μm channel. If W_L is fixed at 520 um, droplets with diameter greater than 525 μm start collecting at upper outlet while the droplets with diameter less than 520 μm are collected at lower outlet. Virtually 100% collection efficiency is achieved for the droplets >540 μm and <510 μm in diameter with a sorting precision ((540-510)/520) of 5.7%. An overall collection efficiency of 75% is obtained for the 510-540 μm diameter range. Figure 56 D-E shows the ability to tune the sorting threshold between 150-225μm in a 450μm channel.

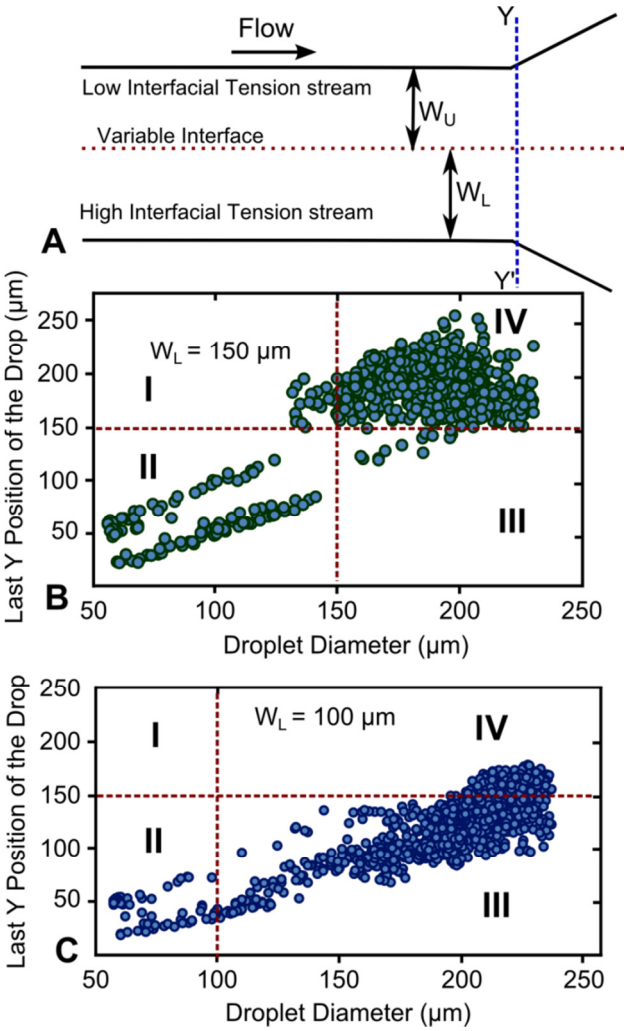

Figure 55: Quantitative analysis of droplet's Y_ position Vs droplet diameter at various interface locations.(A) Channel schematic with Y-Y‘ indicating the plane at which the droplet being analysed. (B Example of case I (C) Example of case II.

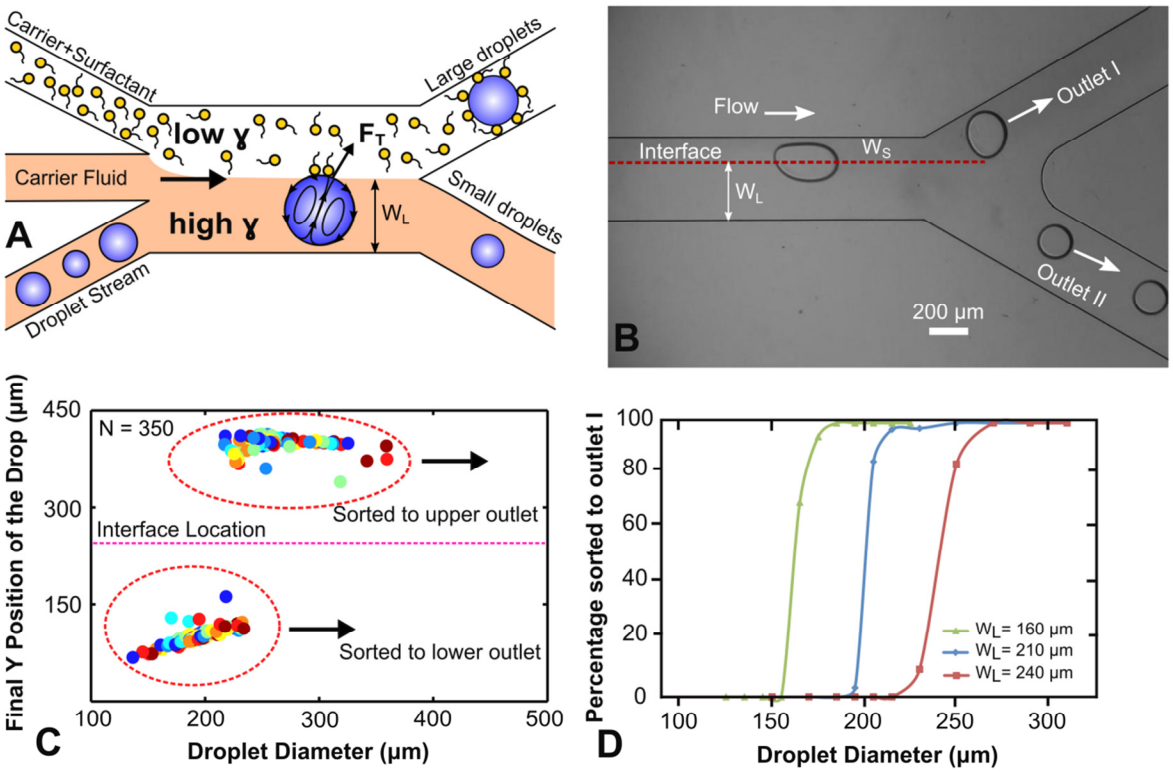

Figure 56: Droplet sorting based on size (A) Chip schematic used to perform size based drop sorting. A carrier fluid containing surfactant solution is flowed through the upper half of the channel, while an unmodified carrier fluid is flowed through the lower half which set up an IFT gradient orthogonal to the channel. (B) Larger droplet (diameter of the droplet is greater than or equal to W_L) touches the interface and migrates to the upper outlet while the smaller droplet will not migrate and is collected at outlet II. (C) Scatter plot of final Y position vs. drop size showing the sorting efficiency (Interface location is set at 225 μm) (D) Illustrates how the interface can be tuned to extract different size droplets from a population. The interface location can be dynamically tuned by adjusting the relative flow rate of the two laminar streams.

This session demonstrated binary size-based sorting of droplets by tensiophoresis, the migration of a droplet due to an IFT gradient. By leveraging microfluidics to precisely control the interface location of the two co-flowing laminar streams which differ in IFT, the size sorting threshold can be dynamically tuned. Our technique can achieve selective size sorting with a resolution of 3.3%. This technique is

simple, passive, and can be used to sort droplet of different size ranges with the same channel design.

4.4.2 Label-Free Droplet Sorting by Chemical Composition

Label-free sensing and sorting is a current challenge in droplet-based high throughput screening. However, the only known technique for sorting droplets based on chemical contents is fluorescent activated sorting using dielectrophoretic [33], piezoelectric [34] or membrane valve actuators [35]. These techniques are both sensitive and fast, but they require fluorescent labeling, along with on-chip structures and an active feedback to control sorting signals. With regard to detection, absorbance detection (colorimetric) techniques are label-free but have poor sensitivity due to shorter optical path lengths. Label-free approaches like Raman spectroscopy have recently been applied to droplets [143] but require complex instrumentation and long integration times. Here, we demonstrate a passive, label-free droplet sorting technique which has the unique ability to sort droplets by their interfacial tension (IFT), without chemical labels or on-chip actuators. IFT based sensing and sorting has significant potential in biological assays, as interfacial properties are sensitive to protein concentration, enzymatic activity, pH, and other chemical parameters.

Droplet Sorting Based on SDS Concentration

Figure 57 illustrates the label free sorting of droplets based on SDS concentration. Droplets containing DI water or 3.5 μM SDS solutions are injected through the lower inlet at the flow rate of 1-3 mL/hr. The upper half of the sorting channel contains oleic acid + 5% Span 85, while the lower half contains the droplets in

pure oleic acid. Pristine droplets initially migrate slowly towards the interface, and upon contact they quickly traverse the boundary to the upper stream Figure 57 A. By contrast, droplets containing SDS do not migrate. The putative cause for the difference in migration profiles is the relative adsorption of external surfactants. SDS (green) adsorbs to the interface, preventing adsorption of the external surfactant (orange) (Figure 57 B). This precludes the formation of an IFT gradient across the droplet, which is necessary for migration. Based on their migration, pristine droplets and SDS droplets collect in outlets A and B, respectively.

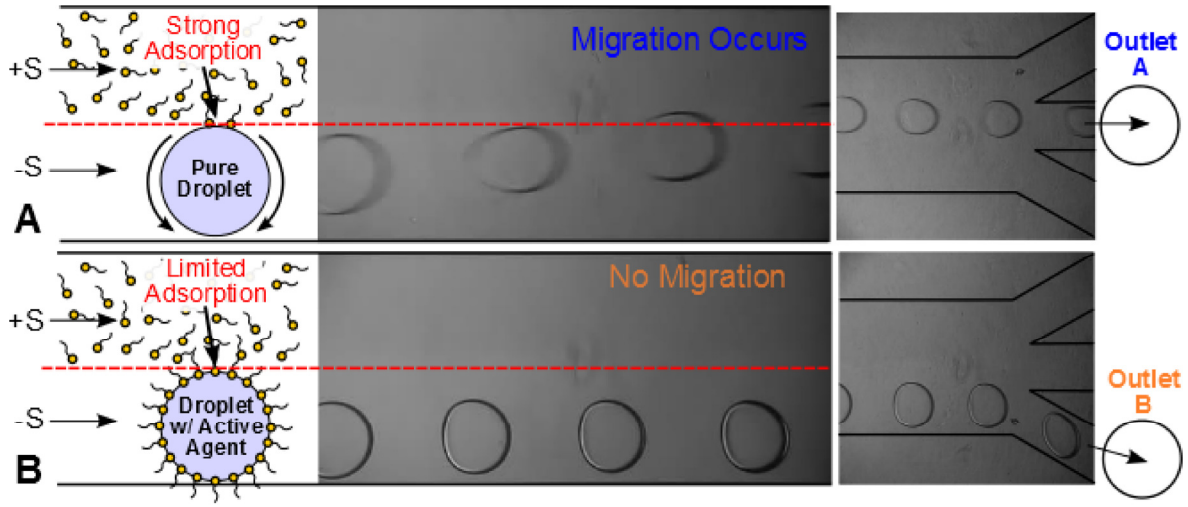

Figure 57: Droplet sorting based on SDS concentration. (A) Pure droplet encounter strong migration and are collected at outlet A (B) Presence of SDS molecules on the surface of the droplet inhibit further adsorption of external surfactants; hence the droplet does not migrate and are redirected to outlet B

Droplet Sorting based on Protein (BSA) Concentration

Tensiophoresis can also be used for the detection of proteins in droplets. Label free detection is desirable for biological assays, particularly those which provide sensitivity in small sample volumes [144]. In many droplet based biological assays, protein adsorption onto the droplet surface is considered a major concern [124]. Here,

we take the advantage of surface adsorption to sort the droplets based on protein concentration. When placed in a surfactant concentration profile, droplets containing protein or any surface active agents (low IFT) will migrate slower than pristine droplets (high IFT). In pristine droplets, surfactant molecules from the high IFT (upper) stream adsorb strongly onto the surface, causing the droplet to migrate rapidly as described earlier (Figure 58 A). Conversely, a droplet containing surface active agents has higher surface coverage, which inhibits adsorption of the surfactant molecules from the continuous phase (Figure 58 A). This slows down or prevents the migration. We demonstrate this concept using water-in-oil droplets containing Bovine Serum Albumin (BSA). A 5mN/m IFT gradient was created by having two streams of oleic acid with surfactant concentrations of zero and 10 %v/v, respectively. Pristine droplets migrates to the upper stream with a velocity of 1.2 mm/s in a while the droplets containing 1μM BSA do not migrate and are collected at lower outlet (Figure 58 B). As the BSA concentration in the droplet increases, the IFT gradient between the droplet and upper stream decreases, and this slows down the migration velocity of the droplet (Figure 58 C). Beyond a certain concentration, the IFT gradient becomes negligible to initiate the droplet migration. There exists a linear relationship between the migration velocity of the droplet and the BSA concentration (Figure 58 D). The concentration of protein in the droplet can be estimated by measuring the migration velocity of the droplets in a surfactant gradient.

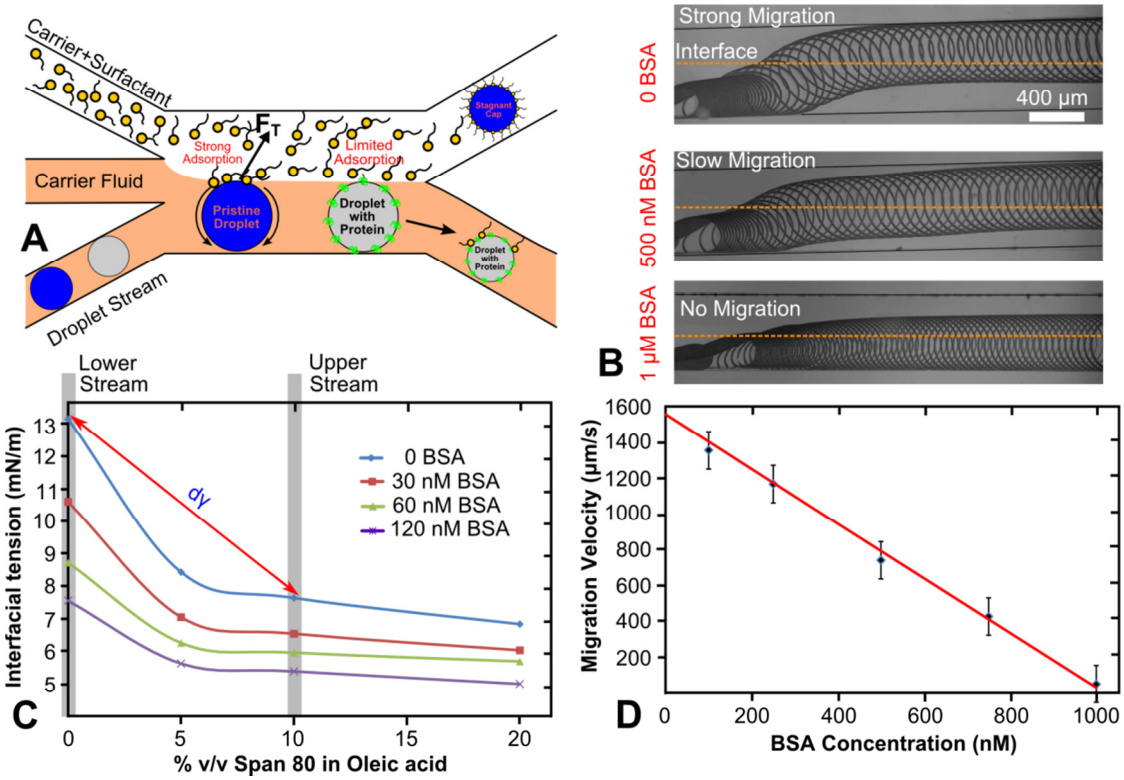

Figure 58: Droplet sorting based on protein concentration. (A) Schematic of the chip used for sorting droplets by protein concentration. Pristine droplet undergoes strong surfactant adsorption and migrates steadily to the upper stream. Conversely, droplet with protein inhibits surfactant adsorption and results in negligible migration. (B) Composite picture showing the droplet trajectories at various BSA concentrations. (C) As BSA concentration increases, the IFT gradient between the droplet and the upper surfactant stream decreases. This reduces the migration velocity. (D) Linear relationship of migration velocity with the BSA concentration. Protein concentration is measured indirectly by calculating the migration velocity of the droplet

In summary, we have demonstrated the concept of tensiophoresis which offers new capabilities in droplet sorting and label-free detection. Using surfactants and microfluidics to generate sharp interfacial tension gradients, we have generated a capillary stresses of several orders greater than thermocapillary approach. Since the capillary force scales linearly with the IFT, tensiophoresis scales favorably to the small length scales.

4.4.3 Deterministic Protein Extraction from Droplets using Recirculation Drag and Tensiophoresis

Introduction

Extracting proteins from biological samples is an important unit operation in clinical proteomics [145]. In single- phase microfluidic devices, protein extraction generally rely on antibodies immobilized on the channel walls [146] or functionalized magnetic beads which are immobilized in the microchannel using an external magnet [123]. Sample flushing results in binding of protein molecules to the specific target. In droplet-based microfluidic systems, an analogous approach may be used: magnetic beads immersed in a plug can bind the biological sample [147], and later be extracted from the drop using external magnets. A second approach extracts proteins in the form of a precipitate by mixing of the sample droplet with the precipitants [148]. These techniques are effective; however, they do require additional steps such as functionalizing the beads or to ensure controlled mixing of precipitants to prevent contamination. In this paper, we report a simple and passive protein segregation and extraction technique which exploits combined effects of micro-scale adsorption [124], hydrodynamic recirculation drag (chapter 3) [149][150] and tensiophoresis [150]

Concept

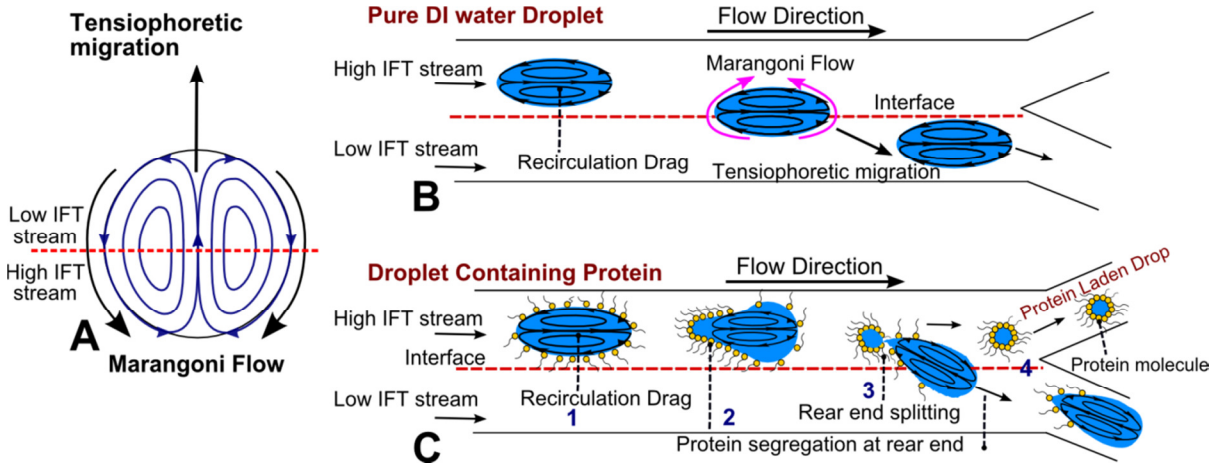

Figure 59: Concept of protein extraction technique. (A) Tensiophoresis basic concept. (B) A pristine water droplet migrates intact to the low IFT stream. (C) In a droplet containing protein, segregation occurs in 4 steps: 1) Protein molecules adsorb to the surface of the droplet; 2) Protein molecules are convected to the rear of the droplet by hydrodynamic recirculation flow; 3) The rear end of the drop containing protein molecules splits and remains in the upper stream while the remainder of the drop undergoes tensiophoretic migration to the lower stream; 4) The two fractions flow to different outlets following a bifurcation.

The protein extraction process includes four steps (Figure 59 C): (1) Protein adsorption: Proteins strongly adsorb to the droplet's liquid-liquid interface due to hydrophobic interactions. (2) Protein segregation: The adsorbed proteins are then convected to the rear of the drop by recirculation flows which occur naturally inside a moving droplet/plug [72]. The aggregation of proteins at the rear boundary locally reduces the interfacial tension (IFT), causing a visible deformation in that region. (3) Protein extraction: Protein extraction occurs as a result of tensiophoretic migration and splitting. Reported previously by our group [150], tensiophoresis is the migration of droplets between two laminar streams of differing interfacial tension (IFT) (Figure 58 A). A pristine droplet (with a clean interface) rapidly migrates to the low IFT stream as a result of non-uniform interfacial stresses which generate Marangoni flow (Figure 59 B). Here we find that a droplet containing a non-uniform surface concentration of protein will

undergo splitting during migration. The protein-free front region of the drop migrates to the low IFT stream. However, the rear portion (saturated with adsorbed proteins) does not migrate because it does not have a mobile interface to initiate surface flow. Furthermore, the high protein concentration in this region reduces the IFT and weakens the droplet boundary. As a result, when the protein free region migrates, the protein laden region splits off and remains in the upper stream. (4) Collection/Separation: The extracted drops containing proteins are directed to the upper outlet, while the remaining drops proceed to the lower outlet (Figure 59 C). The four-step process occurs spontaneously, enabling continuous flow operation.

Experimental Set up

To demonstrate protein extraction from droplets, a tertiary microfluidic junction with a 1000 μm wide extraction channel was fabricated in polydimethylsiloxane (PDMS) using soft lithography. Droplets with various concentrations of BSA/GFP were introduced through the upper inlet while the middle and lower inlets were used to inject oleic acid and octanol-1 respectively. The interfacial tension (IFT) of oleic acid and octanol-1 with water is 16 mN/m and 8.5 mN/m respectively [151]. Laminar streams of these two relatively immiscible liquids form a sharp IFT gradient at the interface. The protein extraction was visualized using the fluorescence or bright field microscope with high speed phantom camera. The quantitative analysis of the protein extraction process such as flow velocity, droplet's rear end deformation, size variation of protein laden drop etc were measured using custom built droplet tracking software called droplet morphology and velocimetry (DMV) [142].

Results and Discussion

Figure 60 demonstrates the extraction of BSA. The control experiment (Figure 60 A) illustrates that, when a pristine droplet is subjected to an IFT gradient it migrates intact to the low IFT stream. By contrast, droplets containing 250nM BSA will undergo BSA segregation and extraction due to the combined effect of protein adsorption, hydrodynamic recirculation drag and tensiophoretic migration. Initially, the BSA molecules in the droplet strongly adsorb to the liquid-liquid interface due to the hydrophobic interactions. The adsorbed molecules will get convected to the rear end of the droplet by recirculation drag. The aggregation of BSA molecules at the rear end decreases the IFT locally which results in rear end deformation as well as a slight change in color (Figure 60 B-2). The subsequent tensiophoretic migration breaks apart the BSA-laden fraction from the supernatant, and both travel to separate outlets. The non-protein region, which has a clean interface, undergoes strong migration and it is collected at the lower outlet whereas the BSA laden rear end fraction does not migrate and gets collected at the upper outlet. The migration of the BSA laden drop is inhibited because of the lack of mobile interface to initiate the Marangoni flow. The processes of adsorption, segregation, and extraction occur spontaneously which increases the throughput of the extraction system.

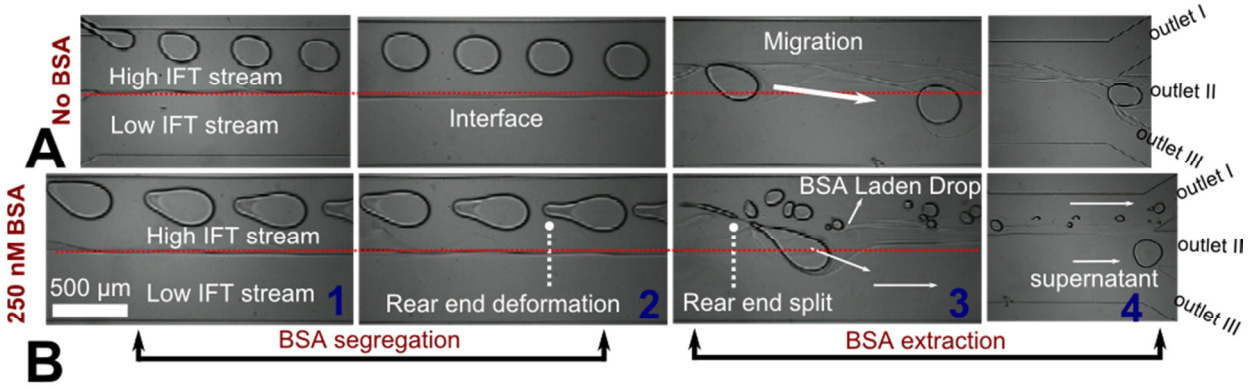

Figure 60: Bovine Serum Albumin (BSA) extraction (A) Control experiment: A pure water droplet migrates steadily into the low IFT stream without any splitting. (B) Droplets containing 250nM BSA. 1) Drop generation. 2) BSA segregation: Hydrodynamic recirculation flow convects the BSA molecules to the rear end of the drop. 3) BSA extraction: Tensiophoretic migration detaches the BSA laden fraction from the supernatant 4) Collection of protein laden drops at outlet I and supernatant at outlet II. Here, the high IFT stream is Oleic acid and low IFT stream is 1-Octanol

Figure 61 shows the quantitative analysis of BSA extraction. Increasing the droplet velocity (Figure 61 A) improves the enrichment (defined as the parent drop area/rear drop area) because high velocity leads to stronger recirculation and increased BSA segregation (Figure 61 A). This results in multiple drop breakoffs thereby improving the enrichment. Therefore, higher flow rates increase the extraction efficiency and throughput of the system. Figure 61 B shows that the size of the extracted drop increases with BSA concentration, suggesting the possibility of using this technique to measure BSA concentration. To visualize the protein extraction, BSA is replaced with GFP (Figure 62). The results show that the GFP extracted droplet fluoresces much brighter than supernatant. It is observed that the extraction efficiency increases as we decrease the GFP concentration.

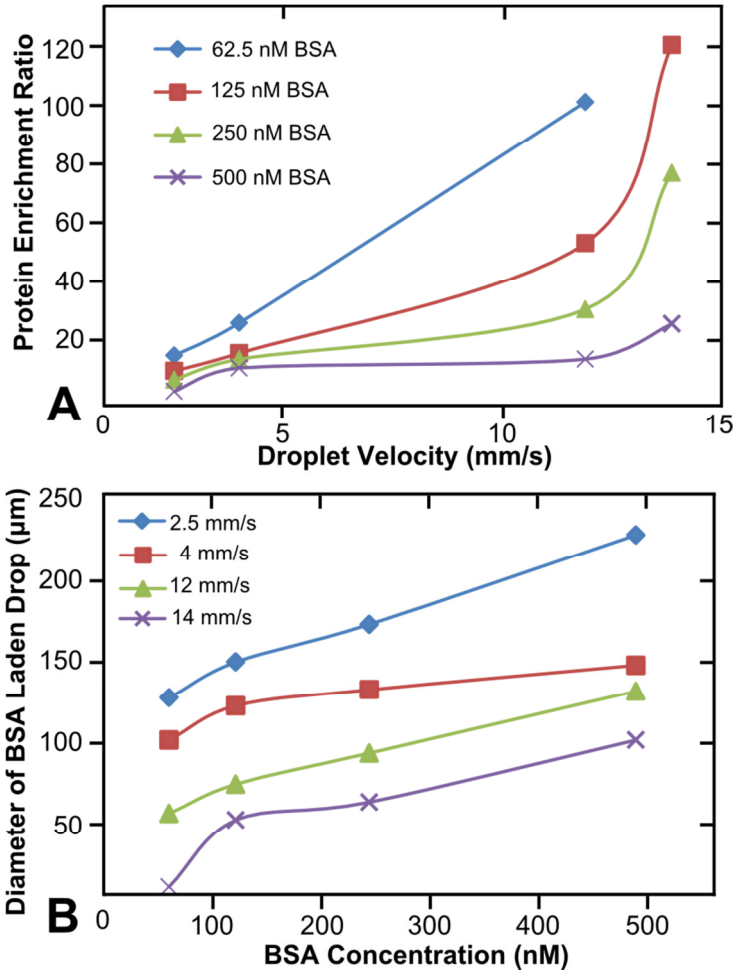

Figure 61: Quantitative analysis of BSA extraction. *(A)Increasing the droplet velocity improves the protein enrichment. Protein enrichment ratio is defined as the parent drop area/rear drop area (B) Size of the extracted drop increases with the protein concentration.*

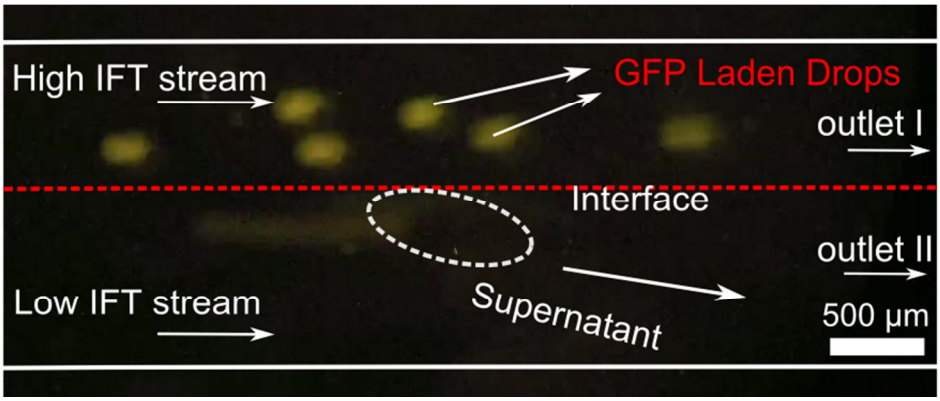

Figure 62: Green Fluorescent Protein (GFP) extraction: The rear end drop with high GFP concentration fluoresces brightly compared to the supernatant. Here, the concentration of GFP used is 500nM.

In summary, we demonstrated a droplet-based protein extraction technique which occurs spontaneously due to the combined effect of recirculation drag and tensiophoretic migration. It is simple technique which does not require multiple steps, and therefore it can be operated in continuous flow mode. It can extract nM concentrations of BSA and GFP from pL droplet samples. These results suggest a simple, passive and high-throughput technique which can achieve high efficiency protein extraction and therefore expand the capabilities of the droplet microfluidics in proteomic assays.

Chapter 5: Conclusions

This thesis addresses two major contributions to the field of droplet microfluidics. 1. Fundamental contribution and 2. Application contribution.

In the fundamental perspective, (a) We demonstrated tensiophoresis, a chemo-mechanical force transduction mechanism used for passive droplet actuation. The unique feature of this technique is that the tensiophoretic force for droplet actuation is derived from the micro-surfactant gradients imposed across the droplet using microfluidic laminar flows which causes the droplet to swim toward the high surfactant concentrated region. Compared to other methods in capillary migration, such as thermocapillarity, this approach can generate >100x larger force and can achieve significant migration velocities without heating the droplet. (b) Using hydrodynamic recirculation flows, we studied the behavior of both hydrophilic (silica beads) and hydrophobic particles (globular proteins) in the microvortex flow. In the case of hydrophilic high density silica particles, gravitational force and recirculation drag are the two forces responsible for particle concentration whereas in hydrophobic species (proteins), the localization is due to the combined effect of microscale surface adsorption and recirculation drag.

In the application perspective, (a) tensiophoresis is the first reported technique which can perform droplet sorting based on size as well as its chemical composition. We demonstrated size based sorting of droplets with wide tuning range at 3.3% resolution and label-free sorting of BSA droplets with 1 femtomole limit of detection. The sensing mechanism is non-specific, which may be a limitation in some cases;

however, this can also be perceived as a potential benefit in that the assay is universal to all surface active species. (b) Utilizing hydrodynamic recirculation flows, we demonstrated a field-free, (i) gravitationally driven approach to perform particle concentration (high density silica beads) and (ii) microscale adsorption driven approach to perform protein localization inside microfluidic plugs. The first notable advantage of this technique is that it is passive, requiring no external components, and it can be controlled simply by changing the flow velocity.

These techniques namely hydrodynamic recirculation drag and tensiophoresis can be used to perform certain applications in droplet based microfluidics including bead based assays, cell based assays, protein extraction studies in clinical proteomics etc. However, realizations of these concepts in real world applications always encounter practical difficulties which are not addressed in this thesis. (i) To perform bead based assays in droplet format, agitation of the sample with beads should occur at high flow rate whereas bead segregation/concentration and bead collection occurs at low flow rate. Since these processes occur at different flow regimes, simultaneous implementation of capture step, concentration step and extraction step would be challenging. (ii) The phenomenon of tensiophoresis is based on the surfactant gradient across the droplet and this technique does not work if the droplet surface is already coated with surfactants. In most of the real world life science applications, the droplet is always stabilized with surfactants and in that case tensiophoresis might not work. In that case, instead of surfactants, one could think about using two miscible liquid streams having different interfacial tension (eg. 1-octanol and oleic acid). (iii) Label-free sensing and sorting of droplets by tensiophoresis works only if the species are surface active

(like to stay at the interface). In the experiments, we have used BSA which is a surface active globular protein and it will not work in the case of non-surface active proteins, hence this technique is not universal for sensing and detection of all kinds of protein molecules.

APPENDIX A: LIST OF PUBLICATIONS

- **G.K. Kurup** and A.S. Basu, "Label-Free Detection of Proteins by Drop Shape Analysis," *Micro Total Analysis Systems (MicroTAS)*, October 2014, San Antonio, Texas, USA.
- **G.K. Kurup** and A.S. Basu, "Viscophoresis: Migration and Sorting of Droplets in a Viscosity Gradient," *Micro Total Analysis Systems (MicroTAS)*, October 2014, San Antonio, Texas, USA.
- **G.K. Kurup** and A.S. Basu, "Microfractionation of Gases Separated by Gas Chromatography," *Micro Total Analysis Systems (MicroTAS)*, October 2014, San Antonio, Texas, USA.
- **G.K. Kurup** and A.S. Basu, "Deterministic Protein Extraction from droplets using Interfacial Drag and Tensiophoresis," *Micro Total Analysis Systems (MicroTAS)*, October 2013, Freiberg, Germany.
- **G.K. Kurup** and A.S. Basu, "Size Based Droplet Sorting with Wide Tuning Range using Tensiophoresis," *Micro Total Analysis Systems (MicroTAS)*, October 2013, Freiberg, Germany
- **G.K. Kurup** and A.S. Basu, "Passive, Label- Free Droplet Sorting based on Chemical Composition using Tensiophoresis," *Micro Total Analysis Systems (MicroTAS)*, October 2012, Okinawa Japan.
- **G.K. Kurup** and A.S. Basu, "Field-Free Particle Segregation and Extraction for Bead-Based Assays in Plugs,"*Micro Total Analysis Systems (MicroTAS)*, October 2012, Okinawa Japan.

- **G.K. Kurup** and A.S. Basu, "Indirect Particle Manipulation using a Scanning Optofluidic Tweezer," *Micro Total Analysis Systems (MicroTAS)*, October 2012, Okinawa Japan.
- **G.K. Kurup** and A.S. Basu,"Field Free Particle Focusing in a Microfluidic Plug," *Biomicrofluidics Special Issue on Multiphase Microfluidics*, vol. 6, pp. 022008, April 2012.
- **G.K. Kurup** and A.S. Basu, "Tensiophoresis: Migration and Sorting of Droplets in an Interfacial Tension Gradient," *Micro Total Analysis Systems (MicroTAS)*, October 2011, Seattle WA.
- **G.K. Kurup** and A.S. Basu, "Optofluidic Tweezers: Manipulation of Oil Droplets with 105 Greater Force than Optical Tweezers," *Micro Total Analysis Systems (MicroTAS)*, October 2011, Seattle WA.
- **G.K. Kurup** and A.S. Basu, "Shape Dependent Laplace Vortices in Deformed Liquid-Liquid Slug Flow," *IEEE Engineering in Medicine and Biology (EMBC)*, September 2011, Boston MA.
- **G.K. Kurup** and A.S. Basu, "Rolling, Aligning, and Trapping Droplets on a Laser Beam using Marangoni Optofluidic Tweezers," *Proc. Intl. Conference on Sensors, Actuators, and Microsystems (Transducers)*, June 2011, Beijing China.
- K. Dadesh, **G. K. Kurup** and A.S. Basu, "High Speed Low-Noise Multiplexed Three Color Absorbance Photometry," *IEEE Engineering in Medicine and Biology (EMBC)*, September 2011, Boston MA.

- **G.K. Kurup** and A.S. Basu, "Hydrodynamic Particle Concentration in a Microfluidic Plug," *Proc. Micro Total Analysis Systems (MicroTAS)*, Oct. 2010, Groningen, The Netherlands.
- **G.K. Kurup** and A.S. Basu, "Multispectral Photometry with a Single Light Detector Using Frequency Division Multiplexing," *Proc. Micro Total Analysis Systems (MicroTAS)*, Oct. 2010, Groningen, The Netherlands.
- V. Trivedi, A. Doshi, **G.K. Kurup**, E. Ereifej, P.J. Vandevord, and A.S. Basu, "A Modular Approach for the Generation, Storage, Mixing, and Detection of Droplet Libraries for High Throughput Screening," *Lab on a Chip*, 2010.

BIBLIOGRAPHY

[1] G. M. Whitesides, “The origins and the future of microfluidics,” *Nature*, vol. 442, no. 7101, pp. 368–373, Jul. 2006.

[2] J. Melin and S. R. Quake, “Microfluidic large-scale integration: the evolution of design rules for biological automation,” *Annu. Rev. Biophys. Biomol. Struct.*, vol. 36, pp. 213–231, 2007.

[3] K. Ahn, C. Kerbage, T. P. Hunt, R. M. Westervelt, D. R. Link, and D. A. Weitz, “Dielectrophoretic manipulation of drops for high-speed microfluidic sorting devices,” *Appl. Phys. Lett.*, vol. 88, no. 2, p. 024104, 2006.

[4] J. Bico and D. QuéRé, “Self-propelling slugs,” *J. Fluid Mech.*, vol. 467, Sep. 2002.

[5] H. Song, D. L. Chen, and R. F. Ismagilov, “Reactions in Droplets in Microfluidic Channels,” *Angew. Chem. Int. Ed.*, vol. 45, no. 44, pp. 7336–7356, Nov. 2006.

[6] J. F. Edd, D. Di Carlo, K. J. Humphry, S. Köster, D. Irimia, D. A. Weitz, and M. Toner, “Controlled encapsulation of single-cells into monodisperse picolitre drops,” *Lab. Chip*, vol. 8, no. 8, p. 1262, 2008.

[7] S. Köster, F. E. Angilè, H. Duan, J. J. Agresti, A. Wintner, C. Schmitz, A. C. Rowat, C. A. Merten, D. Pisignano, A. D. Griffiths, and D. A. Weitz, “Drop-based microfluidic devices for encapsulation of single cells,” *Lab. Chip*, vol. 8, no. 7, p. 1110, 2008.

[8] J.-C. Baret, O. J. Miller, V. Taly, M. Ryckelynck, A. El-Harrak, L. Frenz, C. Rick, M. L. Samuels, J. B. Hutchison, J. J. Agresti, D. R. Link, D. A. Weitz, and A. D. Griffiths, “Fluorescence-activated droplet sorting (FADS): efficient microfluidic cell sorting based on enzymatic activity,” *Lab. Chip*, vol. 9, no. 13, p. 1850, 2009.

[9] S.-Y. Teh, R. Lin, L.-H. Hung, and A. P. Lee, “Droplet microfluidics,” *Lab. Chip*, vol. 8, no. 2, p. 198, 2008.

[10] X. Casadevall i Solvas and A. deMello, “Droplet microfluidics: recent developments and future applications,” *Chem. Commun.*, vol. 47, no. 7, p. 1936, 2011.

[11] A. Huebner, S. Sharma, M. Srisa-Art, F. Hollfelder, J. B. Edel, and A. J. deMello, “Microdroplets: A sea of applications?,” *Lab. Chip*, vol. 8, no. 8, p. 1244, 2008.

[12] T. Thorsen, R. W. Roberts, F. H. Arnold, and S. R. Quake, “Dynamic Pattern Formation in a Vesicle-Generating Microfluidic Device,” *Phys. Rev. Lett.*, vol. 86, no. 18, pp. 4163–4166, Apr. 2001.

[13] T. Nisisako, T. Torii, and T. Higuchi, “Droplet formation in a microchannel networkPresented at the International Symposium on Microchemistry and Microsystems (ISMM 2001), Kawasaki, Japan, September 16?18, 2001.,” *Lab. Chip*, vol. 2, no. 1, p. 24, 2002.

[14] P. Garstecki, M. J. Fuerstman, H. A. Stone, and G. M. Whitesides, “Formation of droplets and bubbles in a microfluidic T-junction—scaling and mechanism of break-up,” *Lab. Chip*, vol. 6, no. 3, p. 437, 2006.

[15] B. Zheng, J. D. Tice, and R. F. Ismagilov, “Formation of Droplets of Alternating Composition in Microfluidic Channels and Applications to Indexing of Concentrations in Droplet-Based Assays,” *Anal. Chem.*, vol. 76, no. 17, pp. 4977–4982, Sep. 2004.

[16] S. L. Anna, N. Bontoux, and H. A. Stone, “Formation of dispersions using ‘flow focusing’ in microchannels,” *Appl. Phys. Lett.*, vol. 82, no. 3, p. 364, 2003.

[17] P. Garstecki, I. Gitlin, W. DiLuzio, G. M. Whitesides, E. Kumacheva, and H. A. Stone, “Formation of monodisperse bubbles in a microfluidic flow-focusing device,” *Appl. Phys. Lett.*, vol. 85, no. 13, p. 2649, 2004.

[18] M. De Menech, P. Garstecki, F. Jousse, and H. A. Stone, “Transition from squeezing to dripping in a microfluidic T-shaped junction,” *J. Fluid Mech.*, vol. 595, Jan. 2008.

[19] P. Garstecki, H. Stone, and G. Whitesides, “Mechanism for Flow-Rate Controlled Breakup in Confined Geometries: A Route to Monodisperse Emulsions,” *Phys. Rev. Lett.*, vol. 94, no. 16, Apr. 2005.

[20] Y.-C. Tan, J. S. Fisher, A. I. Lee, V. Cristini, and A. P. Lee, “Design of microfluidic channel geometries for the control of droplet volume, chemical concentration, and sorting,” *Lab. Chip*, vol. 4, no. 4, p. 292, 2004.

[21] X. Niu, S. Gulati, J. B. Edel, and A. J. deMello, “Pillar-induced droplet merging in microfluidic circuits,” *Lab. Chip*, vol. 8, no. 11, p. 1837, 2008.

[22] P. Singh and N. Aubry, “Transport and deformation of droplets in a microdevice using dielectrophoresis,” *ELECTROPHORESIS*, vol. 28, no. 4, pp. 644–657, Feb. 2007.

[23] C. Priest, S. Herminghaus, and R. Seemann, “Controlled electrocoalescence in microfluidics: Targeting a single lamella,” *Appl. Phys. Lett.*, vol. 89, no. 13, p. 134101, 2006.

[24] J. . Köhler, T. Henkel, A. Grodrian, T. Kirner, M. Roth, K. Martin, and J. Metze, “Digital reaction technology by micro segmented flow—components, concepts and applications,” *Chem. Eng. J.*, vol. 101, no. 1–3, pp. 201–216, Aug. 2004.

[25] R. M. Lorenz, J. S. Edgar, G. D. M. Jeffries, and D. T. Chiu, “Microfluidic and Optical Systems for the On-Demand Generation and Manipulation of Single Femtoliter-Volume Aqueous Droplets,” *Anal. Chem.*, vol. 78, no. 18, pp. 6433–6439, Sep. 2006.

[26] D. Link, S. Anna, D. Weitz, and H. Stone, “Geometrically Mediated Breakup of Drops in Microfluidic Devices,” *Phys. Rev. Lett.*, vol. 92, no. 5, Feb. 2004.

[27] D. N. Adamson, D. Mustafi, J. X. J. Zhang, B. Zheng, and R. F. Ismagilov, “Production of arrays of chemically distinct nanolitre plugs via repeated splitting in microfluidic devices,” *Lab. Chip*, vol. 6, no. 9, p. 1178, 2006.

[28] Sung Kwon Cho, Hyejin Moon, and Chang-Jin Kim, “Creating, transporting, cutting, and merging liquid droplets by electrowetting-based actuation for digital microfluidic circuits,” *J. Microelectromechanical Syst.*, vol. 12, no. 1, pp. 70–80, Feb. 2003.

[29] T. H. Ting, Y. F. Yap, N.-T. Nguyen, T. N. Wong, J. C. K. Chai, and L. Yobas, “Thermally mediated breakup of drops in microchannels,” *Appl. Phys. Lett.*, vol. 89, no. 23, p. 234101, 2006.

[30] H. N. Joensson, M. Uhlén, and H. A. Svahn, “Droplet size based separation by deterministic lateral displacement—separating droplets by cell-induced shrinking,” *Lab. Chip*, vol. 11, no. 7, p. 1305, 2011.

[31] Y.-C. Tan, Y. L. Ho, and A. P. Lee, “Microfluidic sorting of droplets by size,” *Microfluid. Nanofluidics*, vol. 4, no. 4, pp. 343–348, Jun. 2007.

[32] M. Chabert and J.-L. Viovy, “Microfluidic high-throughput encapsulation and hydrodynamic self-sorting of single cells,” *Proc. Natl. Acad. Sci.*, vol. 105, no. 9, pp. 3191–3196, Mar. 2008.

[33] J. J. Agresti, E. Antipov, A. R. Abate, K. Ahn, A. C. Rowat, J.-C. Baret, M. Marquez, A. M. Klibanov, A. D. Griffiths, and D. A. Weitz, “Ultrahigh-throughput screening in drop-based microfluidics for directed evolution,” *Proc. Natl. Acad. Sci.*, vol. 107, no. 9, pp. 4004–4009, Feb. 2010.

[34] T. Franke, A. R. Abate, D. A. Weitz, and A. Wixforth, “Surface acoustic wave (SAW) directed droplet flow in microfluidics for PDMS devices,” *Lab. Chip*, vol. 9, no. 18, p. 2625, 2009.

[35] A. R. Abate, J. J. Agresti, and D. A. Weitz, “Microfluidic sorting with high-speed single-layer membrane valves,” *Appl. Phys. Lett.*, vol. 96, no. 20, p. 203509, 2010.

[36] C. N. Baroud, M. Robert de Saint Vincent, and J.-P. Delville, “An optical toolbox for total control of droplet microfluidics,” *Lab. Chip*, vol. 7, no. 8, p. 1029, 2007.

[37] S. Liu, Y. Gu, R. B. Le Roux, S. M. Matthews, D. Bratton, K. Yunus, A. C. Fisher, and W. T. S. Huck, “The electrochemical detection of droplets in microfluidic devices,” *Lab. Chip*, vol. 8, no. 11, p. 1937, 2008.

[38] Y. Zhang, H.-H. Kim, and A. Heller, “Enzyme-Amplified Amperometric Detection of 3000 Copies of DNA in a 10-μL Droplet at 0.5 fM Concentration,” *Anal. Chem.*, vol. 75, no. 13, pp. 3267–3269, Jul. 2003.

[39] L. M. Fidalgo, G. Whyte, B. T. Ruotolo, J. L. P. Benesch, F. Stengel, C. Abell, C. V. Robinson, and W. T. S. Huck, “Coupling Microdroplet Microreactors with Mass

Spectrometry: Reading the Contents of Single Droplets Online," *Angew. Chem. Int. Ed.*, vol. 48, no. 20, pp. 3665–3668, May 2009.

[40] X. Z. Niu, B. Zhang, R. T. Marszalek, O. Ces, J. B. Edel, D. R. Klug, and A. J. deMello, "Droplet-based compartmentalization of chemically separated components in two-dimensional separations," *Chem. Commun.*, no. 41, p. 6159, 2009.

[41] M. Petersson, J. Nilsson, L. Wallman, T. Laurell, J. Johansson, and S. Nilsson, "Sample enrichment in a single levitated droplet for capillary electrophoresis," *J. Chromatogr. B. Biomed. Sci. App.*, vol. 714, no. 1, pp. 39–46, Aug. 1998.

[42] G. Cristobal, L. Arbouet, F. Sarrazin, D. Talaga, J.-L. Bruneel, M. Joanicot, and L. Servant, "On-line laser Raman spectroscopic probing of droplets engineered in microfluidic devices," *Lab. Chip*, vol. 6, no. 9, p. 1140, 2006.

[43] M. P. Cecchini, J. Hong, C. Lim, J. Choo, T. Albrecht, A. J. deMello, and J. B. Edel, "Ultrafast Surface Enhanced Resonance Raman Scattering Detection in Droplet-Based Microfluidic Systems," *Anal. Chem.*, vol. 83, no. 8, pp. 3076–3081, Apr. 2011.

[44] M. R. Bringer, C. J. Gerdts, H. Song, J. D. Tice, and R. F. Ismagilov, "Microfluidic systems for chemical kinetics that rely on chaotic mixing in droplets," *Philos. Trans. R. Soc. Math. Phys. Eng. Sci.*, vol. 362, no. 1818, pp. 1087–1104, May 2004.

[45] W. W. Yang, Y. C. Lu, Z. Y. Xiang, and G. S. Luo, "Monodispersed microcapsules enclosing ionic liquid of 1-butyl-3-methylimidazolium hexafluorophosphate," *React. Funct. Polym.*, vol. 67, no. 1, pp. 81–86, Jan. 2007.

[46] B. G. De Geest, J. P. Urbanski, T. Thorsen, J. Demeester, and S. C. De Smedt, “Synthesis of Monodisperse Biodegradable Microgels in Microfluidic Devices,” *Langmuir*, vol. 21, no. 23, pp. 10275–10279, Nov. 2005.

[47] D. T. Chiu, R. M. Lorenz, and G. D. M. Jeffries, “Droplets for Ultrasmall-Volume Analysis,” *Anal. Chem.*, vol. 81, no. 13, pp. 5111–5118, Jul. 2009.

[48] I. Shestopalov, J. D. Tice, and R. F. Ismagilov, “Multi-step synthesis of nanoparticles performed on millisecond time scale in a microfluidic droplet-based system,” *Lab. Chip*, vol. 4, no. 4, p. 316, 2004.

[49] J. R. Burns and C. Ramshaw, “The intensification of rapid reactions in multiphase systems using slug flow in capillaries,” *Lab. Chip*, vol. 1, no. 1, p. 10, 2001.

[50] B. Ahmed, D. Barrow, and T. Wirth, “Enhancement of Reaction Rates by Segmented Fluid Flow in Capillary Scale Reactors,” *Adv. Synth. Catal.*, vol. 348, no. 9, pp. 1043–1048, Jun. 2006.

[51] K.-I. Sotowa, K. Irie, T. Fukumori, K. Kusakabe, and S. Sugiyama, “Droplet Formation by the Collision of Two Aqueous Solutions in a Microchannel and Application to Particle Synthesis,” *Chem. Eng. Technol.*, vol. 30, no. 3, pp. 383–388, Mar. 2007.

[52] H. Song, H.-W. Li, M. S. Munson, T. G. Van Ha, and R. F. Ismagilov, “On-Chip Titration of an Anticoagulant Argatroban and Determination of the Clotting Time within Whole Blood or Plasma Using a Plug-Based Microfluidic System,” *Anal. Chem.*, vol. 78, no. 14, pp. 4839–4849, Jul. 2006.

[53] Z. T. Cygan, J. T. Cabral, K. L. Beers, and E. J. Amis, “Microfluidic Platform for the Generation of Organic-Phase Microreactors,” *Langmuir*, vol. 21, no. 8, pp. 3629–3634, Apr. 2005.

[54] E. M. Chan, A. P. Alivisatos, and R. A. Mathies, “High-Temperature Microfluidic Synthesis of CdSe Nanocrystals in Nanoliter Droplets,” *J. Am. Chem. Soc.*, vol. 127, no. 40, pp. 13854–13861, Oct. 2005.

[55] M. S. Long, C. D. Jones, M. R. Helfrich, L. K. Mangeney-Slavin, and C. D. Keating, “Dynamic microcompartmentation in synthetic cells,” *Proc. Natl. Acad. Sci.*, vol. 102, no. 17, pp. 5920–5925, Mar. 2005.

[56] V. Noireaux and A. Libchaber, “A vesicle bioreactor as a step toward an artificial cell assembly,” *Proc. Natl. Acad. Sci.*, vol. 101, no. 51, pp. 17669–17674, Dec. 2004.

[57] A. Huebner, M. Srisa-Art, D. Holt, C. Abell, F. Hollfelder, A. J. deMello, and J. B. Edel, “Quantitative detection of protein expression in single cells using droplet microfluidics,” *Chem. Commun.*, no. 12, p. 1218, 2007.

[58] V. Taly, D. Pekin, A. E. Abed, and P. Laurent-Puig, “Detecting biomarkers with microdroplet technology,” *Trends Mol. Med.*, vol. 18, no. 7, pp. 405–416, Jul. 2012.

[59] W. Wang, Z.-X. Li, R. Luo, S.-H. Lü, A.-D. Xu, and Y.-J. Yang, “Droplet-based micro oscillating-flow PCR chip,” *J. Micromechanics Microengineering*, vol. 15, no. 8, pp. 1369–1377, Aug. 2005.

[60] B. J. Hindson, K. D. Ness, D. A. Masquelier, P. Belgrader, N. J. Heredia, A. J. Makarewicz, I. J. Bright, M. Y. Lucero, A. L. Hiddessen, T. C. Legler, T. K. Kitano,

M. R. Hodel, J. F. Petersen, P. W. Wyatt, E. R. Steenblock, P. H. Shah, L. J. Bousse, C. B. Troup, J. C. Mellen, D. K. Wittmann, N. G. Erndt, T. H. Cauley, R. T. Koehler, A. P. So, S. Dube, K. A. Rose, L. Montesclaros, S. Wang, D. P. Stumbo, S. P. Hodges, S. Romine, F. P. Milanovich, H. E. White, J. F. Regan, G. A. Karlin-Neumann, C. M. Hindson, S. Saxonov, and B. W. Colston, "High-Throughput Droplet Digital PCR System for Absolute Quantitation of DNA Copy Number," *Anal. Chem.*, vol. 83, no. 22, pp. 8604–8610, Nov. 2011.

[61] T. Hatakeyama, D. L. Chen, and R. F. Ismagilov, "Microgram-Scale Testing of Reaction Conditions in Solution Using Nanoliter Plugs in Microfluidics with Detection by MALDI-MS," *J. Am. Chem. Soc.*, vol. 128, no. 8, pp. 2518–2519, Mar. 2006.

[62] A. R. Wheeler, H. Moon, C. A. Bird, R. R. Ogorzalek Loo, C.-J. "C. J. . Kim, J. A. Loo, and R. L. Garrell, "Digital Microfluidics with In-Line Sample Purification for Proteomics Analyses with MALDI-MS," *Anal. Chem.*, vol. 77, no. 2, pp. 534–540, Jan. 2005.

[63] K. P. Nichols and J. G. E. Gardeniers, "A Digital Microfluidic System for the Investigation of Pre-Steady-State Enzyme Kinetics Using Rapid Quenching with MALDI-TOF Mass Spectrometry," *Anal. Chem.*, vol. 79, no. 22, pp. 8699–8704, Nov. 2007.

[64] B. T. C. Lau, C. A. Baitz, X. P. Dong, and C. L. Hansen, "A Complete Microfluidic Screening Platform for Rational Protein Crystallization," *J. Am. Chem. Soc.*, vol. 129, no. 3, pp. 454–455, Jan. 2007.

[65] H. Song and R. F. Ismagilov, “Millisecond Kinetics on a Microfluidic Chip Using Nanoliters of Reagents,” *J. Am. Chem. Soc.*, vol. 125, no. 47, pp. 14613–14619, Nov. 2003.

[66] G. K. Batchelor, *An introduction to fluid dynamics*. Cambridge, U.K.; New York, NY: Cambridge University Press, 1999.

[67] K. Sritharan, C. J. Strobl, M. F. Schneider, A. Wixforth, and Z. Guttenberg, “Acoustic mixing at low Reynold’s numbers,” *Appl. Phys. Lett.*, vol. 88, no. 5, p. 054102, 2006.

[68] G. G. Yaralioglu, I. O. Wygant, T. C. Marentis, and B. T. Khuri-Yakub, “Ultrasonic Mixing in Microfluidic Channels Using Integrated Transducers,” *Anal. Chem.*, vol. 76, no. 13, pp. 3694–3698, Jul. 2004.

[69] C. Eckart, “Vortices and Streams Caused by Sound Waves,” *Phys. Rev.*, vol. 73, no. 1, pp. 68–76, Jan. 1948.

[70] S. C. Hur, A. J. Mach, and D. Di Carlo, “High-throughput size-based rare cell enrichment using microscale vortices,” *Biomicrofluidics*, vol. 5, no. 2, p. 022206, 2011.

[71] H. K. Moffatt, “Viscous and resistive eddies near a sharp corner,” *J. Fluid Mech.*, vol. 18, no. 01, p. 1, Mar. 2006.

[72] G. K. Kurup and A. S. Basu, “Field-free particle focusing in microfluidic plugs,” *Biomicrofluidics*, vol. 6, no. 2, p. 022008, 2012.

[73] C.-C. Chang and R.-J. Yang, “Electrokinetic mixing in microfluidic systems,” *Microfluid. Nanofluidics*, vol. 3, no. 5, pp. 501–525, Jun. 2007.

[74] Y. Ben and H.-C. Chang, “Nonlinear Smoluchowski slip velocity and micro-vortex generation,” *J. Fluid Mech.*, vol. 461, Jul. 2002.

[75] D. Kim, A. Raj, L. Zhu, R. I. Masel, and M. A. Shannon, “Non-equilibrium electrokinetic micro/nano fluidic mixer,” *Lab. Chip*, vol. 8, no. 4, p. 625, 2008.

[76] A. Kumar, S. J. Williams, and S. T. Wereley, “Experiments on opto-electrically generated microfluidic vortices,” *Microfluid. Nanofluidics*, vol. 6, no. 5, pp. 637–646, Aug. 2008.

[77] A. O. El Moctar, N. Aubry, and J. Batton, “Electro-hydrodynamic micro-fluidic mixerElectronic supplementary information (ESI) available: Video of effect of electric field on channel flow mixing. See http://www.rsc.org/suppdata/lc/b3/b306868b/,” *Lab. Chip*, vol. 3, no. 4, p. 273, 2003.

[78] A. Ashkin, J. M. Dziedzic, J. E. Bjorkholm, and S. Chu, “Observation of a single-beam gradient force optical trap for dielectric particles,” *Opt. Lett.*, vol. 11, no. 5, p. 288, May 1986.

[79] P. Y. Chiou, A. T. Ohta, and M. C. Wu, “Massively parallel manipulation of single cells and microparticles using optical images,” *Nature*, vol. 436, no. 7049, pp. 370–372, Jul. 2005.

[80] S. Park, C. Pan, T.-H. Wu, C. Kloss, S. Kalim, C. E. Callahan, M. Teitell, and E. P. Y. Chiou, “Floating electrode optoelectronic tweezers: Light-driven dielectrophoretic droplet manipulation in electrically insulating oil medium,” *Appl. Phys. Lett.*, vol. 92, no. 15, p. 151101, 2008.

[81] Pei-Yu Chiou, Zehao Chang, and M. C. Wu, “Droplet Manipulation With Light on Optoelectrowetting Device,” *J. Microelectromechanical Syst.*, vol. 17, no. 1, pp. 133–138, Feb. 2008.

[82] S.-Y. Park and P.-Y. Chiou, “Light-Driven Droplet Manipulation Technologies for Lab-on-a-Chip Applications,” *Adv. Optoelectron.*, vol. 2011, pp. 1–12, 2011.

[83] K. T. Kotz, K. A. Noble, and G. W. Faris, “Optical microfluidics,” *Appl. Phys. Lett.*, vol. 85, no. 13, p. 2658, 2004.

[84] A. S. Basu and Y. B. Gianchandani, “Virtual microfluidic traps, filters, channels and pumps using Marangoni flows,” *J. Micromechanics Microengineering*, vol. 18, no. 11, p. 115031, Nov. 2008.

[85] S. R. Hodges, O. E. Jensen, and J. M. Rallison, “The motion of a viscous drop through a cylindrical tube,” *J. Fluid Mech.*, vol. 501, pp. 279–301, Feb. 2004.

[86] A. Ghaini, A. Mescher, and D. W. Agar, “Hydrodynamic studies of liquid–liquid slug flows in circular microchannels,” *Chem. Eng. Sci.*, vol. 66, no. 6, pp. 1168–1178, Mar. 2011.

[87] M. N. Kashid, I. Gerlach, S. Goetz, J. Franzke, J. F. Acker, F. Platte, D. W. Agar, and S. Turek, “Internal Circulation within the Liquid Slugs of a Liquid−Liquid Slug-Flow Capillary Microreactor,” *Ind. Eng. Chem. Res.*, vol. 44, no. 14, pp. 5003–5010, Jul. 2005.

[88] J. D. Tice, H. Song, A. D. Lyon, and R. F. Ismagilov, “Formation of Droplets and Mixing in Multiphase Microfluidics at Low Values of the Reynolds and the Capillary Numbers,” *Langmuir*, vol. 19, no. 22, pp. 9127–9133, Oct. 2003.

[89] M. N. Kashid and D. W. Agar, “Hydrodynamics of liquid–liquid slug flow capillary microreactor: Flow regimes, slug size and pressure drop,” *Chem. Eng. J.*, vol. 131, no. 1–3, pp. 1–13, Jul. 2007.

[90] G. K. Kurup and A. S. Basu, “Shape dependent Laplace vortices in deformed liquid-liquid slug flow,” 2011, pp. 4034–4037.

[91] S. L. Anna, N. Bontoux, and H. A. Stone, “Formation of dispersions using "flow focusing’’ in microchannels,” *Appl. Phys. Lett.*, vol. 82, no. 3, pp. 364–366, 2003.

[92] T. Thorsen, R. W. Roberts, F. H. Arnold, and S. R. Quake, “Dynamic pattern formation in a vesicle-generating microfluidic device,” *Phys. Rev. Lett.*, vol. 86, no. 18, pp. 4163–4166, 2001.

[93] J. Bico and D. QuéRé, “Self-propelling slugs,” *J. Fluid Mech.*, vol. 467, pp. 101–127, Sep. 2002.

[94] F. P. Bretherton, “The motion of long bubbles in tubes,” *J. Fluid Mech.*, vol. 10, no. 02, p. 166, 1961.

[95] C. N. Baroud, F. Gallaire, and R. Dangla, “Dynamics of microfluidic droplets,” *Lab. Chip*, vol. 10, no. 16, p. 2032, 2010.

[96] A. Ghaini, A. Mescher, and D. W. Agar, “Hydrodynamic studies of liquid–liquid slug flows in circular microchannels,” *Chem. Eng. Sci.*, vol. 66, no. 6, pp. 1168–1178, Mar. 2011.

[97] G. K. Kurup and A. S. Basu, “Shape Dependent Laplace Vortices in Deformed Liquid-Liquid Slug Flow,” in *Proc. IEEE Engineering in Medicine and Biology Conference (EMBC)*, Boston, MA, 2011.

[98] G. I. Taylor, “Deposition of a viscous fluid on the wall of a tube,” *J. Fluid Mech.*, vol. 10, no. 02, p. 161, 1961.

[99] M. N. Kashid, I. Gerlach, S. Goetz, J. Franzke, J. F. Acker, F. Platte, D. W. Agar, and S. Turek, “Internal Circulation within the Liquid Slugs of a Liquid−Liquid Slug-Flow Capillary Microreactor,” *Ind. Eng. Chem. Res.*, vol. 44, no. 14, pp. 5003–5010, Jul. 2005.

[100] H. Song, D. L. Chen, and R. F. Ismagilov, “Reactions in droplets in microfluidic channels,” *Angew. Chem. Int. Ed*, vol. 45, no. 44, p. 7336, 2006.

[101] S. R. Hodges, O. E. Jensen, and J. M. Rallison, “The motion of a viscous drop through a cylindrical tube,” *J. Fluid Mech.*, vol. 501, pp. 279–301, Feb. 2004.

[102] C. King, E. Walsh, and R. Grimes, “PIV measurements of flow within plugs in a microchannel,” *Microfluid. Nanofluidics*, vol. 3, no. 4, pp. 463–472, 2007.

[103] T. C. Thulasidas, M. A. Abraham, and R. L. Cerro, “Flow patterns in liquid slugs during bubble-train flow inside capillaries,” *Chem. Eng. Sci.*, vol. 52, no. 17, pp. 2947–2962, Sep. 1997.

[104] M. Kashid and D. Agar, “Hydrodynamics of liquid–liquid slug flow capillary microreactor: Flow regimes, slug size and pressure drop,” *Chem. Eng. J.*, vol. 131, no. 1–3, pp. 1–13, Jul. 2007.

[105] N. Pamme, “Continuous flow separations in microfluidic devices,” *Lab. Chip*, vol. 7, no. 12, p. 1644, 2007.

[106] X. Xuan, J. Zhu, and C. Church, “Particle focusing in microfluidic devices,” *Microfluid. Nanofluidics*, vol. 9, no. 1, pp. 1–16, Mar. 2010.

[107] D. Di Carlo, D. Irimia, R. G. Tompkins, and M. Toner, “Continuous inertial focusing, ordering, and separation of particles in microchannels,” *Proc. Natl. Acad. Sci.*, vol. 104, no. 48, pp. 18892–18897, 2007.

[108] A. A. S. Bhagat, S. S. Kuntaegowdanahalli, and I. Papautsky, “Continuous particle separation in spiral microchannels using dean flows and differential migration.,” *Lab. Chip*, vol. 8, no. 11, pp. 1906–1914, 2008.

[109] D. Huh, J. H. Bahng, Y. Ling, H.-H. Wei, O. D. Kripfgans, J. B. Fowlkes, J. B. Grotberg, and S. Takayama, “Gravity-Driven Microfluidic Particle Sorting Device with Hydrodynamic Separation Amplification,” *Anal. Chem.*, vol. 79, no. 4, pp. 1369–1376, Feb. 2007.

[110] S. K. Cho, Y. Zhao, and C.-J. ?CJ? Kim, “Concentration and binary separation of micro particles for droplet-based digital microfluidics,” *Lab. Chip*, vol. 7, no. 4, p. 490, 2007.

[111] J. K. Valley, S. NingPei, A. Jamshidi, H.-Y. Hsu, and M. C. Wu, “A unified platform for optoelectrowetting and optoelectronic tweezers,” *Lab. Chip*, vol. 11, pp. 1292–1297, 2011.

[112] R. S. Sista, A. E. Eckhardt, V. Srinivasan, M. G. Pollack, S. Palanki, and V. K. Pamula, “Heterogeneous immunoassays using magnetic beads on a digital microfluidic platform,” *Lab. Chip*, vol. 8, no. 12, pp. 2188–2196, 2008.

[113] U. Lehmann, C. Vandevyver, V. K. Parashar, and M. A. M. Gijs, “Droplet-Based DNA Purification in a Magnetic Lab-on-a-Chip,” *Angew. Chem. Int. Ed.*, vol. 45, no. 19, pp. 3062–3067, May 2006.

[114] J. Pipper, M. Inoue, L. F.-P. Ng, P. Neuzil, Y. Zhang, and L. Novak, “Catching bird flu in a droplet,” *Nat. Med.*, vol. 13, no. 10, pp. 1259–1263, Sep. 2007.

[115] A. Shields, W. P. Ott, and J. C. Van Uchelen, “Application of similarity principles and turbulence research to bed-load movement,” Caltech Library Soil Conservation Service, 1936.

[116] M. C. Miller, I. N. McCAVE, and P. D. Komar, “Threshold of sediment motion under unidirectional currents,” *Sedimentology*, vol. 24, no. 4, pp. 507–527, Aug. 1977.

[117] L. Svarovsky, *Solid-liquid separation*. Oxford; Boston: Butterworth-Heinemann, 2000.

[118] A. Einstein, “Eine neue bestimmung der moleküldimensionen,” *Ann. Phys.*, vol. 324, no. 2, pp. 289–306, 1906.

[119] L. E. Nielsen and R. F. Landel, *Mechanical properties of polymers and composites*. Marcel Dekker Inc, 1994.

[120] M. Elimelech, J. Gregory, X. Jia, and R. Williams, *Particle deposition and aggregation: measurement, modelling and simulation*. Butterworth-Heinemann, 1998.

[121] T. Taha and Z. F. Cui, “Hydrodynamics of slug flow inside capillaries,” *Chem. Eng. Sci.*, vol. 59, no. 6, pp. 1181–1190, 2004.

[122] K. Sun, N. Ramgir, and S. Bhansali, “An immunoelectrochemical sensor for salivary cortisol measurement,” *Sens. Actuators B Chem.*, vol. 133, no. 2, pp. 533–537, Aug. 2008.

[123] S. Bronzeau and N. Pamme, “Simultaneous bioassays in a microfluidic channel on plugs of different magnetic particles,” *Anal. Chim. Acta*, vol. 609, no. 1, pp. 105–112, Feb. 2008.

[124] L. S. Roach, H. Song, and R. F. Ismagilov, “Controlling Nonspecific Protein Adsorption in a Plug-Based Microfluidic System by Controlling Interfacial Chemistry Using Fluorous-Phase Surfactants,” *Anal. Chem.*, vol. 77, no. 3, pp. 785–796, Feb. 2005.

[125] J. L. Anderson, “Colloid Transport by Interfacial Forces,” *Annu. Rev. Fluid Mech.*, vol. 21, no. 1, pp. 61–99, Jan. 1989.

[126] M. Washizu, “Electrostatic actuation of liquid droplets for micro-reactor applications,” *IEEE Trans. Ind. Appl.*, vol. 34, no. 4, pp. 732–737, Aug. 1998.

[127] J. R. Millman, K. H. Bhatt, B. G. Prevo, and O. D. Velev, “Anisotropic particle synthesis in dielectrophoretically controlled microdroplet reactors,” *Nat. Mater.*, vol. 4, no. 1, pp. 98–102, Dec. 2004.

[128] D. C. Prieve, J. L. Anderson, J. P. Ebel, and M. E. Lowell, “Motion of a particle generated by chemical gradients. Part 2. Electrolytes,” *J. Fluid Mech.*, vol. 148, no. -1, p. 247, Apr. 2006.

[129] S. Duhr and D. Braun, “From the Cover: Why molecules move along a temperature gradient,” *Proc. Natl. Acad. Sci.*, vol. 103, no. 52, pp. 19678–19682, Dec. 2006.

[130] R. Piazza, “Thermophoresis: moving particles with thermal gradients,” *Soft Matter*, vol. 4, no. 9, p. 1740, 2008.

[131] R. S. Subramanian, *The motion of bubbles and drops in reduced gravity*. Cambridge; New York: Cambridge University Press, 2001.

[132] N. O. Young, J. S. Goldstein, and M. J. Block, “The motion of bubbles in a vertical temperature gradient,” *J. Fluid Mech.*, vol. 6, no. 03, p. 350, Mar. 2006.

[133] R. Balasubramaniam and A.-T. Chai, “Thermocapillary migration of droplets: An exact solution for small marangoni numbers,” *J. Colloid Interface Sci.*, vol. 119, no. 2, pp. 531–538, Oct. 1987.

[134] R. S. Subramanian, “The Stokes force on a droplet in an unbounded fluid medium due to capillary effects,” *J. Fluid Mech.*, vol. 153, no. -1, p. 389, Apr. 2006.

[135] R. Balasubramaniam and R. S. Subramanian, “The migration of a drop in a uniform temperature gradient at large Marangoni numbers,” *Phys. Fluids*, vol. 12, no. 4, p. 733, 2000.

[136] M. Hähnel, V. Delitzsch, and H. Eckelmann, “The motion of droplets in a vertical temperature gradient,” *Phys. Fluids Fluid Dyn.*, vol. 1, no. 9, p. 1460, 1989.

[137] T. Cosgrove, *Colloid science principles, methods and applications*. Chichester, U.K.: Wiley, 2010.

[138] E. P. Lewandowski, J. A. Bernate, P. C. Searson, and K. J. Stebe, “Rotation and Alignment of Anisotropic Particles on Nonplanar Interfaces,” *Langmuir*, vol. 24, no. 17, pp. 9302–9307, Sep. 2008.

[139] M. J. M. Hill, “On a Spherical Vortex.,” *Proc. R. Soc. Lond.*, vol. 55, no. 331–335, pp. 219–224, Jan. 1894.

[140] S. S. Alves, S. P. Orvalho, and J. M. T. Vasconcelos, “Effect of bubble contamination on rise velocity and mass transfer,” *Chem. Eng. Sci.*, vol. 60, no. 1, pp. 1–9, Jan. 2005.

[141] C. D. Eggleton, Y. P. Pawar, and K. J. Stebe, “Insoluble surfactants on a drop in an extensional flow: a generalization of the stagnated surface limit to deforming interfaces,” *J. Fluid Mech.*, vol. 385, pp. 79–99, Apr. 1999.

[142] A. S. Basu, “Droplet morphometry and velocimetry (DMV): a video processing software for time-resolved, label-free tracking of droplet parameters,” *Lab. Chip*, vol. 13, no. 10, p. 1892, 2013.

[143] G. Wang, C. Lim, L. Chen, H. Chon, J. Choo, J. Hong, and A. J. deMello, “Surface-enhanced Raman scattering in nanoliter droplets: towards high-sensitivity detection of mercury (II) ions,” *Anal. Bioanal. Chem.*, vol. 394, no. 7, pp. 1827–1832, May 2009.

[144] M. T. Guo, A. Rotem, J. A. Heyman, and D. A. Weitz, “Droplet microfluidics for high-throughput biological assays,” *Lab. Chip*, vol. 12, no. 12, p. 2146, 2012.

[145] A. Arora, G. Simone, G. B. Salieb-Beugelaar, J. T. Kim, and A. Manz, “Latest Developments in Micro Total Analysis Systems,” *Anal. Chem.*, vol. 82, no. 12, pp. 4830–4847, Jun. 2010.

[146] K. Sun, N. Ramgir, and S. Bhansali, “An immunoelectrochemical sensor for salivary cortisol measurement,” *Sens. Actuators B Chem.*, vol. 133, no. 2, pp. 533–537, Aug. 2008.

[147] U. Lehmann, C. Vandevyver, V. K. Parashar, and M. A. M. Gijs, “Droplet-Based DNA Purification in a Magnetic Lab-on-a-Chip,” *Angew. Chem. Int. Ed.*, vol. 45, no. 19, pp. 3062–3067, May 2006.

[148] M. J. Jebrail and A. R. Wheeler, “Digital Microfluidic Method for Protein Extraction by Precipitation,” *Anal. Chem.*, vol. 81, no. 1, pp. 330–335, Jan. 2009.

[149] M. N. Kashid, I. Gerlach, S. Goetz, J. Franzke, J. F. Acker, F. Platte, D. W. Agar, and S. Turek, “Internal Circulation within the Liquid Slugs of a Liquid−Liquid Slug-Flow Capillary Microreactor,” *Ind. Eng. Chem. Res.*, vol. 44, no. 14, pp. 5003–5010, Jul. 2005.

[150] *15th International Conference on miniaturized systems for chemistry and life sciences: Microtas 2011*. San Diego, CA: Chemical and Biological Microsystems Society, 2011.

[151] A. T. Florence and D. Attwood, *Physicochemical principles of pharmacy*. London: Chicago : Pharmaceutical Press, 2006.

ABSTRACT

MICROVORTICES IN DROPLETS: GENERATION AND APPLICATIONS

by

GOPAKUMAR KAMALAKSHAKURUP

August 2014

Advisor: Dr. Amar S. Basu

Major: Electrical Engineering

Degree: Doctor of Philosophy

The emerging field of droplet microfluidics deals with the manipulation of nL-fL droplets encapsulated within an immiscible carrier phase. The droplets are used as reaction containers for biochemical assays, enabling drastic reduction in assay volumes needed for modern life sciences research. To achieve this, basic laboratory processes such as mixing, detection, and metering must be emulated in the droplet format. Three important unit operations relevant to high throughput screening include 1) the concentration of particles and species within droplets, which is necessary for heterogeneous assays; 2) sensing the biochemical contents of a droplet; and 3) the sorting of droplets based on physical or chemical properties, which is important for single cell and proteomic assays. Currently, particle concentration in droplets requires active components, such as on-chip electrodes or magnets, along with charged or magnetic particles. Similarly, sensing and sorting droplets by chemical composition is based on flow cytometry, which also requires on-chip electrodes, feedback control, and chemical labeling. It is desirable to avoid active field techniques due to complexity, size,

and cost constraints, and replace them with more simple and passive techniques. In this thesis, we utilize microvortices, the rotational motion of fluid, to enhance the capabilities of droplet microfluidics in the above three areas. The microvortices are generated using two methods: (i) hydrodynamic recirculation drag and (ii) tensiophoresis.

In the first method, species concentration is accomplished by exploiting the shear-induced vortices that occur naturally inside a droplet/plug as it moves through a microchannel. Prior studies utilized these flows for enhancing mixing or interphase mass transfer. This work exploits microvortices together with two other independent phenomena—sedimentation of particles and interfacial adsorption of proteins—to concentrate both types of species at the rear of the droplet, where they can be extracted from the drop. In the latter case, the protein localization at the rear of drop reduces the interfacial tension locally resulting in an asymmetry in the drop shape. Under laminar flow, the shape deformation is deterministic and can serve as a sensitive, label-free indicator of protein concentration in proteomic screening.

In the second method, label-free sorting of droplets is accomplished by a novel droplet actuation technique termed Tensiophoresis. A microchemical gradient across the droplet is transduced into a microvortex flow which propels the droplets up the chemical gradient. Using laminar flow to precisely control the gradient, droplets can be sorted by size with 3.3% resolution over a wide turning range. Droplets can be also sorted based on chemical composition because tensiophoresis is inhibited by surface active agents adsorbed on the droplet surface. Studies conducted using Bovine Serum Albumin (BSA) show that the droplet migration velocity scales inversely with protein concentration in

the droplet, and migration velocity can be correlated to protein concentration with a 1 femtomole limit of detection.

As modern life sciences research becomes increasingly reliant on high throughput workflows, microdroplet technology can meet the growing demand to perform screening at ultra-high throughputs with reduced sample volume. This thesis contributes three important unit operations which expand the capabilities of droplet-based workflows in proteomics, cell biology, and other areas of biomedical research.

AUTOBIOGRAPHICAL STATEMENT

Gopakumar Kamalakshakurup (G.K. Kurup) received a Bachelor of Technology in Electrical & Electronics engineering from Government College of Engineering Kerala, India in 2006 and Master of Technology in Microsystems from Indian Institute of Technology, Kharagpur in 2009, all with honors. Presently, he is persuing PhD in Electrical Engineering from Wayne State University. His dissertation, under Prof. Amar S. Basu, is in the area of droplet microfluidics titled “Microvortices in Droplets: Generation & Applications”. Gopakumar has worked with BioRad Laboratories in developing novel droplet transport techniques for genomic applications, and served as a teaching assistant during his PhD career at Wayne State University. He has received MHRD fellowship from Government of India, Thomas C Rumble Fellowship from Wayne State University, Wayne State University Travel award, and silver medal for best academic performance in undergraduate curriculum. His work on Optofluidic tweezers has resulted in US patent.